Theory of Nanostructures

Clive Emary

February 16, 2009

Contents

Chapter 1

Introduction

1.1 What is a nanostructure?

Strictly speaking, a *nanostructure* is any structure with one or more dimensions measuring in the nanometer (10^{-9}m) range. Various definitions refine this further, stating that a nanostructure should have a characteristic dimension lying between 1nm and 100nm, putting nanostructures as intermediate in size between a molecule and a bacterium. In this lecture, we will take a slightly more flexible definition and allow "nanostructure" to include larger structures — providing that the object's size of the plays an essential role in determining its physical properties.

Experimentalists now have access to a huge array of nanostructures, both self-assembled (e.g. fullerenes, nanotubes, ...), and directly fabricated (e.g. quantum wires, lateral quantum dots, ...). The picture set in the lectures should give an idea of the diversity of such structures, as revealed through the techniques of electron and atomic-force microscopy.

1.2 Mesoscopic transport

Nanostructures are typically probed either optically (spectroscopy, photoluminescence, ...) or in transport experiments. In this lecture series we will mainly concentrate on the latter (we will, however, discuss the optics of quantum dots; in particular in the context of quantum computation). This field of investigation is often given the name *mesoscopic transport*, and the following considerations give an idea of the significance of this term.

We would expect that the resistance R of a bulk 3-dimensional sample

of a material to be given by

$$R = \frac{L}{\sigma A}, \tag{1.1}$$

where L and A are the length and cross-sectional area of the sample, and σ is the conductivity. A sample for which Eq. (1.1) holds is said to be *Ohmic*, and this behaviour is well described by (semi-)classical transport theory (such as the Boltzmann Equation of Chapter 3 2).

If, however, the sample is small enough that the considerations leading up to Eq. (1.1) do not hold, non-Ohmic behaviour can result. This typically occurs when the characteristic dimension of the device is smaller than one or more of the following length scales:

- the de Broglie wavelength of the electrons (given by their kinetic energy)
- their mean free path, (distance between collisions)
- and their phase coherence length (distance over which an electron can interfere with itself).

Such a sample, or device, is then described as being *mesoscopic* — one that is bigger than atomic, or 'microscopic', dimensions but yet small enough not to exhibit the Ohmic properties of bulk, or 'macroscopic' materials. The important length scales listed above vary considerably with material properties, temperature, applied voltage, etc, and so the size-scale at which mesoscopic effects occur is highly variable, and not ridgedly fixed at the literal nano-scale.

A mesoscopic device may also be thought of as one being big enough to be successfully manipulated in experiment, and yet small enough to be interesting!

1.3 Why study nanostructures?

Understanding the nanoworld makes up one of the frontiers of modern science. One reason for this is that technology based on nanostructures promises to be hugely important economically. Nowhere is this more evident than in semiconductor industry. Moore's law makes the observation that the number of transistors that can be inexpensively placed on an integrated circuit doubles approximately every two years. If the size of IC chips stay approximately the same, then the linear dimension of the transistors

must half every four years. Current transistor fabrication already runs at 45nm, and Intel claim that they will have 32nm technology in commercial devices by 2009. Understanding how electrons behave over such tiny distant scales is therefore of very obvious importance to the electronics, communication and computation industries. One potentially game-changing future application that we will discuss in this course is the use of nanostructures to perform quantum information processing tasks, and in particular to build a quantum computer.

Nanostructures and nanomaterials are having real-world impact elsewhere. For example, the Quantum Hall effect, for which K. von Klitzing earned the Nobel prize, now serves as a measurement standard for resistance. Quantum dots are making quite a name for themselves in many modern application areas such as Photovoltaic devices, QD lasers, and as even as fluorescent tracers in biological and medical settings.

The theory of nanostructures is an intellectually very rewarding topic. There are fundamental questions: what is the origin of resistance? what can we tell about an structure just by counting the electrons flowing through it?, and what role does information play in the nanoworld? Their pursuit involves a broad range of physical concepts and theories, from simple confinement effects familiar from introductory quantum mechanics through to the complex many-body physics of the Kondo and fractional quantum Hall effects. Furthermore, analogies to atomic and molecular physics abound, as do formal similarities between mesoscopic transport and quantum optics. More traditional condensed matter and quantum many-body theory all have the role to play in understanding, an learning how to control, nanostructures.

1.4 Literature

- S. Datta, *Electronic Transport in Mesoscopic Systems*, Cambridge University Press, Cambridge, 1995.
- D. Ferry and S. Goodnick, *Transport in Nanostructures*, Cambridge University Press, Cambridge, 1997.
- M. Büttiker, Phys. Rev. B **46** 12485 (1992).
- Ya. M. Blanter, and M. Büttiker, *Shot Noise in Mesoscopic Conductors*, Phys. Rep. **336**, 1 (2000); `cond-mat/9910158`.
- L. Sohn, L. Kouwenhoven and G. Schön, *Mesoscopic Electron Transport*, NATO ASI Series E, Vol. 345 (Kluwer Academic, Dordrecht, 1996).
- J. Rammer, *Quantum Transport Theory*, Perseus Books, Reading MA 1998.
- J. Jäckle *Einführung in die Transporttheorie*, Vieweg 1978.
- H. Bruus and K. Flensberg, *Many-Body Quantum Theory in Condensed Matter Physics, An Introduction*, Oxford University Press, Oxford 2004.
- N. W. Ashcroft and N. D. Mermin, *Solid State Physics*, Brooks Cole 1976.
- J. M. Ziman, *Principles of the theory of solids*, Cambridge University Press, Cambridge, 1964.

Chapter 2

Semi-classical transport theory

In this course, we are primarily interested in transport through nanostructures. However, it is instructive, to first review the semi-classical Boltzmann theory of transport in bulk materials to become familiar with some concepts and language, and also have a benchmark with which to compare.

2.1 Physical length scales

The transport properties of a device are determined by a set of characteristic length scales and their relationship to the physical dimensions of the device. As presaged in the introduction, we expect a conductor to shows Ohmic behaviour only when its dimensions are greater than all of these length scales, which vary widely from material to material and also with temperature, applied field, impurity concentration etc. The relevant length scales are: (following E. Schöll in *Theory of Transport properties of semiconductor nanostructures*, Chapman & Hall 1998)

- **Mean free path, l_m:** The average distance an electron travels before it experiences *elastic scattering* which destroys its initial momentum. The dominant elastic scattering mechanism is impurity scattering. The mean-free path is related to the (transport) momentum relaxation time $\tau_{\rm tr}$ by $l_m = v\tau_{\rm tr}$ where v is the average carrier speed.
- **Phase-relaxation length, l_ϕ:** The average distance an electron travels before information about its initial phase is lost. *Inelastic* scattering, such as occurs in electron-phonon interactions, is responsible for

this dephasing, since in such collisions the energy of the electron is changed, and its quantum-mechanical phase is randomised. Impurity scattering may also contribute to phase relaxation if the impurity has internal degrees of freedom. In high-mobility semiconductors, the phase relaxation time τ_ϕ can be of the same order or shorter than the momentum relaxation time, and $l_\phi = v_F \tau_\phi$ with Fermi velocity v_F. In low mobility samples, however, τ_m can be considerably shorter than τ_ϕ and diffusive motion may occur over a phase coherent region; then $l_\phi^2 = D\tau_\phi$ with diffusion constant $D = v_F \tau_m/2$.

- **de Broglie wavelength, λ:** An electron with wavenumber k has a de Broglie wavelength of $\lambda = 2\pi/k$. In three-dimensions, this can be expressed in terms of the electron energy E as $\lambda = \sqrt{h^2/2m^*E}$ with m^* the effective electron mass. The de Broglie length defines the scale on which quantum-mechanical effects become important.

- **Magnetic length, l_B:** In the presence of a magnetic inductance B, electron energy is quantised in integer multiples of $\hbar\omega_c$, where ω_c is the cyclotron frequency. The magnetic length $l_B = \sqrt{\hbar/eB}$ characterises the extent of the electron cyclotron orbit.

Depending on the relation of system size L to the above lengths, different transport regimes can be distinguished:

- **Classical diffusive transport:** For macroscopic dimensions $L \gg l_m, l_\phi$, carriers experience frequent elastic and inelastic collisions such their momentum and phase are relaxed. The average velocity of the electron is given by its drift velocity $v = -\mu F$ with mobility $\mu = e\tau_m/m^*$ from Drude theory.

- **Coherent transport:** For system sizes smaller that the phase relaxation length l_ϕ, quantum-mechanical wavefunction of the carriers has a well-defined phase throughout the system. Quantum interference effects such as Aharonov-Bohm oscillations or universal conductance fluctuations may observed in transport.

- **Ballistic transport:** If the size of the system L is smaller than l_m, carriers can cross the device without scattering.

- **Quantum size effects:** If the de Broglie wavelength is greater than one or more of the system dimensions, size quantisation of the carrier wave functions will occur. Propagation in those directions is not possible and the density of states of the system is modified accordingly.

2.2 The Boltzmann Equation

A transport theory include must include not just the dynamics of carriers under the influence of external fields, but also stochastic effects arising from carrier interactions with impurities, phonons, contacts, etc. The Boltzmann Equation is a transport theory that operates in the classical diffusive regime in which the electrons are described by a distribution function $f(\mathbf{r}, \mathbf{p}, t)$, which gives the local concentration of carriers in state $\mathbf{p}$ in the neighbourhood of point $\mathbf{r}$ in space. The dynamics of $f(\mathbf{r}, \mathbf{p}, t)$ under an applied Lorentz force are governed by Newton's laws, and the dissipation is incorporated via a *scattering* or *collision integral*, $I_{\mathbf{r},\mathbf{p},t}[f]$. The Boltzmann equation is a semi-classical theory since $f(\mathbf{r}, \mathbf{p}, t)$ is a classical distribution function in phase space, with well defined $\mathbf{r}$ and $\mathbf{p}$ coordinates, but the scattering integral, as well as the equilibrium function $f^{(0)}(\mathbf{r}, \mathbf{p}, t)$, are obtained from quantum mechanical considerations. The consistency of this approach requires that the distribution function varies little over the de Broglie wave length of the electron. Furthermore, in order that collisions may be treated in a simple way, we require a low carrier density (only binary collisions), that the time between collisions is much greater than the durations of the collisions, and that density gradients are small over the range of the interparticle potential.

The Boltzmann equation posits that the total rate of change of the electronic distribution is given by scattering

$$\frac{d}{dt} f(\mathbf{r}, \mathbf{p}, t) = I_{\mathbf{r},\mathbf{p},t}[f] \tag{2.1}$$

This is made more intuitive by separating the dependencies of $f(\mathbf{r}, \mathbf{p}, t)$ such that, by the chain rule, we can write

$$\frac{\partial}{\partial t} f(\mathbf{r}, \mathbf{p}, t) = -\left.\frac{\partial \mathbf{r}}{\partial t}\right|_{\mathbf{p}} \cdot \nabla_{\mathbf{r}} f(\mathbf{r}, \mathbf{p}, t) - \left.\frac{\partial \mathbf{p}}{\partial t}\right|_{\mathbf{r}} \cdot \nabla_{\mathbf{p}} f(\mathbf{r}, \mathbf{p}, t) + I_{\mathbf{r},\mathbf{p},t}[f]\,. \tag{2.2}$$

We now see that the time-dependence of the distribution function is given by three terms: a diffusive term, a term arising from the applied fields and the collision term. The behaviour of $f(\mathbf{r}, \mathbf{p}, t)$ can thus be pictured in terms of these three contributions acting on a small phase-space volume centred at $\mathbf{r}, \mathbf{p}$.

We will consider only elastic scattering here and restrict ourselves to a single band in a three-dimensional sample. In this case, the scattering

integral can be written as

$$\begin{aligned} I_{\mathbf{r},\mathbf{p},t}[f] &= \int \frac{d^3p'}{(2\pi\hbar)^3} W(\mathbf{p},\mathbf{p}') \\ &\qquad \times \left\{ f(\mathbf{r},\mathbf{p}',t)\left(1-f(\mathbf{r},\mathbf{p},t)\right) - f(\mathbf{r},\mathbf{p},t)\left(1-f(\mathbf{r},\mathbf{p}',t)\right) \right\} \\ &= -\int \frac{d^3p'}{(2\pi\hbar)^3} W(\mathbf{p},\mathbf{p}') \left\{ f(\mathbf{r},\mathbf{p},t) - f(\mathbf{r},\mathbf{p}',t) \right\} \end{aligned} \tag{2.3}$$

Scattering from state $\mathbf{p}$ to $\mathbf{p}'$ decreases $f(\mathbf{r},\mathbf{p},t)$ and the probability of this process is proportional to $f(\mathbf{r},\mathbf{p},t)$ and $1-f(\mathbf{r},\mathbf{p}',t)$, as the final state must be empty. Furthermore, there is a basic transition probability $W(\mathbf{p},\mathbf{p}')$ that we must calculate from a microscopic model of the collision process, typically with Fermi's golden rule. The scattering integral also includes the reverse process of scattering from$\mathbf{p}'$ to $\mathbf{p}$ and from the principle of *microscopic reversibility*, we know that $W(\mathbf{p},\mathbf{p}') = W(\mathbf{p}',\mathbf{p})$, whence the second line above. This integral has the property that

$$\int \frac{d^3p}{(2\pi\hbar)^3} \epsilon_{\mathbf{p}} I_{\mathbf{r},\mathbf{p},t}[f] = 0, \tag{2.4}$$

illustrating energy-conserving nature of the scattering.

We now write Eq. (2.2) in more familiar terms. We first identify $\partial\mathbf{r}/\partial t|_{\mathbf{p}}$ as $\mathbf{v}_{\mathbf{p}}$, the velocity of an electron in state $\mathbf{p}$. Then, from Hamilton's equations of motion with Hamiltonian $\mathcal{H}$, we have

$$\left.\frac{\partial \mathbf{p}}{\partial t}\right|_{\mathbf{r}} = -\frac{\partial \mathcal{H}}{\partial \mathbf{r}}, \tag{2.5}$$

which is nothing other than the force acting on the electron. With this force arising from applied electric and magnetic fields, we have

$$\left.\frac{\partial \mathbf{p}}{\partial t}\right|_{\mathbf{r}} = e\left(\mathbf{E} + \mathbf{v}_{\mathbf{p}} \times \mathbf{B}\right). \tag{2.6}$$

Putting this altogether, we obtain

$$\boxed{\frac{\partial}{\partial t} f(\mathbf{r},\mathbf{p},t) + \mathbf{v}_{\mathbf{p}} \cdot \nabla_{\mathbf{r}} f(\mathbf{r},\mathbf{p},t) + e\left(\mathbf{E} + \mathbf{v}_{\mathbf{p}} \times \mathbf{B}\right) \cdot \nabla_{\mathbf{p}} f(\mathbf{r},\mathbf{p},t) = I_{\mathbf{r},\mathbf{p},t}[f]} \tag{2.7}$$

This is the Boltzmann equation. It is an integro-differential equation and in general very difficult to solve.

Normally we are interested in the steady state, $\partial f(\mathbf{r},\mathbf{p},t)/\partial t = 0$. Furthermore, it is usually sufficient to treat the applied electric field as inducing only a small perturbation in the electron distribution, such that we can work to first order in the field — or in other words, calculate the linear response of the system to an applied electric field. We therefore assume that the distribution function can be written as

$$f(\mathbf{r},\mathbf{p}) = f^{(0)}(\mathbf{r},\mathbf{p}) + f^{(1)}(\mathbf{r},\mathbf{p}), \tag{2.8}$$

where $f^{(0)}$ is equilibrium distribution and $f^{(1)}$ is response term of order $\mathbf{E}$. For the equilibrium distribution, we take the Fermi-Dirac distribution

$$f^{(0)}(\mathbf{r},\mathbf{p}) = \frac{1}{\exp\left((\epsilon_{\mathbf{p}} - \mu)/k_B T\right) + 1} \tag{2.9}$$

with chemical potential μ, temperature T and Boltzmann's constant k_B. We allow both μ and T to be functions of $\mathbf{r}$ (we should therefore, speak of quasi-chemical potential). Inserting these forms into Eq. (2.7) and linearising, we obtain

$$\begin{aligned}\left(-\frac{\partial f^{(0)}(\mathbf{r},\mathbf{p})}{\partial \epsilon_p}\right)\mathbf{v}_{\mathbf{p}} \cdot \left\{-\frac{\epsilon-\mu}{T}\nabla T + e\left(\mathbf{E} - \frac{1}{e}\nabla\mu\right)\right\} \\ = -I_{\mathbf{r},\mathbf{p}}[f] + \mathbf{v}_{\mathbf{p}} \cdot \nabla_{\mathbf{r}} f^{(1)}(\mathbf{r},\mathbf{p}) + e\left(\mathbf{v}_{\mathbf{p}} \times \mathbf{B}\right) \cdot \nabla_{\mathbf{p}} f^{(1)}(\mathbf{r},\mathbf{p})\end{aligned} \tag{2.10}$$

which is the linearised steady-state Boltzmann equation.

One typically is interested in a homogeneous sample, in which there are no T or μ gradients, and the distribution function is a function of $\mathbf{p}$ only. In this case, we have

$$\boxed{-e\left(\frac{\partial f^{(0)}(\mathbf{p})}{\partial \epsilon_p}\right)\mathbf{v}_{\mathbf{p}} \cdot \mathbf{E} = -I_{\mathbf{p}}[f] + e\left(\mathbf{v}_{\mathbf{p}} \times \mathbf{B}\right) \cdot \nabla_{\mathbf{p}} f^{(1)}(\mathbf{p}).} \tag{2.11}$$

2.3 Electrical conductivity

Equation (2.11) allows us to derive the conductivity of the sample as determined by impurity scattering. In zero magnetic field, we have

$$e\left(\frac{\partial f^{(0)}(\mathbf{p})}{\partial \epsilon_{\mathbf{p}}}\right)\mathbf{v}_{\mathbf{p}} \cdot \mathbf{E} = I_{\mathbf{p}}[f] \tag{2.12}$$

We assume the scattering to be elastic and that the impurity potential is spherically symmetric. This means that

$$W\left(\mathbf{p},\mathbf{p}'\right) = W\left(\hat{\mathbf{p}}\cdot\hat{\mathbf{p}}',\epsilon_{\mathbf{p}}\right)\delta\left(\epsilon_{\mathbf{p}}-\epsilon_{\mathbf{p}'}\right), \tag{2.13}$$

where $\hat{\mathbf{p}}$ is a unit vector in the direction of $\mathbf{p}$. One way of making further progress (see Jammer, Ch 5.4) is to expand W in terms of Legendre polynomials, $\mathbb{P}_l$:

$$W\left(\hat{\mathbf{p}}\cdot\hat{\mathbf{p}}',\epsilon_{\mathbf{p}}\right) = \sum_{l=0} W_l(\epsilon_{\mathbf{p}})\mathbb{P}_l(\hat{\mathbf{p}}\cdot\hat{\mathbf{p}}'). \tag{2.14}$$

Making an analogous expansion for the distribution function,

$$f^{(1)}(\mathbf{p}) = \sum_{l=1} f_l^{(1)}(\epsilon_{\mathbf{p}})\mathbb{P}_l(\hat{\mathbf{p}}\cdot\hat{\mathbf{E}}), \tag{2.15}$$

the collision integral becomes

$$I_{\mathbf{p}}[f] = -\mathcal{D}(\epsilon_{\mathbf{p}})\sum_{l=0} f_l^{(1)}(\epsilon_{\mathbf{p}})\mathbb{P}_l(\hat{\mathbf{p}}\cdot\hat{\mathbf{E}})\left\{W_0(\epsilon_{\mathbf{p}}) - \frac{1}{2l+1}W_l(\epsilon_{\mathbf{p}})\right\}, \tag{2.16}$$

where $\mathcal{D}(\epsilon)$ is the density of electronic states at energy ϵ. Substituting these results into linearised Boltzmann equation Eq. (2.12), we obtain the solution

$$\begin{aligned} f_l^{(1)}(\epsilon_{\mathbf{p}}) &= 0;\ \forall l \neq 1 \\ f_1^{(1)}(\epsilon_{\mathbf{p}}) &= \left\{\frac{1}{3}W_1(\epsilon_{\mathbf{p}}) - W_0(\epsilon_{\mathbf{p}})\right\}^{-1}\frac{eEv_{\mathbf{p}}}{\mathcal{D}(\epsilon_{\mathbf{p}})}\frac{\partial f^{(0)}(\epsilon_{\mathbf{p}})}{\partial\epsilon_{\mathbf{p}}}. \end{aligned} \tag{2.17}$$

This result may be written as

$$f^{(1)}(\epsilon_{\mathbf{p}}) = -e\mathbf{E}\cdot\mathbf{v}_p\tau_{\mathrm{tr}}(\epsilon_{\mathbf{p}})\frac{\partial f^{(0)}(\epsilon_{\mathbf{p}})}{\partial\epsilon_{\mathbf{p}}} \tag{2.18}$$

with the *transport relaxation time*

$$\begin{aligned} \tau_{\mathrm{tr}}^{-1}(\epsilon_{\mathbf{p}}) &= \mathcal{D}(\epsilon_{\mathbf{p}})\left\{W_0(\epsilon_{\mathbf{p}}) - \frac{1}{3}W_1(\epsilon_{\mathbf{p}})\right\} \\ &= \mathcal{D}(\epsilon_p)\int\frac{d\hat{\mathbf{p}}'}{4\pi}W\left(\hat{\mathbf{p}}\cdot\hat{\mathbf{p}}',\epsilon_{\mathbf{p}}\right)\left(1-\hat{\mathbf{p}}\cdot\hat{\mathbf{p}}'\right) \end{aligned} \tag{2.19}$$

The factor $(1-\hat{\mathbf{p}}\cdot\hat{\mathbf{p}}')$ can be expressed as $(1-\cos\theta)$ where θ is the angle between the two vectors. It weights the contributions of scattered vectors.

If $\mathbf{p}'$ is parallel to $\mathbf{p}$ then $\theta = 0$ and this weighting factor is zero — elastic forward scattering does not, obviously, relax the electron momentum. Conversely, with $\mathbf{p}'$ anti-parallel to $\mathbf{p}$, this weighting factor is maximal, and correspondingly, backscattering is seen to be the most effective.

Let us write

$$f(\mathbf{p}) = f^{(0)}(\epsilon_{\mathbf{p}}) + \mathbf{p} \cdot \mathbf{g}(\epsilon_{\mathbf{p}}), \tag{2.20}$$

with

$$\mathbf{g}(\epsilon_{\mathbf{p}}) = -e\mathbf{E}\frac{\tau_{\rm tr}(\epsilon_{\mathbf{p}})}{m}\frac{\partial f^{(0)}(\epsilon_{\mathbf{p}})}{\partial \epsilon_p}. \tag{2.21}$$

Then $f^{(1)}(\mathbf{p}) = \mathbf{p} \cdot \mathbf{g}(\epsilon_{\mathbf{p}})$ and the collision integral becomes

$$I_{\mathbf{p}}[f] = I_{\mathbf{p}}[f_0 + \mathbf{p} \cdot \mathbf{g}] = -\frac{\mathbf{p} \cdot \mathbf{g}(\epsilon_{\mathbf{p}})}{\tau_{\rm tr}(\epsilon_{\mathbf{p}})} = -\frac{f(\epsilon_{\mathbf{p}}) - f^{(0)}(\epsilon_{\mathbf{p}})}{\tau_{\rm tr}(\epsilon_{\mathbf{p}})}. \tag{2.22}$$

From this we can see the significance of the relaxation time. Consider Eq. (2.1); let system reach steady-state and then switch off all fields. We have

$$\frac{\partial}{\partial t} f(\epsilon_{\mathbf{p}}, t) = -\frac{f(\epsilon_{\mathbf{p}}, t) - f^{(0)}(\epsilon_{\mathbf{p}})}{\tau_{\rm tr}(\epsilon_{\mathbf{p}})} \tag{2.23}$$

which we solve to give

$$f(\epsilon_{\mathbf{p}}, t) = f^{(0)}(\epsilon_{\mathbf{p}}) + f^{(1)}(\epsilon_{\mathbf{p}}) e^{-t/\tau_{\rm tr}(\epsilon_{\mathbf{p}})}, \tag{2.24}$$

showing that, starting from the transport steady-state, the $\mathbf{p}$th-component of the distribution relaxes back to its equilibrium distribution with a time constant $\tau_{\rm tr}(\epsilon_{\mathbf{p}})$.

Now we are in possesion of the steady-state distribution, we can simply calculate the stationary current density:

$$\mathbf{j} = \frac{2e}{m}\int \frac{d^3p}{(2\pi\hbar)^3}\mathbf{p} f(\mathbf{p}) \tag{2.25}$$

$$= \frac{4e^2}{3m}\int d\epsilon \mathcal{D}(\epsilon)\epsilon\tau_{\rm tr}(\epsilon)\left(-\frac{\partial f^{(0)}(\epsilon)}{\partial \epsilon}\right)\mathbf{E}. \tag{2.26}$$

The derivative of the Fermi function is peaked at the Fermi surface with a width $\sim k_B T$ Since the rest of the integral is slowly varying over this scale,

we can can approximate $\left(-\partial f^{(0)}/\partial\epsilon\right) \sim \delta(\epsilon - \epsilon_F)$ and take the remaining quantities in the integral to be evaluated at the Fermi energy ϵ_F. With help of the 3D density of states, $\mathcal{D}(\epsilon) = \sqrt{2m^3\epsilon_F}/(2\pi^2\hbar^3)$, Fermi energy $\epsilon_F = \hbar^2 k_F^2/(2m)$, and Fermi wavenumber $k_F = (3\pi^2 n)^{1/3}$, the current density can be evaluated as

$$\mathbf{j} \;=\; \frac{e^2 n \tau_{\rm tr}(\epsilon_F)}{m}\mathbf{E} \tag{2.27}$$

The relationship between the components of the current density and the electric field can be written as

$$j_\alpha = \sum_\beta \sigma_{\alpha\beta} E_\beta \tag{2.28}$$

where $\boldsymbol{\sigma}$ is the conductivity tensor. For the isotropic model that we are discussing here, the tensor is diagonal

$$\sigma_{\alpha\beta} = \sigma_0 \delta_{\alpha,\beta} \tag{2.29}$$

with

$$\sigma_0 = \frac{n e^2 \tau_{\rm tr}(\epsilon_F)}{m}, \tag{2.30}$$

which is Drude's result. From this, we obtain Ohm's law

$$R = \frac{m}{n e^2 \tau_{\rm tr}(\epsilon_F) L}. \tag{2.31}$$

It is customary to express the conductivity as

$$\sigma = n|e|\mu, \tag{2.32}$$

in terms of the carrier *mobility*

$$\mu = \frac{|e|\tau_{\mathbf{tr}}}{m}. \tag{2.33}$$

Entertainingly, this same result for the conductivity can be obtained from three very different theoretical analyses — semiclassically as above, within the classical considerations of the Drude model, and also in the full quantum-mechanical calculation via the Kubo formula.

2.4 The Hall effect

We now want to understand transport in the presence of both electric and magnetic fields. Let us start with Eq. (2.11) with the assumption of a relaxation time

$$e\left(\frac{\partial f_p^{(0)}}{\partial \epsilon_p}\right)\mathbf{v_p}\cdot\mathbf{E}+e\left(\mathbf{v_p}\times\mathbf{B}\right)\cdot\nabla_{\mathbf{p}}\left(\mathbf{p}\cdot\mathbf{g}(\epsilon_{\mathbf{p}})\right)=-\frac{\mathbf{p}\cdot\mathbf{g}(\epsilon_{\mathbf{p}})}{\tau_{\rm tr}(\epsilon_{\mathbf{p}})} \tag{2.34}$$

Omitting the details (see, e.g. Rammer Ch 5.4.2, Ziman Ch 7.12), this equation can be solved for the linear response function $\mathbf{g}$. We obtain

$$\begin{aligned}\mathbf{g}(\epsilon_{\mathbf{p}}) &= -\frac{e\tau_{\rm tr}(\epsilon_{\mathbf{p}})}{m}\frac{\partial f^{(0)}(\epsilon_{\mathbf{p}})}{\partial\epsilon_{\mathbf{p}}}\frac{1}{1+\left(\omega_c\tau_{\rm tr}(\epsilon_{\mathbf{p}})\right)^2}\\ &\quad\times\left[\mathbf{E}+\left(\omega_c\tau_{\rm tr}(\epsilon_{\mathbf{p}})\right)^2\mathbf{E}_{\parallel}+\frac{e\tau_{\rm tr}(\epsilon_{\mathbf{p}})}{m}\mathbf{E}\times\mathbf{B}\right],\end{aligned} \tag{2.35}$$

where $\mathbf{E}_{\parallel}$ is the electric field parallel to $\mathbf{B}$ and $\omega_c = |e|B/m$ is the cyclotron frequency. From this result and the expression for the current density Eq. (2.25), we obtain the conductivity tensor for $\mathbf{B} = B\hat{\mathbf{z}}$ as

$$\boldsymbol{\sigma}=\frac{\sigma_0}{1+\left(\omega_c\tau_{\rm tr}\right)^2}\begin{pmatrix}1 & -\omega_c\tau_{\rm tr} & 0\\ \omega_c\tau_{\rm tr} & 1 & 0\\ 0 & 0 & 1+\left(\omega_c\tau_{\rm tr}\right)^2\end{pmatrix} \tag{2.36}$$

This conductivity obeys the Onsager relations

$$\sigma_{\alpha\beta}(\mathbf{B})=\sigma_{\beta\alpha}(-\mathbf{B}) \tag{2.37}$$

which stem from fundamental considerations about the behaviour of systems under time-reversal. Inverting Eq. (2.36), we get the resistivity tensor

$$\boldsymbol{\rho}=\boldsymbol{\sigma}^{-1}=\rho_0\begin{pmatrix}1 & \omega_c\tau_{\rm tr} & 0\\ -\omega_c\tau_{\rm tr} & 1 & 0\\ 0 & 0 & 1\end{pmatrix} \tag{2.38}$$

with $\rho_0 = \sigma_0^{-1}$. An isotropic sample, therefore, shows no magnetoresistance, i.e. ρ_{xx} does not depend on magnetic field for an isotropic dispersion $\epsilon_{\mathbf{p}} = \epsilon(|\mathbf{p}|)$.

In a Hall bar experiment, a current flowing the x direction, say, gets deflected by the magnetic field in the z direction, say, leading to a voltage

appearing in the y-direction. This voltage is known as the Hall voltage and is determined by state state condition conditions, $j_y = 0$, such that

$$\frac{E_y}{E_x} = -\frac{\sigma_{yx}}{\sigma_{yy}}. \tag{2.39}$$

The Hall coefficient is then

$$R_{\mathrm{H}} \equiv \frac{E_y}{B j_x} = \frac{1}{ne}, \tag{2.40}$$

and the Hall voltage is

$$V_{\mathrm{H}} \equiv E_y L_y = L_y B j_x \frac{1}{ne}. \tag{2.41}$$

A hall bar experiment therefore probes both sign and density of charge carriers.

2.5 Thermal Conductivity

The Boltzmann equation, Eq. (2.7), can also be used to investigate the behaviour of conduction electrons under the influence of a thermal gradient. Omitting the details here (Rammer Ch5.4.3 or Ziman Ch7.8), we note that linearising Eq. (2.7) in terms of both the applied electric field and the thermal gradient applied across the sample, we can derive a relationship between electrical (σ) and thermal (κ) conductivities:

$$\kappa = \frac{\pi^2}{3} k_B^2 T \frac{\sigma_0}{e^2}. \tag{2.42}$$

This is known as the *Wiedemann-Franz law* and holds quite generally providing that we only have elastic scattering. This result can be easily understood: In electrical conduction each electron carries a charge e and is acted on by the field $e\mathbf{E}$. The current per unit field is therefore proportional to e^2. In thermal conduction, each electron carries an energy $k_B T$, and is acted on by a thermal force $k_B \nabla T$. The heat current per unit thermal gradient is then $k_B^2 T$. The ratio of the two transport coefficients must be there be proportional to $k_B^2 T/e^2$ and the numerical factor arises because we are only considering electrons near the Fermi surface.

2.6 Other scattering mechanisms

At low temperatures, elastic scatting from impurities is the dominant form of electron scattering. However, there are many other scattering mechanisms that can play an important role in transport. For example, surface roughness leads to additional elastic scattering, whereas interactions with lattice vibrations (both acoustic and optical phonons) gives rise to inelastic scattering. To some extent, all these mechanisms can be incorporated in a relaxation time approach as described in Ferry and Goodnick, Section 2.7.

Chapter 3

Quantum confinement

3.1 Two-dimensional electron gas and lateral quantum dots

Many important developments in mesoscopic transport have taken place in the two-dimensional electron gas (2DEG), and are likely to continue to do so in the future. The 2DEG typically used in transport experiments is formed at the interface in an AlGaAs-GaAs semiconductor heterojunction, as described in Fig. 3.1. The AlGaAs is doped with Si donors using a process known as modulation doping, which allows the donors to be situated a small distance from the interface (spacer layer width $\sim$ 5nm) . This has the important consequence that the 2DEG is physically separated from the the donor ions, which minimises the scattering from these ions and facilitates the very high mobilities obtainable in the 2DEG. Table 3.1 gives some typical mobilities for comparison.

Quantum dots (and other more exotic structures) can be created in a

material	temperature	μ (cm^d/(Vs))
organic semiconductor	room	$< 10^1$
Si	room	10^2-10^3
C-nanotube	room	10^5
graphene	low	10^5
2DEG	low	10^5-10^7

Table 3.1: Some example electron mobilities. Here, a "low" temperature means $\sim$ 20mK, a temperature typical of mesoscopic experiments.

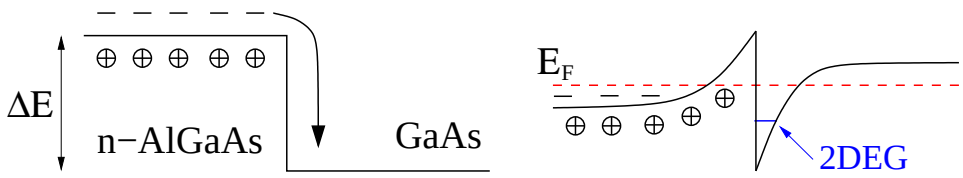

Figure 3.1: Formation of a 2DEG in AlGaAs–GaAs heterojunction. Left picture shows the conduction band just after the two materials are brought into contact with one another (or so we imagine). AlGaAs has a wider gap than GaAs and the conduction band edges are offset by an amount ΔE. Electrons from the donors in the n-doped AlGaAs move across junction to lower energy states in GaAs, leaving charged donor ions behind. The combination of the band edge offset with the potential due to donor ions produces the band edge in the right-hand sketch — a narrow triangular well is formed at the interface and it is here that the 2DEG is located.

2DEG through the use of top gates — metal electrodes deposited on the semiconductor surface. Application of a negative voltage to these gates deforms the electrostatic potential at the 2DEG, and can deplete the electron gas underneath the gate. These depleted zones can be used to define QDs. Figure 3.2 shows samples with single and double QDs. Lateral QD size ranges from $\sim \mu$m at the large end, down to 10s of nm — small enough to contain just a few (0,1,2,...) electrons.

Example numbers from Hanson, et al., Rev. Mod. Phys. **79**, 1217 (2007); cond-mat/0610433: The 2DEG is situated 50-100nm below surface, and has a width of 10nm. Electron mobility and density: 10^5-10^7 cm^2/(Vs) and (1-5)$\times 10^{15}$m^{-2} respectively. Fermi wavelength of the electrons: 40nm. Temperature: $\sim$ 20mK.

3.2 Single-particle, single-band effective mass approximation

Before discussing the effects of confinement, we should make explicit the approximations with in which we shall work. Although transport in semiconductors can be mediated by both electron and hole flow, in mesoscopic experiments it is usually just the electrons that are involved. Mesoscopic samples are usually *degenerate*, which means that the conduction band is highly populated with electrons. Furthermore, transport energy scales are

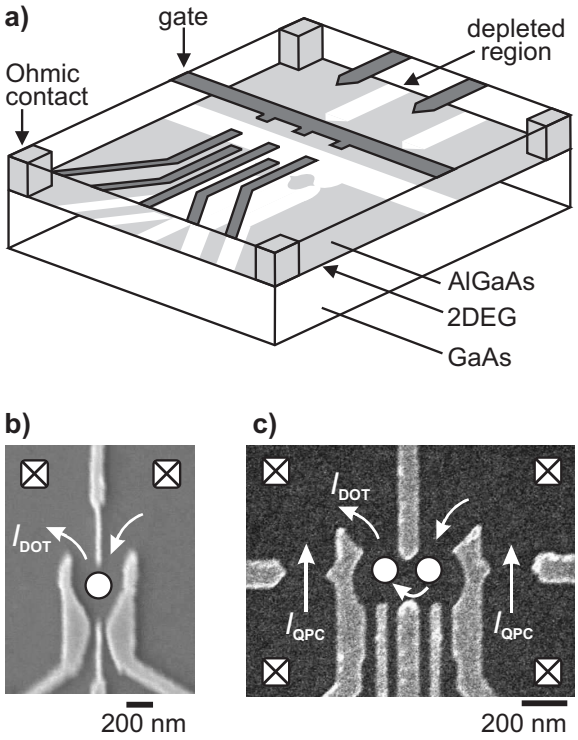

Figure 3.2: Definition of lateral quantum dots in a 2DEG with top gates. From Hanson, et al., Rev. Mod. Phys. **79**, 1217 (2007); cond-mat/0610433

low cf. the band gap and therefore inter-band transitions are avoided. Thus we need only consider only a single band — the conduction band (CB) — and the electrons that reside in it.

We describe an electron moving in the CB with the *effective mass equation*:

$$\left[E_c + \frac{1}{2m^*}\left(i\hbar\boldsymbol{\nabla} + e\mathbf{A}\right)^2 + U(\mathbf{r})\right]\Psi(\mathbf{r}) = E\Psi(\mathbf{r}) \tag{3.1}$$

Here m^* is the effective mass, $\mathbf{A}$ is the vector potential, and E_c is the bottom of the CB. The function $\Psi(\mathbf{r})$ is the smooth envelope of the electrons wavefunction, with the effects of the lattice potential having been incorporated in the effective mass, which we assume isotropic and homogeneous. The potential $U(\mathbf{r})$ describes then the large-scale confinement potential experienced by the electron.

We consider the electrons to be non-interacting. Strict justification of this comes from the Landau theory, in which an interacting electron gas is re-described in terms of non-interacting *quasi-particles* with renormalised energy (as compared to original particles) and a finite lifetime. Providing this lifetime is long compared to any experimentally relevant processes, the quasi-particle picture is a valid one, and this is generally the case in semiconductors. We may also appeal to *a posteriori* justification, as we will see that this simple treatment is sufficient to describe a wide range of interesting mesoscopic transport experiments.

3.3 Effects of confinement

In the triangular quantum well of Fig. 3.1, confinement in one spatial dimension is much stronger than in the other two. With z singled out as the strongly confined dimension, we may therefore approximate the confinement potential as $U(\mathbf{r}) = U(z)U(x,y)$. With magnetic field in the z direction, i.e. perpendicular to the plane of the interface, the effective mass Schrödinger Equation, Eq. (3.1), admits the separable solution $\Psi(\mathbf{r}) = \phi_n(z)\psi(x,y)$, with $\phi_n(z)$ the nth quantised solution of the one-dimensional problem in the z direction. Index $n = 1, 2, \ldots$ defines a set of *sub-bands*; if we consider the electrons to be unconfined in the plane of the interface, then the full eigenfunctions of Eq. (3.1) with $U(\mathbf{r}) = U(z)$ are

$$\Psi(\mathbf{r}) = \phi_n(z)e^{ik_x x}e^{ik_y y} \tag{3.2}$$

with dispersion

$$E(n,k) = E_c + \epsilon_n + \frac{\hbar^2}{2m^*}\left(k_x^2 + k_y^2\right) \tag{3.3}$$

with ϵ_n, the eigen-energies from z-confinement.

The density of states (per unit energy, per unit surface area) of such a quasi-infinite two-dimensional system is

$$\mathcal{D}(E) = \sum_n \frac{m^*}{\pi\hbar^2}\theta\left(E - \epsilon_n - E_c\right) = \sum_n \mathcal{D}_0\theta\left(E - \epsilon_n - E_c\right), \tag{3.4}$$

with $\theta(E)$ the unit step function and where a factor 2 for spin has been included. Within the nth subband then, the density of states is constant, with value $n\mathcal{D}_0$. For GaAs, with effective mass $m^* = 0.07m_e$, $\mathcal{D}_0 = 2.9 \times 10^{10}/(\text{cm.meV})$.

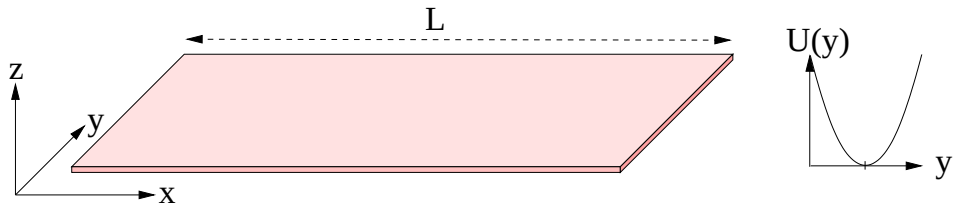

Figure 3.3: Sketch of a 2DEG, establishing co-ordinate system. Strong confinement is in the z direction, and much weaker parabolic confinement in the y direction. The extent of the sample in the x-direction is large cf. extent in y and z directions.

Confinement in the z direction is strong enough that experiments are usually restricted to the lowest $n = 1$ sub-band. In both 2DEGs and SAQD the z-confinement is ~ 10 times that in the x-y plane. Thus, sub-bands $n \geq 2$ play no significant role and we can neglect the z direction altogether — reducing the original 3D problem to a two-dimensional one with effective 2D Schrödinger equation

$$\left[E_s + \frac{1}{2m^*}\left(i\hbar\boldsymbol{\nabla} + e\mathbf{A}\right)^2 + U(x,y)\right]\psi(x,y) = E\psi(x,y) \tag{3.5}$$

with $E_s = E_c + \epsilon_1$, and 2D vector operators.

3.4 Transverse modes in 2DEG

Consider a uniform 2D conductor, much longer than it is wide (Fig. 3.3). We will consider transport parallel to the long axis of the conductor (x direction), assuming that the motion is essentially unconfined in this direction. In the transverse (y) direction, we model the confinement with a harmonic potential, such that we write

$$U(x,y) = U(y) = \frac{1}{2}m^*\omega_0^2 y^2, \tag{3.6}$$

with ω_0 the *confinement energy* in the y direction. Harmonic confinement is a convenient mathematical form as it leads to analytical solutions. It also provides a reasonable approximations to confinements found in experiment.

We consider an applied magnetic field perpendicular to the 2DEG (in the z direction), and choose a gauge such that the vector potential is written

$$\mathbf{A} = -\hat{\boldsymbol{e}}_x By; \qquad A_x = -By; \qquad A_y = 0. \tag{3.7}$$

The 2D Schrödinger equation, Eq. (3.5), can then be written

$$\left[E_s + \frac{1}{2m^*}\left(p_x + eBy\right)^2 + \frac{1}{2m^*}p_y^2 + U(y)\right]\psi(x,y) = E\psi(x,y), \tag{3.8}$$

with $p_x = -i\hbar\partial/\partial x$ and $p_y = -i\hbar\partial/\partial y$. This has solution

$$\psi(x,y) = \frac{1}{\sqrt{L}}e^{ikx}\chi(y) \tag{3.9}$$

with plane wave in x direction (normalised to length L) and the transverse function $\chi(y)$ given by the solution of the 1D problem

$$\left[E_s + \frac{1}{2m^*}p_y^2 + \frac{1}{2m^*}\left(\hbar k + eBy\right)^2 + \frac{1}{2}m^*\omega_0^2 y^2\right]\chi(y) = E\chi(y). \tag{3.10}$$

Let us define the cyclotron frequency

$$\omega_c = \frac{|eB|}{m^*}, \tag{3.11}$$

and the length

$$y_k = \frac{\hbar k}{eB}. \tag{3.12}$$

We have then

$$\left[E_s + \frac{1}{2m^*}p_y^2 + \frac{1}{2}m^*\omega_c^2\left(y + y_k\right)^2 + \frac{1}{2}m^*\omega_0^2 y^2\right]\chi(y) = E\chi(y). \tag{3.13}$$

Completing the square, we have

$$\left[E_s + \frac{m^*}{2}\frac{\omega_0^2\omega_c^2}{\widetilde{\omega}^2}y_k^2 + \frac{1}{2m^*}p_y^2 + \frac{1}{2}m^*\widetilde{\omega}^2\left(y + \frac{\omega_c^2}{\widetilde{\omega}^2}y_k\right)^2\right]\chi(y) = E\chi(y), \tag{3.14}$$

with

$$\widetilde{\omega}^2 = \omega_c^2 + \omega_0^2 \tag{3.15}$$

This, then, has the form of a displaced Harmonic oscillator, and from elementary quantum mechanics, we have the solutions

$$\chi_{n,k}(y) = u_n\left(q + \frac{\omega_c^2}{\widetilde{\omega}^2}q_k\right), \tag{3.16}$$

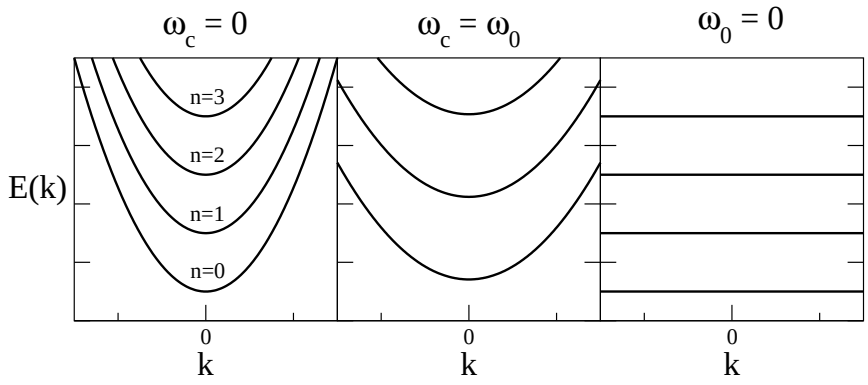

Figure 3.4: Dispersion relation for a 2DEG with transverse harmonic confinement and perpendicular magnetic field. The three plots are for different choices of ω_0 and ω_c, the confinement and cyclotron frequencies, respectively.

with $u_n(x)$ the usual simple-harmonic oscillator eigenfunctions written in terms of the dimensionless displacements $q = y/\widetilde{l}$ and $q_k = y_k/\widetilde{l}$ with length

$$\widetilde{l} = \sqrt{\frac{\hbar}{m^*\widetilde{\omega}}}. \tag{3.17}$$

The corresponding dispersion relation is

$$\begin{aligned} E &= E_s + \frac{m^*}{2}\frac{\omega_0^2\omega_c^2}{\widetilde{\omega}^2}y_k^2 + \left(n+\frac{1}{2}\right)\hbar\widetilde{\omega} \\ &= E_s + \left(n+\frac{1}{2}\right)\hbar\widetilde{\omega} + \frac{\hbar^2k^2}{2m^*}\frac{\omega_0^2}{\widetilde{\omega}^2}, \end{aligned} \tag{3.18}$$

with $n = 0, 1, 2, \ldots$. This result is illustrated in Fig. 3.4

The first thing to notice is that due to the confinement in the y-direction, we obtain a series of sub-bands, labelled with quantum number n. In contrast to the z-direction, however, here the confining potential is relatively weak, and more than just the lowest of sub-band will play a role in transport. In analogy with optical wave guides, these sub bands are known as *transverse modes* and they play a crucial role in determining the transport properties of low-dimensional conductors. We also note that the dispersion of a given transverse mode is of plane-wave form (i.e. quadratic) but with a renormalised mass $m^* \to m^*\left(1+\omega_c^2/\omega_0^2\right)$ — increasing the magnetic field

increases this renormalised mass of the electrons and makes the dispersion relation flatter. Figure 3.4 highlights two limiting cases:

- **Zero field:** For $B \to 0$, we have $\omega_c \to 0$ and $\widetilde{\omega} \to \omega_0$ such that

$$E = E_s + \left(n + \frac{1}{2}\right)\hbar\omega_0 + \frac{\hbar^2 k^2}{2m^*}, \tag{3.19}$$

  as expected.

- **Zero confinement** For $\omega_0 \to 0$, we have $\widetilde{\omega} \to \omega_c$ and

$$E = E_s + \left(n + \frac{1}{2}\right)\hbar\omega_c, \tag{3.20}$$

  in which case, quantum number n therefore the familiar Landau levels with quantisation energy given by the cyclotron frequency. NB: there is no dispersion in this limit.

3.5 Quantum dots: Fock-Darwin Spectrum

A useful model for the electronic confinement of a quantum dot is the two-dimensional, symmetric parabolic potential

$$U(x, y) = \frac{m^*}{2}\omega_0^2\left(x^2 + y^2\right). \tag{3.21}$$

The corresponding Hamiltonian of an electron in the dot is

$$H = \frac{1}{2m^*}\left(\mathbf{p} + e\mathbf{A}\right)^2 + \frac{m^*}{2}\omega_0^2\left(x^2 + y^2\right). \tag{3.22}$$

By using the symmetric gauge for the vector potential $\mathbf{A} = (-By/2, Bx/2, 0)$ it can be shown (homework!) that the energy spectrum the dot is given by

$$E_{n_+,n_-} = (n_+ + 1)\,\hbar\Omega + \frac{1}{2}\hbar\omega_c n_-, \tag{3.23}$$

with

$$\Omega^2 = \omega_0^2 + \frac{\omega_c^2}{4}, \tag{3.24}$$

and quantum numbers

$$n_\pm = n_x \pm n_y; \quad \text{for} \quad n_x, n_y = 0, 1, 2, \ldots. \tag{3.25}$$

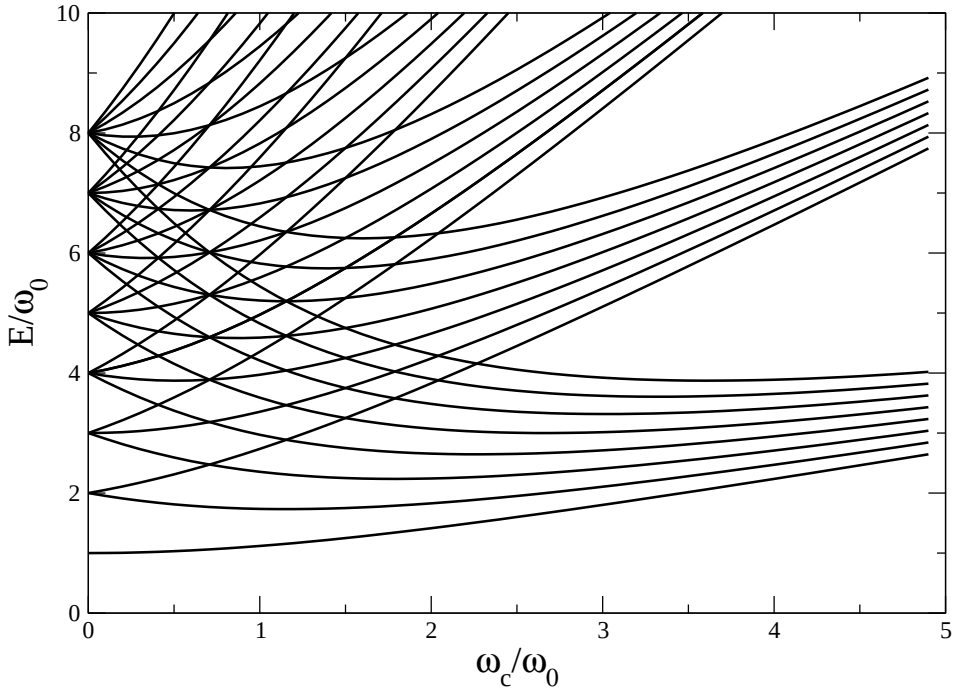

Figure 3.5: Fock-Darwin spectrum of symmetric quantum dot up to quantum number $n = 7$.

This result is known as the Fock-Darwin spectrum after the physicists who initially discussed the problem in the 1930s (nothing to do with quantum dots). This spectrum is plotted in Fig. 3.5. For $B = 0$ we have the regularly-spaced spectrum of a two-dimensional symmetric harmonic oscillator. In the high-field limit, the spectrum goes over into that of the Landau levels with the effects of the dot confinement playing an ever decreasing role.

Chapter 4

Scattering theory

4.1 Resistance of a ballistic conductor

Consider a small conductor (length L, cross section A) connected to two contacts which, by necessity, are large compared with the sample. Ohm's law states that the conductance of the sample will be $G = \sigma A/L$, where the conductivity σ is a size-independent material property. If Ohm's law were to hold as we decreased the length of the sample, we would therefore expect the conductance to diverge as L^{-1}. This is consistent with the Drude picture, in which the resistance arises from electron scattering within the sample; if the sample length is much shorter than the mean-free path l_m, the electrons are not scattered at all, whence an infinite conductance.

A conductor with $L \ll l_m$ is said to be ballistic and experimentally, an infinite conductance is not what is observed. Rather, as L is decreased, the resistance saturates to a finite value G_c^{-1}, the contact resistance. As the name suggests, the contact conductance arises from the contact of the mesoscopic sample and the outside world. Essentially, electronic motion within the mesoscopic conductor is quantum confined (as discussed in the previous chapter) such that, for a given voltage bias, only a finite many transverse modes are supported in the sample. Each channel can only carry a finite current and thus the conductance of the sample saturates. The resistance occurs naturally as a consequence of trying to drive a current from the large electron reservoirs of the contacts into and through a very narrow constriction.

In this chapter we learn how to calculate this conductance not just for ballistic conductors but more generally, using the *scattering* or *Landauer-Büttiker* formalism. We follow here the treatment in the review by Blanter

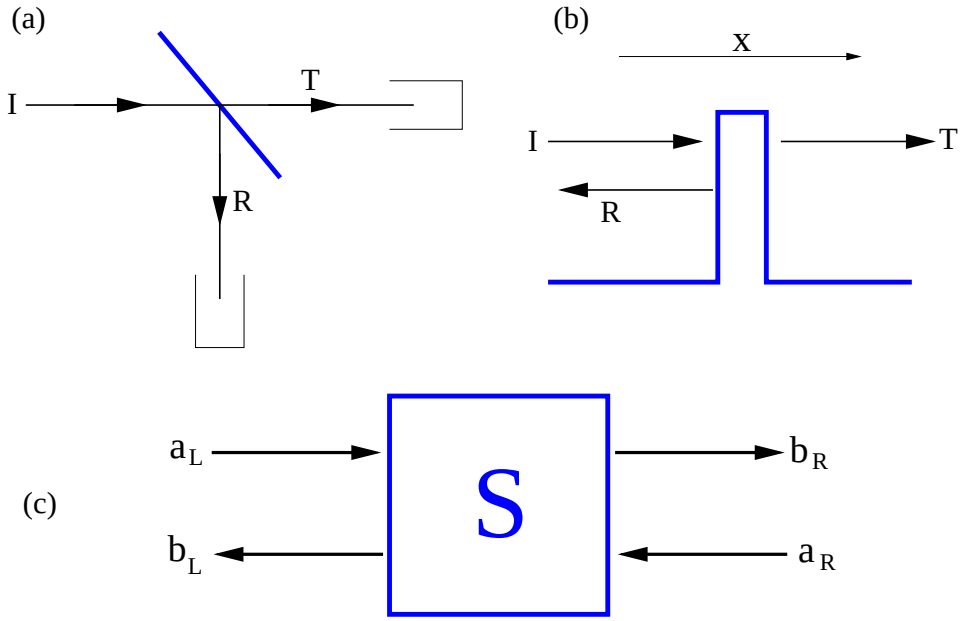

Figure 4.1: Scattering. (a) Incident photons (I) are scattered at a beam-splitter into transmitted (T) and reflected (R) components. (b) Similarly scattered are electrons incident on a potential barrier. (c) In general, particles can impinge on a scatterer from both the left and right. Incoming amplitudes (or mode annihilation operators in the second quantised version), a_L, a_R are related to the outgoing modes b_L, b_R through scattering matrix $\mathbf{S}$.

and Büttiker.

4.2 Electron scattering

In this chapter we will consider devices that are smaller that the phase-relaxation length $L < l_\phi$, such that transport through the device is *phase coherent*. This is important as it means we can consider electronic wave-functions coherent across the whole device, along the lines of those discussed in Chapter 3.

The Landau er Büttiker approach treats the mesoscopic sample simply as a scatterer of electron waves. This makes a rather direct analogy between the phase coherent transport of electrons through a mesoscopic device and

the scattering of photons in optics by a beamsplitter, for example. Fig. 4.1a shows an incident light beam (labelled I) impinging on an optical beam splitter. A component of the incident beam is transmitted (T), and a component is reflected (R). A similar situation occurs in Fig. 4.1b, where an electron beam is partitioned into reflected and transmitted components as it impinges on a finite potential barrier.

This idea of an incoming particle being scattered into reflected and transmitted components is fruitfully described by the *scattering matrix* **S**. For definiteness, let us consider Fig. 4.1b and assume that energy and momentum are conserved in the scattering. Allowing an incident electron plane-wave to strike the barrier from the left, the total wave function of the system including scattering is

$$\begin{aligned} \psi_L(L) &= e^{ikx} + re^{-ikx}; & x < 0 \\ \psi_L(R) &= te^{ikx}; & x > 0 \end{aligned} \tag{4.1}$$

where coefficient r and t are the (complex) amplitudes for reflection and transmission, respectively. Similarly, an electron incident from the right gives

$$\begin{aligned} \psi_R(L) &= t'e^{-ikx}; & x < 0 \\ \psi_R(R) &= e^{-ikx} + r'e^{ikx}; & x > 0 \end{aligned} \tag{4.2}$$

where the coefficients r' and t' need not be the same as r and t (although they will be for a symmetric barrier). These states are called *scattering states*. A general input state $a_L e^{ikx} + a_R e^{-ikx}$ with initial amplitudes $a_{L,R}$ therefore gives rise a total wave function:

$$\begin{aligned} \Psi(L) &= a_L \left(e^{ikx} + re^{-ikx} \right) + a_R t' e^{-ikx} \\ &= a_L e^{ikx} + \left(a_L r + a_R t' \right) e^{-ikx}; \qquad x < 0 \\ \Psi(R) &= a_L t e^{ikx} + a_R \left(e^{-ikx} + r' e^{ikx} \right) \\ &= a_R e^{-ikx} + \left(a_L t + a_R r' \right) e^{ikx}; \qquad x > 0 \end{aligned} \tag{4.3}$$

Introducing coefficients $b_{L,R}$ to describe the amplitudes of the outgoing modes, we can write these wavefunctions simply as

$$\begin{aligned} \Psi(L) &= a_L e^{ikx} + b_L e^{-ikx} \\ \Psi(R) &= a_R e^{-ikx} + b_R e^{ikx} \end{aligned} \tag{4.4}$$

Comparison of these two forms shows that the input and output coefficients are related as

$$\begin{pmatrix} b_L \\ b_R \end{pmatrix} = \begin{pmatrix} r & t' \\ t & r' \end{pmatrix} \begin{pmatrix} a_L \\ a_R \end{pmatrix} = \mathbf{S} \begin{pmatrix} a_L \\ a_R \end{pmatrix}. \tag{4.5}$$

This defines scattering matrix S which relates output mode amplitudes to input ones.

Where does the **S** matrix come from? Or rather, how are the coefficients r,t,r' and t' determined? Well, the answer is that they must be determined by a precise quantum mechanical calculation of the behaviour of the electrons at the scatterer. An illustrative example is the scattering matrix of the potential barrier of Fig. 4.1b, for which one must invoke the continuity of the wavefunction and its first derivative at the interfaces of the potential barrier to determine **S**.

4.2.1 The scattering matrix

The preceding scattering matrix just describes a single outgoing and a single incoming mode in each of the left and right regions. We can easily generalise to the multimode case, with N_L modes on the left and N_R on the right. Labeling an incoming amplitude in mode m on the right as a_{Lm} and so on, we can collect all such amplitudes into vectors, writing.

$$\mathbf{b} = \begin{pmatrix} b_{L1} \\ \vdots \\ b_{LN_L} \\ b_{R1} \\ \vdots \\ b_{RN_R} \end{pmatrix}; \qquad \mathbf{a} = \begin{pmatrix} a_{L1} \\ \vdots \\ a_{LN_L} \\ a_{R1} \\ \vdots \\ a_{RN_R} \end{pmatrix} \tag{4.6}$$

We then relate input and output modes with a scattering matrix

$$\mathbf{b} = \mathbf{S}\mathbf{a}. \tag{4.7}$$

The scattering matrix **S** is of dimension $(N_L + N_R) \times (N_L + N_R)$ and has the block structure

$$\mathbf{S} = \begin{pmatrix} \mathbf{s}_{LL} & \mathbf{s}_{LR} \\ \mathbf{s}_{RL} & \mathbf{s}_{RR} \end{pmatrix} = \begin{pmatrix} \mathbf{r} & \mathbf{t}' \\ \mathbf{t} & \mathbf{r}' \end{pmatrix}, \tag{4.8}$$

where, in the second form, the subblocks represent transmission ($\mathbf{t}$ and $\mathbf{t}'$) and reflection ($\mathbf{r}$ and $\mathbf{r}'$) processes.

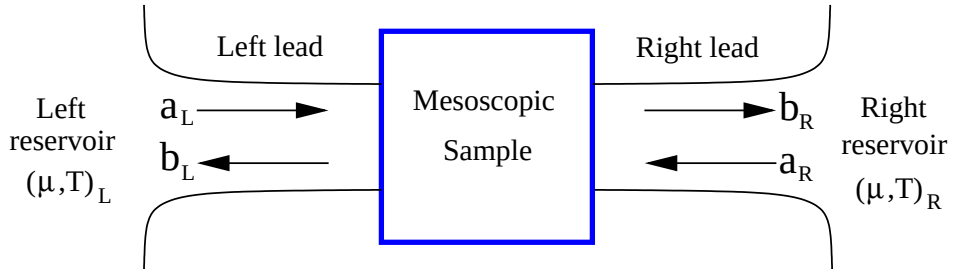

Figure 4.2: In the scattering theory of a two-probe mesoscopic transport experiment, five components of the set-up are identified: left and right reservoirs, left and right leads, and the sample itself. The reservoirs act as a sink and thermalised source for electrons. The left and right leads are considered to be narrow ballistic conductors with N_L and N_R transverse modes respectively within in the transport window. Finally, the mesoscopic sample itself is considered as scatterer, with scattering matrix $\mathbf{S}$.

Flux conservation requires that $\mathbf{S}$ is unitary. This has the consequence that

$$\mathbf{r}^\dagger\mathbf{r} + \mathbf{t}^\dagger\mathbf{t} = \mathbf{r}'^\dagger\mathbf{r}' + \mathbf{t}'^\dagger\mathbf{t}' = \mathbb{1}, \tag{4.9}$$

$$\mathbf{r}^\dagger\mathbf{t}' + \mathbf{t}^\dagger\mathbf{r}' = \mathbf{t}'^\dagger\mathbf{r} + \mathbf{r}'^\dagger\mathbf{t} = 0,$$

$$\mathbf{r}\mathbf{t}^\dagger + \mathbf{t}'\mathbf{r}'^\dagger = \mathbf{t}\mathbf{r}^\dagger + \mathbf{r}'\mathbf{t}'^\dagger = 0. \tag{4.10}$$

If time-reversal symmetry applies, $\mathbf{S}$ is also symmetric. Since the transformation between $\mathbf{a}$ and $\mathbf{b}$ is unitary, the canonical commutation relations for $\mathbf{b}$ and the same as those for $\mathbf{a}$.

4.3 The Landauer-Büttiker formalism

We will use a scattering matrix to relate states entering and leaving our mesoscopic sample. In order to describe transport, however, we need more ingredients than just the scattering matrix. As Fig. 4.2 shows, we identify five components of the set-up: the sample itself, left and right leads, and the left and right reservoirs. This is a two-probe set-up (L and R), but we will generalise to the multi-probe case later. We will use the indices $\alpha, \beta = L, R$ to label the left and right leads and reservoirs.

4.3.1 Reservoirs

The reservoirs are assumed to be macroscopic conductors, large and in thermal equilibrium. Each is described by a temperature T_α and chemical potential μ_α, set by the external circuit. Normally, we set the temperatures equal. The electrons in reservoir α are distributed according to the Fermi distribution:

$$f_\alpha(E) = \frac{1}{\exp\left((E-\mu_\alpha)/k_B T_\alpha\right)+1}. \tag{4.11}$$

Electrons entering the reservoirs are completely thermalised to this distribution before being returned to the leads and the only role that the reservoirs play is to provide thermalised electrons.

4.3.2 Leads

Sign convention (after M. Büttiker, Phys. Rev. B **46**, 12485 (1992)): In each lead α, we define a local coordinate x_α such that the positive sense of x_α is taken towards the sample. Incoming plane waves are always e^{ikx_α}, outgoing waves e^{-ikx_α}. [1] This convention makes particular sense when we consider multi-probe geometries. We also define the vector $\mathbf{r}_{\perp\alpha}$ perpendicular to x_α in lead α.

The leads are assumed to be perfect (ballistic) conductors, and narrow compared with the reservoirs. We describe electrons in lead α with the Hamiltonian

$$H_\alpha = \frac{1}{2m^*}p_{x\alpha}^2 + \frac{1}{2m^*}p_{\perp\alpha}^2 + U(\mathbf{r}_\perp), \tag{4.12}$$

with $U(\mathbf{r}_\perp)$ the perpendicular confinement potential, as in the previous chapter. The eigenfunctions of H_α are

$$\phi^\pm_{\alpha n k_n}(x_\alpha, \mathbf{r}_{\perp\alpha}) = \chi_{\alpha n}(\mathbf{r}_{\perp\alpha})e^{\pm k_n x_\alpha}, \tag{4.13}$$

with χ satisfying the transverse problem:

$$\left\{\frac{1}{2m^*}p_{\perp\alpha}^2 + U(\mathbf{r}_\perp)\right\}\chi_{\alpha n}(\mathbf{r}_{\perp\alpha}) = \epsilon_{\alpha n}\chi_{\alpha n}. \tag{4.14}$$

The dispersion relationship is then

$$E_{\alpha n}(k_{\alpha n}) = \frac{\hbar^2 k_{\alpha n}^2}{2m^*} + \epsilon_{\alpha n}, \tag{4.15}$$

[1] This is different to the convention of Eqns. (4.1) to (4.4) in which the left to right is fixed as the positive x direction for both incoming and outgoing waves.

with $\epsilon_{\alpha n}$ the energy of the transverse mode n in lead α. Although index n is in principle unbounded, for our purposes we need only consider a finite number of modes in each lead, N_α, since higher modes will lie outside the energy range of interest. This energy range, or 'transport window' is given approximately by the bias across the sample.

The contact between the leads and the reservoirs is assumed to be *reflectionless*, which means that any electron impinging on the reservoir is fully absorbed by it. In practise, this can be realised with the 'horn' shaped contacts along the lines of Fig. 4.2.

4.3.3 Scattering states

We will describe the mesoscopic sample is described solely in terms of its scattering matrix $\mathbf{S}$, which describes phase-coherent elastic scattering between the N_L electron modes of lead L and the N_R modes of lead R. The scattering matrix is taken as an input to our theory, and as such must be calculated by other means, such as the wave function matching mentioned in the previous section.

Proceeding as before, let us now construct the scattering states of our problem. Injecting an electron into mode m of lead α, the total wavefunction is, in lead α,

$$\psi_{\alpha m}(\alpha) = \sum_n \delta_{mn}\phi^+_{\alpha n k_{\alpha n}} + \sqrt{\frac{v_{\alpha m}}{v_{\alpha n}}} s_{\alpha\alpha nm}\phi^-_{\alpha n k_{\alpha n}}, \tag{4.16}$$

and in lead β,

$$\psi_{\alpha m}(\beta) = \sum_n \sqrt{\frac{v_{\alpha m}}{v_{\beta n}}} s_{\beta\alpha nm}\phi^-_{\beta n k_{\alpha n}}. \tag{4.17}$$

Here, $s_{\alpha\beta nm}$ are elements of the scattering matrix which, in general depends on the wavenumber/energy at which scattering takes place. These expressions have been written such that the electron velocity in mode (α, m):

$$v_{\alpha m} = \frac{dE_{\alpha m}}{d(\hbar k_{\alpha m})} = \frac{\hbar k_{\alpha m}}{m^*} = \sqrt{\frac{2m^*}{E_{\alpha m} - \epsilon_{\alpha m}}} \tag{4.18}$$

appears explicitly. This may be thought of as a consequences of the normalisation of our wavefunctions, or of a free choice we make about the definition of $\mathbf{S}$ — when we move to an energy representation, these factors will conveniently cancel.

The scattering states $\psi_{\alpha m}$, together with any possible bound states in the conductor, form a complete set of states for a single electron (J. E. G Farina, Quantum theory of scattering processes, Pergamon, Oxford, 1973). A general electronic state in the device-lead system can therefore be written as

$$\Psi(\mathbf{r},t) = \frac{1}{\sqrt{2\pi}} \sum_{\alpha m} \int dk_{\alpha m} \psi_{\alpha m}(k_{\alpha m}, \mathbf{r}) e^{-i\omega_{\alpha m}(k)t} a_{\alpha m}(k_{\alpha m}) \tag{4.19}$$

with $\omega_{\alpha m}(k) = E_{\alpha m}/\hbar$ and $a_{\alpha m}(k_{\alpha m})$, the amplitudes of the incoming wave components.

4.3.4 Second Quantisation

We now move to a second-quantised formalism through the introduction of fermionic creation and annihilation operators for incoming and outgoing modes. Still in momentum space, the canonical anti-commutation relations for the incoming operators read

$$\left\{ \hat{a}_{\alpha m}(k), \hat{a}^{\dagger}_{\beta n}(k') \right\} = \delta_{\alpha\beta}\delta_{nm}\delta\left(k - k'\right). \tag{4.20}$$

with other anti-commutators equal to zero. Identifying the wavefunction amplitudes of Eq. (4.19) with these operators , we can write the electron field operator at $(\mathbf{r}, t)$ as

$$\hat{\Psi}(\mathbf{r},t) = \frac{1}{\sqrt{2\pi}} \sum_{\alpha m} \int dk_{\alpha m} \psi_{\alpha m}(k_{\alpha m}, \mathbf{r}) e^{-i\omega_{\alpha m}(k)t} \hat{a}_{\alpha m}(k_{\alpha m}). \tag{4.21}$$

For all subsequent developments, it is more convenient to work in the energy (rather than k) representation. For this we need to find the relations analogous to Eq. (4.20) in energy space. Consider the delta function $\delta(k - k')$. An important identity for the delta function reads

$$\delta(f(x)) = \sum_i \frac{1}{|f'(x_i)|} \delta(x - x_i) \text{ with } x_i \text{ roots of } f(x_i) = 0. \tag{4.22}$$

Taking into account the preceding $\delta_{\alpha\beta}\delta_{nm}$ factors, we can thus write

$$\begin{aligned} \delta\left(k - k'\right) &= \delta\left(\frac{\sqrt{2m}}{\hbar} \left(\sqrt{E - \epsilon_{\alpha m}} - \sqrt{E' - \epsilon_{\alpha m}} \right) \right) \\ &= \frac{1}{\hbar} \sqrt{\frac{m^*}{2\left(E - \epsilon_{\alpha m}\right)}} \delta\left(E - E'\right) \\ &= \frac{1}{\hbar v_{\alpha m}(E)} \delta\left(E - E'\right) \end{aligned} \tag{4.23}$$

Therefore, in order that the commutation relations preserve their canonical form in the energy representation, we define

$$\hat{a}_{\alpha m}(E) = \frac{1}{\sqrt{\hbar v_{\alpha m}(k)}}\hat{a}_{\alpha m}(k)\,;\ \text{and}\ \ \hat{a}^{\dagger}_{\alpha m}(E) = \frac{1}{\sqrt{\hbar v_{\alpha m}(k)}}\hat{a}^{\dagger}_{\alpha m}(k)\,, \tag{4.24}$$

such that

$$\left\{\hat{a}^{\dagger}_{\alpha m}(E), \hat{a}^{\dagger}_{\beta n}(E')\right\} = \delta_{\alpha\beta}\delta_{nm}\delta\left(E - E'\right), \tag{4.25}$$

with the velocities cancelling. In order to convert the field operator of Eq. (4.21) into the energy representation we introduce the density of states $\mathcal{D}(E)$, such that $\int dk \rightarrow \int dE\ \mathcal{D}(E)$. As the motion in both transverse directions is confined, the appropriate density of states is the one-dimensional result

$$\mathcal{D}(E) = \frac{1}{4}\frac{1}{\pi\hbar}\sqrt{\frac{2m^*}{E}} = \frac{1}{2\pi\hbar v_{\alpha m}(E)}. \tag{4.26}$$

This value is quarter of the value that one usually expects for a 1D DOS, the reason being that here we have not included spin (spin up and spin down count as two separate channels), and we only consider states propagating in a single incoming direction (i.e. just k and not $\pm k$). These results allow us to write the field operator as

$$\hat{\Psi}(\mathbf{r}, t) = \sum_{\alpha m}\int \frac{dE_{\alpha m}}{\sqrt{2\pi\hbar v_{\alpha m}}}\psi_{\alpha m}(E_{\alpha m}, \mathbf{r})e^{-i\omega_{\alpha m}(E)t}\hat{a}_{\alpha m}(E_{\alpha m}). \tag{4.27}$$

In second quantisation, we can relate outgoing operators annihilators $\hat{b}_{\beta n}(E)$ to incoming ones via the scattering matrix, just as we did for the amplitudes in section 4.2.1

$$\hat{b}_{\beta n}(E) = s_{\beta\alpha nm}\hat{a}_{\alpha m}(E). \tag{4.28}$$

Arranging the operators into vectors, we have

$$\hat{\mathbf{b}}(E) = \mathbf{S}\hat{\mathbf{a}}(E). \tag{4.29}$$

and for the corresponding creation operators,

$$\hat{\mathbf{b}}^{\dagger}(E) = \mathbf{S}^{\dagger}\hat{\mathbf{a}}^{\dagger}(E). \tag{4.30}$$

The scattering matrix here obeys the same properties as discussed in the previous section.

4.3.5 The Landauer current formula

Employing the scattering states from Eq. (4.16), we can express the left-lead field operator Eq. (4.27) as

$$\begin{aligned}\hat{\Psi}_L(\mathbf{r},t) &= \sum_{mn}\int \frac{dE}{\sqrt{2\pi\hbar v_{Lm}}} e^{-i\omega_{Lm}(E)t} \\ &\quad \times \left\{\delta_{mn}\phi^+_{Ln} + \sqrt{\frac{v_{Lm}}{v_{Ln}}} s_{LLnm}\phi^-_{Ln}(E)\right\}\hat{a}_{Lm}(E) \\ &= \sum_{m=1}^{N_L(E)}\int \frac{dE}{\sqrt{2\pi\hbar v_{Lm}}} e^{-i\omega_{Lm}(E)t} \\ &\quad \times \left\{\phi^+_{Lm}(E)\hat{a}_{Lm}(E) + \phi^-_{Lm}(E)\hat{b}_{Lm}(E)\right\}.\end{aligned} \tag{4.31}$$

Following the standard QM expression, the current operator in the left lead, far from the sample can be expressed as:

$$\hat{I}_L(x,t) = \frac{\hbar e}{2im}\int d\mathbf{r}_{\perp L}\left[\hat{\Psi}^\dagger_L(\mathbf{r},t)\frac{\partial}{\partial x}\hat{\Psi}_L(\mathbf{r},t) - \left(\frac{\partial}{\partial x}\hat{\Psi}^\dagger_L(\mathbf{r},t)\right)\hat{\Psi}_L(\mathbf{r},t)\right] \tag{4.32}$$

Evaluating the derivatives with field operators from Eq. (4.31) yields a lengthy expression. This expression contains the velocity $v(E)$ and by recognising that this is a slowly-varying functions of energy, we can approximate the current operator as

$$\hat{I}_L(t) = \frac{e}{2\pi\hbar}\sum_n \int dE dE' e^{i(E-E')t/\hbar}\left[\hat{a}^\dagger_{Ln}(E)\hat{a}_{Ln}(E') - \hat{b}^\dagger_{Ln}(E)\hat{b}_{Ln}(E')\right]. \tag{4.33}$$

Setting $E' = E + \hbar\omega$ and integrating over ω gives

$$\boxed{\hat{I}_L(t) = \frac{e}{2\pi\hbar}\sum_n \int dE\left[\hat{n}^+_{Ln}(E,t) - \hat{n}^-_{Ln}(E,t)\right],} \tag{4.34}$$

where $\hat{n}^+_{Ln}(E,t)$ are the time-dependent occupation numbers for incoming and outgoing electrons in mode n of the left lead. We thus arrive at the physically appealing result that the current in a given lead is given by the difference in occupation between left- and right- moving electrons in that lead.

Let us define the A matrix for the left lead:

$$A^{mn}_{\alpha\beta}(L;E,E') = \delta_{mn}\delta_{\alpha L}\delta_{\beta L} - \sum_k s^\dagger_{L\alpha;mk}(E)s_{L\beta;kn}(E'), \tag{4.35}$$

with $s_{L\alpha;mk}(E)$ the scattering matrix element relating $\hat{b}_{Lm}(E)$ to $\hat{a}_{\alpha k}(E)$. The current operator then assumes a bilinear form in terms of input operators only:

$$\hat{I}_L(t) = \frac{e}{2\pi\hbar}\sum_{\alpha\beta}\sum_{mn}\int dEdE' e^{i(E-E')t/\hbar}\hat{a}^\dagger_{\alpha m}(E)A^{mn}_{\alpha\beta}(L;E,E')\hat{a}_{\beta n}(E'). \tag{4.36}$$

Inserting the definition of matrix A and comparing with Eq. (4.33), we see that the δ-function part of A gives number operator for incoming modes and the second term gives the number operator for outgoing modes.

We are now in a position to use this current operator to obtain an expression for the average current in the left lead $\langle I_L\rangle$. Incoming modes are populated by electrons coming from the reservoirs. We assume that each incoming mode is in thermal equilibrium with the corresponding reservoir, and thus the electrons in mode m of lead α are distributed according to the Fermi function $f_\alpha(E_m)$. The bilinear product of incoming mode operators therefore have the following expectation value:.

$$\langle \hat{a}^\dagger_{\alpha m}(E)\hat{a}_{\beta n}(E')\rangle = \delta_{\alpha\beta}\delta_{mn}\delta\left(E-E'\right)f_\alpha(E). \tag{4.37}$$

Taking the expectation value of the current operator of Eq. (4.36) directly yields the average current as

$$\boxed{\langle\hat{I}_L\rangle = \frac{e}{2\pi\hbar}\int dE\ \mathrm{Tr}\left[\mathbf{t}^\dagger(E)\mathbf{t}(E)\right]\left[f_L(E)-f_R(E)\right]}, \tag{4.38}$$

where $\mathbf{t}(E)$ is the off-diagonal transmission subblock of the scattering matrix.

4.3.6 Linear Response

Equation (4.38) gives the current for a general voltage, but we are often just interested in small applied fields where a linear approximation will suffice. Let us set a voltage bias V across sample such that the chemical potentials

read $\mu_L = \mu + eV/2$ and $\mu_R = \mu - eV/2$, with μ the equilibrium value. We have then

$$f_L(E) - f_R(E) = f(E - E_F - eV/2) - f(E - E_F + eV/2) \tag{4.39}$$

In the limit of small bias, we can approximate this as

$$eV\left(\frac{f(E-\mu-eV/2) - f(E-\mu+eV/2)}{eV}\right) \to eV\left(-f'(E-\mu)\right) \tag{4.40}$$

with $f(E) = \left[1 + e^{E/k_BT}\right]^{-1}$ and $f'(E) = \frac{d}{dE}f(E)$. The current becomes

$$\langle \hat{I}_L \rangle = \frac{e^2 V}{2\pi\hbar} \int dE \ \mathrm{Tr}\left[\mathbf{t}^\dagger(E)\mathbf{t}(E)\right]\left(-\frac{\partial f(E-\mu)}{\partial E}\right), \tag{4.41}$$

and the corresponding conductance

$$G = \frac{\langle I_L \rangle}{V} = \frac{e^2}{h} \int dE \ \mathrm{Tr}\left[\mathbf{t}^\dagger(E)\mathbf{t}(E)\right]\left(-\frac{\partial f(E-\mu)}{\partial E}\right). \tag{4.42}$$

At low temperatures, the derivative of the Fermi functions gives us a delta function, such that at small bias and temperature we have

$$f_L(E) - f_R(E) \to eV\delta\left(E - E_F\right), \tag{4.43}$$

where, in this last step, we have written μ in its zero-temperature limit of E_F. The linear (or equilibrium) conductance then becomes

$$G = \frac{e^2}{h}\mathrm{Tr}\left[\mathbf{t}^\dagger(E_F)\mathbf{t}(E_F)\right]. \tag{4.44}$$

The matrix $\mathbf{t}^\dagger\mathbf{t}$ has eigenvalues T_n which are real, and these are the *transmission probabilities*. The corresponding representation is called the *eigenchannel representation*. In this representation, the current of Eq. (4.38), reads

$$\langle \hat{I}_L \rangle = \frac{e}{2\pi\hbar} \sum_n \int dE \ T_n(E)\left[f_L(E) - f_R(E)\right]. \tag{4.45}$$

and the linear response conductance can therefore be written as

$$\boxed{G = \frac{e^2}{h} \sum_n \int dE \ T_n(E)\left(-\frac{\partial f(E-\mu)}{\partial E}\right).} \tag{4.46}$$

At low temperatures this becomes simply

$$\boxed{G = \frac{e^2}{h} \sum_n T_n; \qquad T_n = T_n(E_F).} \tag{4.47}$$

This is the *Landauer conductance formula*. It states that each channel contributes a unit of conductance $G_0 = e^2/h$ multiplied by the transmission probability of the channel. This is quite a nice picture of what is happening and somewhat in tune with intuition.

A final version of this result makes use of the probabilities $T_{RL;mn} = |s_{RL;mn}|^2$ for transmission of a carrier from channel n in the left lead to channel m in the right. In this basis, the *natural basis*, the conductance reads

$$G = \frac{e^2}{h} \sum_{mn} T_{mn}. \tag{4.48}$$

Note that linear response is not only valid when the applied bias is small, but also for the case when the transmission coefficients are only weakly dependent on energy.

4.4 Examples

4.4.1 Quantum point contact

A quantum point contact (QPC) is a narrow constriction in a 2DEG, see Fig. 4.3a, through which transport is essentially ballistic. In terms of the Landauer-Büttiker approach, this means that each channel has transmission probability equal to unity when the channel lies within the transport window, and zero otherwise. The total transmission coefficient for the system is then

$$T(E) = \sum_n \theta(E - \epsilon_n) \tag{4.49}$$

where $\theta(E)$ is the step-function as usual, and ϵ_n are the mode energies.

With such a simple scattering matrix, the (linear, low temperature) conductance is simply found from Eq. (4.47) to be

$$G = \frac{e^2}{n} \sum_n \theta(E - \epsilon_n) = \frac{e^2}{h} N_L, \tag{4.50}$$

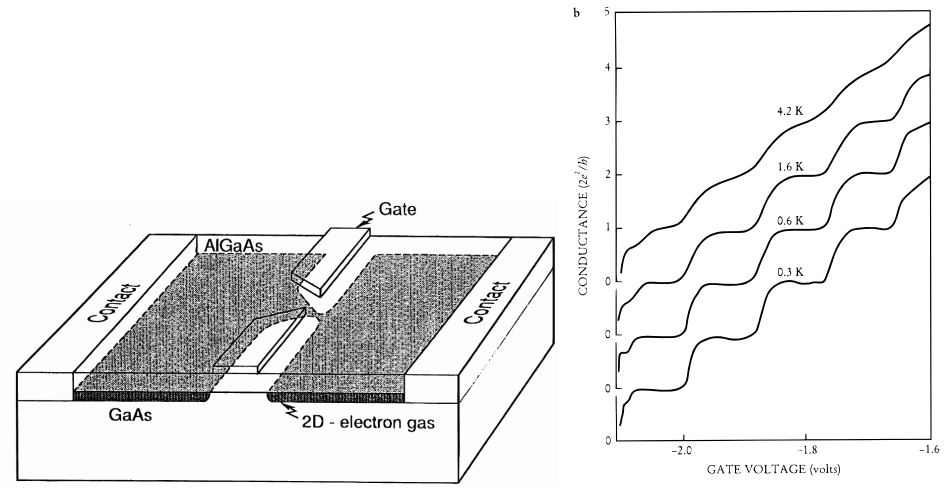

Figure 4.3: Left: Quantum point contact formed in a 2DEG with top gates. Right: conductance quantisation in units of $2e^2/h$. The resulting conductance steps are smeared out when the thermal energy becomes comparable to the energy separation of the modes. From H. van Houten and C.W.J. Beenakker, `cond-mat/0512609` (adapted from the experiment of B. J. van Wees, Phys. Rev. Lett. **60**, 848 (1988)).

where N_L is the number of modes in the transport window. With zero magnetic field, spin-up and spin-down channels are degenerate, and we write $N_L = 2M$, where M is the number of orbital channels. We thus find the QPC condutnace to be

$$\boxed{G = \frac{2e^2}{h} M,} \tag{4.51}$$

which shows conductance quantisation in units of

$$\frac{2e^2}{h} = \frac{1}{12.5\text{k}\Omega}. \tag{4.52}$$

This value, 12.5kΩ, is the resistance of a single channel — and it is certainly not negligible. The conductance of a QPC from experiment is plotted in Fig. 4.3b. Clearly seen is a sequence of conductance steps as the applied bias is increased and more modes are brought within the transport window. The height of the each steps is always $2e^2/h$, but the position of the steps

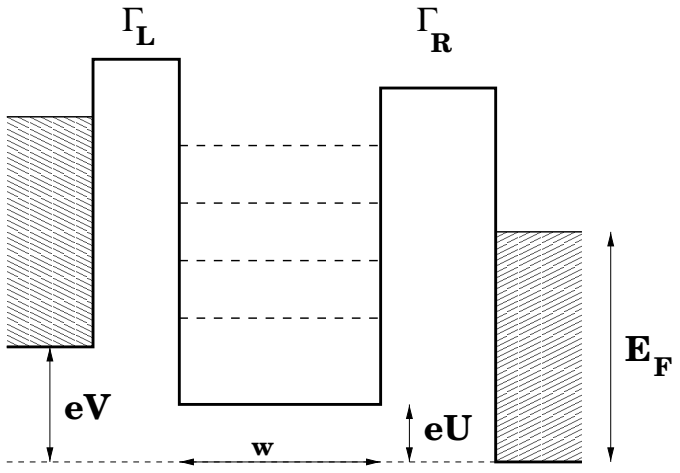

Figure 4.4: Resonant tunnel barriers. From Ya. M. Blanter, and M. Büttiker, `cond-mat/9910158`.

depends on the values of the mode energies and hence on the precise form of the transverse confinement potential. With a simple harmonic potential, the positions of the steps will be regularly spaced.

The effects of temperature and the Zeeman splitting on the QPC conductance are discussed in a homework exercise.

4.4.2 Resonant tunnel barrier

We now consider an example in which the interesting behaviour arises from the structure of the scatterer, and not from the transverse confinement. To this end we consider that the leads have a single (spin-degenerate) mode such that, from Eq. (4.47), the conductance is simply

$$G = \frac{2e}{h} T(E), \tag{4.53}$$

with $T(E)$ the transmission amplitude of the scatterer, and we where we have included a factor of 2 for both spin directions, which we assume are scattered identically.

As our scatterer, we take the resonant tunnel barrier structure sketched in Fig. 4.4, which serves as a model for both quantum wells and quantum dots. If we consider the structure to be purely one-dimensional with transmission probabilities T_L and T_R for the L and R barriers, the total

transmission coefficient of the device is

$$T(E) = \frac{T_L T_R}{1 + (1 - T_L)(1 - T_R) - 2\sqrt{(1 - T_L)(1 - T_R)}\cos\phi(E)}, \quad (4.54)$$

with $\phi(E)$ the phase accumulated in crossing the enclosed region $\phi(E) = 2w\sqrt{2mE}/\hbar$. This expression has a series of maxima which occur at resonant energies E_n^r such that the phase is $\phi^r(E) = 2\pi n$. NB: this result comes from a wavefunction matching calculation or something similar: see homework exercise or Ferry & Goodnick. For simplicity, we expand Eq. (4.54) about its resonances, assuming that the spacing between the resonances is greater than their broadening, and obtain

$$T(E) \approx \sum_n T_n^{\max} \frac{\Gamma_n^2/4}{(E - E_n^r)^2 + \Gamma_n^2/4} \quad (4.55)$$

where

$$T_n^{\max} = \frac{4\Gamma_{Ln}\Gamma_{Rn}}{\Gamma_n^2} \quad (4.56)$$

is the maximum transmission probability on resonance, $\Gamma_{\alpha n} = \hbar\nu_n T_\alpha$ is the partial width, with attempt frequency $\nu_n^{-1} = (\hbar/2)(d\phi/dE_n^r) = w/v_n$ with velocity $v_n = \sqrt{2E_n^r/m}$, and the total width of the nth resonant level is $\Gamma_n = \Gamma_{Ln} + \Gamma_{Rn}$. $T(E)$ thus consists of a string of Breit-Wigner resonances.

The resulting conductance is shown in Fig. 4.5, from which we clearly see this resonance structure. Note that the broadening of the peaks is given by Γ and not temperature. One further interesting point is that, even if the transmission probability of the individual barriers is very low, if they are symmetric, the transmission coefficient of the complete structure is unity. This may be understood in terms of multiple-internal reflections in the inter-barrier region.

4.5 The Macroscopic limit

We now analyse the predictions of this Landauer result as we increase the size of the conductor. Let us assume that all M channels are equally transmissive (probability T), such that the conductance is

$$G = \frac{2e^2}{h} MT. \quad (4.57)$$

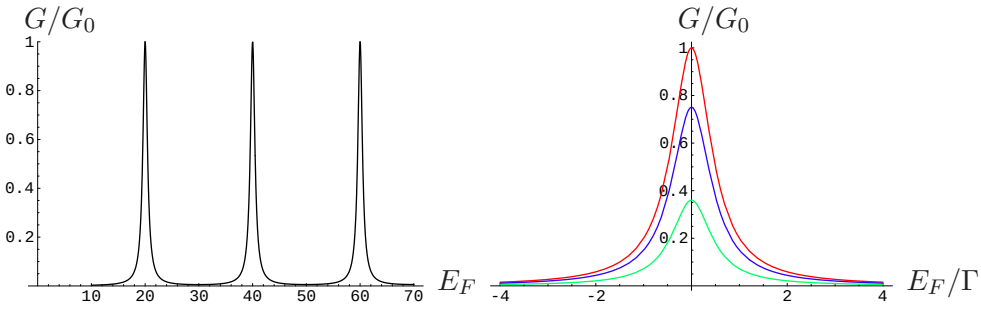

Figure 4.5: The conductance G/G_0 with $G_0 = 2e^2/h$ for the resonant tunnel barrier model assumed to have a transmission coefficient given by Eq. (4.55). We set $\Gamma_n = \Gamma$, $\Gamma_{Ln} = \Gamma_L$, $\Gamma_{Rn} = \Gamma_R$ and $E_n^r = n\hbar\omega$.. Left: The conductance shows distinct peaks at the resonance energies, with $\Gamma_L = \Gamma_R$, $\hbar\omega = 20\Gamma$ Right: Close-up of a single resonance for $\Gamma_L = 1/2$(red), $\Gamma_L = 1/4$(blue), $\Gamma_L = 1/10$(green). The transmission is unity on resonance for symmetric barriers, regardless of the magnitude of $\Gamma_L = \Gamma_R$.

4.5.1 Wide conductor

For a wide conductor we can estimate M, the number of modes by assuming periodic boundary conditions, for which the allowed values of k_y are spaced by $2\pi/W$, with conductor width W. At energy $E_F = \hbar^2 k_F^2/2m$ a wave can only propagate if its wavevector lies in the range $-k_F < k_y < k_F$, and the number of such states is therefore $2k_F/(2\pi/W) = k_F W/\pi$. Strictly, we have to take the integer part

$$M = \text{int}(k_F W/\pi) = \text{int}(W/(\lambda_F/2)). \tag{4.58}$$

Assuming a Fermi wavelength of 30nm, the number of modes in a 15 μm wide FET is of the order 1000, such that the contact resistance is $\sim 12.5\Omega$.

4.5.2 Ohm's law

What happens if we now increase the length of the conductor? Using result Eq. (4.58), the conductance of our wide sample is

$$G = \frac{2e^2}{h}\frac{k_F W}{\pi}T = e^2 W \mathcal{D}_0 \frac{v_F T}{\pi} \tag{4.59}$$

with $\mathcal{D}_0 = m/\pi\hbar^2$, the 2DEG DOS. The transmission probability for a conductor of length L is

$$T(L) = \frac{L_0}{L + L_0}, \tag{4.60}$$

where L_0 is a length of the order of the mean-free path. Proof of this relation is left for the homework set. It therefore follows that the conductance is

$$G = \frac{W}{L + L_0} e^2 \mathcal{D}_0 \frac{v_F L_0}{\pi}. \tag{4.61}$$

This result can be understood in terms of the diffusive theory of (classical) transport in which the current density arises from a gradient in electron concentration

$$\mathbf{J} = -eD\nabla n, \tag{4.62}$$

with D the diffusion coefficient. Comparison with $\mathbf{J} = \sigma\mathbf{E}$ yields the relationship between D and the Ohm's law conductivity:

$$\sigma = e^2 \mathcal{D}_0 D \tag{4.63}$$

This is the *Einstein relation* for degenerate semiconductors. Returning to Eq. (4.61), we can identify $v_F L_0/\pi$ with the diffusion coefficient D, and use the Einstein relation to write

$$G = \frac{\sigma W}{L + L_0}. \tag{4.64}$$

Separating out two contributions, we have

$$G^{-1} = G_\Omega^{-1} + G_c^{-1} = \frac{L}{\sigma W} + \frac{L_0}{\sigma W}, \tag{4.65}$$

where the first term is the Ohm's law resistance, which scales with the length, and the second is the contact resistance, which has value independent of the length of the conductor. In the macroscopic limit $G_\Omega^{-1} \gg G_c^{-1}$, and we recover Ohm's law.

4.6 Multiterminal conductance

The Landauer-Büttiker formalism can be extended to devices with multiple contacts. Consider a number of reservoirs labelled with index α, each with

its own equilibrium Fermi distribution $f_\alpha(E)$. At a given energy, lead α supports $N_\alpha(E)$ transverse modes. Introduce annihilation operators $\hat{a}_{\alpha m}$ and $\hat{b}_{\alpha m}$ for incoming and outgoing modes in mode m of channel α, which are once again related by a scattering relation which, in terms of components, reads

$$\hat{b}_{\alpha m}(E) = \sum_{\beta n} s_{\alpha\beta;mn}(E)\hat{a}_{\beta n}(E). \tag{4.66}$$

The matrix s is of course unitary. As in Eq. (4.35) we introduce the matrix:

$$A^{mn}_{\beta\gamma}(\alpha; E, E') = \delta_{mn}\delta_{\alpha\beta}\delta_{\alpha\gamma} - \sum_k s^\dagger_{\alpha\beta;mk}(E)s_{\alpha\gamma;kn}(E'), \tag{4.67}$$

such that the current operator in lead α becomes

$$\hat{I}_\alpha(t) = \frac{e}{2\pi\hbar}\sum_{\beta\gamma}\sum_{mn}\int dEdE' e^{i(E-E')t/\hbar}\hat{a}^\dagger_{\beta m}(E)A^{mn}_{\beta\gamma}(\alpha; E, E')\hat{a}_{\gamma n}(E'). \tag{4.68}$$

The signs of currents are chosen so that they are positive for incoming electrons.

Consider a voltage V_β applied to reservoir β such that $\mu_\beta = \mu + eV_\beta$ with μ the equilibrium chemical potential of all leads. The average current in linear response is then

$$\langle I_\alpha\rangle = \frac{e^2}{2\pi\hbar}\sum_\beta V_\beta \int dE \left(-\frac{\partial f}{\partial E}\right)\left[N_\alpha\delta_{\alpha\beta} - \mathrm{Tr}\left(s^\dagger_{\alpha\beta}s_{\alpha\beta}\right)\right], \tag{4.69}$$

where the trace is taken over the channel index of lead α. Defining the differential conductance matrix $G_{\alpha\beta}$ via

$$G_{\alpha\beta} = \left.\frac{d\langle I_\alpha\rangle}{dV_\beta}\right|_{V_\beta=0}, \tag{4.70}$$

we have, in linear regime,

$$\langle I_\alpha\rangle = \sum_\beta G_{\alpha\beta}V_\beta \tag{4.71}$$

with elements of the conductance tensor

$$G_{\alpha\beta} = \frac{e^2}{h}\int dE \left(-\frac{\partial f}{\partial E}\right)\left[N_\alpha\delta_{\alpha\beta} - \mathrm{Tr}\left(s^\dagger_{\alpha\beta}s_{\alpha\beta}\right)\right], \tag{4.72}$$

At low temperature we have

$$G_{\alpha\beta} = \frac{e^2}{h}\left[N_\alpha \delta_{\alpha\beta} - \mathrm{Tr}\left(s^\dagger_{\alpha\beta} s_{\alpha\beta}\right)\right]. \tag{4.73}$$

In both Eq. (4.72) and Eq. (4.73), the scattering matrix is evaluated at the Fermi energy.

4.6.1 Three-terminal device

As an example, let us consider a three terminal device. From Eq. (4.71) the currents are related to the voltages via

$$\begin{pmatrix} I_1 \\ I_2 \\ I_3 \end{pmatrix} = \begin{pmatrix} G_{11} & G_{12} & G_{13} \\ G_{21} & G_{22} & G_{23} \\ G_{31} & G_{32} & G_{33} \end{pmatrix} \begin{pmatrix} V_1 \\ V_2 \\ V_3 \end{pmatrix} \tag{4.74}$$

At low temperatures, and with M_i spin-dependent channels in each channel i, Eq. (4.73) means that this can be written

$$\begin{pmatrix} I_1 \\ I_2 \\ I_3 \end{pmatrix} = \frac{2e^2}{h} \begin{pmatrix} M_1 - \bar{R}_{11} & -\bar{T}_{12} & -\bar{T}_{13} \\ -\bar{T}_{21} & M_2 - \bar{R}_{22} & -\bar{T}_{23} \\ -\bar{T}_{31} & -\bar{T}_{32} & M_3 - \bar{R}_{33} \end{pmatrix} \begin{pmatrix} V_1 \\ V_2 \\ V_3 \end{pmatrix}, \tag{4.75}$$

with

$$\bar{R}_{\alpha\alpha} = \mathrm{Tr}\left(s^\dagger_{\alpha\alpha} s_{\alpha\alpha}\right); \quad \bar{T}_{\alpha\beta} = \mathrm{Tr}\left(s^\dagger_{\alpha\beta} s_{\alpha\beta}\right) \tag{4.76}$$

To find the resistances, we could in principle invert the conduction matrix. However, we can make life simpler for ourselves by first noting that Kirchoff's law implies that $I_1 + I_2 + I_3 = 0$, and that, since the results can only depend on voltage differences, we can, without loss of generality, set $V_3 = 0$. We then have

$$\begin{pmatrix} I_1 \\ I_2 \end{pmatrix} = \begin{pmatrix} G_{11} & G_{12} \\ G_{21} & G_{22} \end{pmatrix} \begin{pmatrix} V_1 \\ V_2 \end{pmatrix}, \tag{4.77}$$

which we can easily invert to give

$$\begin{pmatrix} V_1 \\ V_2 \end{pmatrix} = \begin{pmatrix} R_{11} & R_{12} \\ R_{21} & R_{22} \end{pmatrix} \begin{pmatrix} I_1 \\ I_2 \end{pmatrix}. \tag{4.78}$$

If we drive a current from terminal 3 to terminal 1 and measure the voltage across terminals 2 and 3, the resistance is

$$\begin{aligned} R_{3t} &= \frac{V}{I} = \left.\frac{V_2}{I_1}\right|_{I_2=0} = R_{21} \\ &= \frac{-G_{21}}{G_{11}G_{22} - G_{12}G_{21}} \\ &= \frac{\bar{T}_{21}}{(M_1 - \bar{R}_{11})(M_2 - \bar{R}_{22}) - \bar{T}_{12}\bar{T}_{21}}. \end{aligned} \tag{4.79}$$

If we instead drive the current from terminal 3 to terminal 2, and measure the voltage across terminals 1 and 3, we find

$$R'_{3t} = \frac{V'}{I'} = \left.\frac{V_1}{I_2}\right|_{I_1=0} = R_{12}, \tag{4.80}$$

which yields the same as before but with $\bar{T}_{12}$ in the numerator instead of $\bar{T}_{21}$.

Chapter 5

The quantum Hall effect

Consider a 2DEG in a perpendicular magnetic field of flux density B. According to the semi-classical (Ohmic) prediction of Chapter 2, we should expect the longitudinal resistance R_L to be independent of magnetic field strength, and the transverse, or Hall, resistance R_H to increase linearly with B. However, if this experiment is carried out at high B-field strength, with a high-mobility sample at low temperature the experimentally measured resistances appear as shown in Fig. 5.1. The significant features are

- At low fields, there is agreement with Ohmic predictions
- As B is increased, longitudinal resistance R_L shows oscillations with frequency $\sim 1/B$.
- The Hall resistance R_H shows a series of pronounced plateaus.
- Within these plateaus at high fields, the longitudinal resistance is extremely close to zero . This is particularly surprising because the terminals between which this resistance is measured can be some millimeters apart!

The latter of these two points go under the name of the *quantum Hall effect*, for which Klaus von Klitzing won the 1985 Nobel prize.

5.1 Shubnikov-de Haas oscillations

The oscillation of the longitudinal resistance with increasing B-field is known from bulk materials, and is called the *Shubnikov-de Haas effect* after its discoverers in 1930 (in a Bismuth sample, incidentally). The explanation of

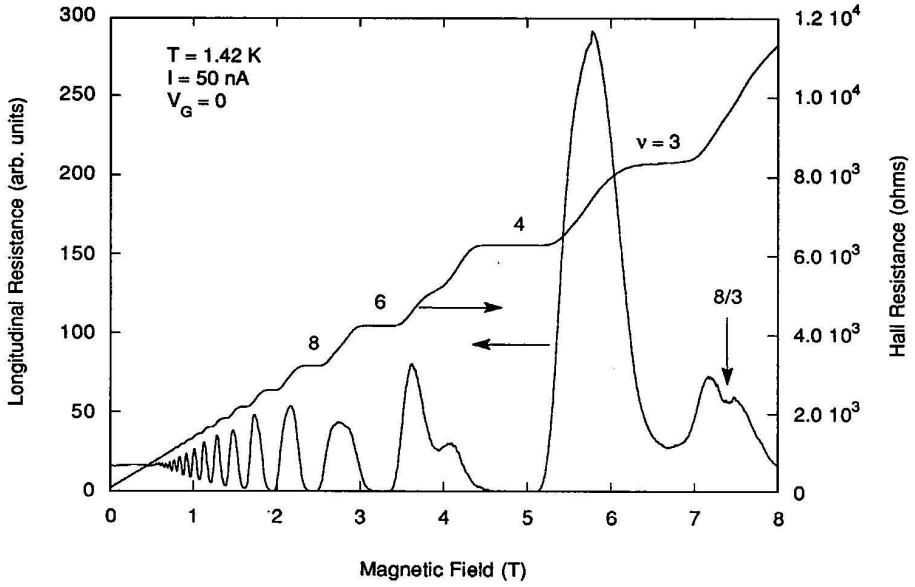

Figure 5.1: Shubnikov-de Haas oscillations and the integer quantum Hall effect. Experimental results for the longitudinal and Hall resistances of a 2DEG as a function of magnetic field. Figure from Ferry & Goodnick.

these oscillations relies on the concept of the Landau level (LL) introduced in previously. In Chapter 3 we saw that in the presence of a perpendicular B-field, the electronic states in a 2DEG split into a series of Landau levels. These we label with an index $n_{\rm LL} = 0, 1, 2, \ldots$ (corresponding to the first,second, third,... LL), such that the dispersion is

$$E_n = E_s + \hbar\omega_c \left(n_{\rm LL} + \tfrac{1}{2}\right), \tag{5.1}$$

with $\omega_c = eB/m$, the cyclotron frequency. How many electronic states are there is a Landau level? To find out, first consider the density of states of a single-subband 2DEG:

$$\mathcal{D}(E) = \mathcal{D}_0\theta(E - E_s); \qquad \mathcal{D}_0 = \frac{m}{\pi\hbar^2}. \tag{5.2}$$

The corresponding density of states consists of a set of discrete peaks, as in Fig. 5.2. We can write

$$\mathcal{D}(E) \approx \mathcal{D}_0^{\rm LL} \sum \delta\left(E - E_s - \hbar\omega_c \left(n_{\rm LL} + \tfrac{1}{2}\right)\right), \tag{5.3}$$

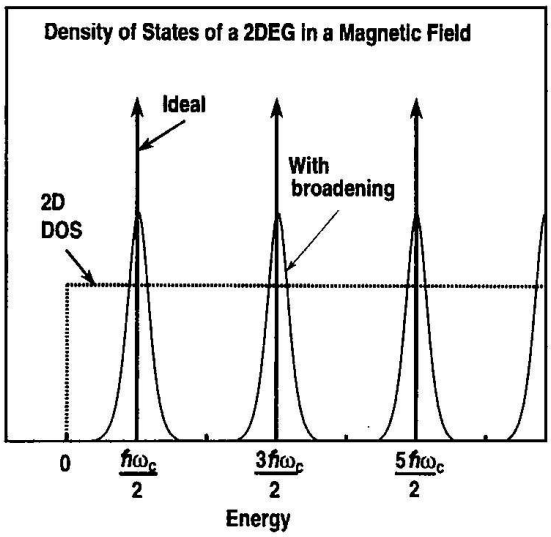

Figure 5.2: Density of states of a 2DEG in magnetic field. By comparing the DOS with and without magnetic field, we can calculate the number of states within each Landau level. From Ferry & Goodnick.

where the forefactor $\mathcal{D}_0^{\mathrm{LL}}$ is the number of states per unit area in a single Landau level. By comparison of the density of states with and without magnetic field, Fig. 5.2, this forefactor can be determined as

$$\mathcal{D}_0^{\mathrm{LL}} = \frac{2eB}{h}. \tag{5.4}$$

In reality, and as drawn in Fig. 5.2, the delta-functions are broadened by scattering into peaks of finite width. At low B, this broadening is greater than the separation of the peaks and we recover the Ohmic results.

We first imagine a situation in which B is kept constant,and the electron density n is altered by changing a gate voltage. Due to the discrete form of the DOS, the Fermi level of the system will undergo a series of jumps as we change the electron density. Increasing n when E_F is inside a Landau level simply increases the number of electrons in that level, with only a very small change in E_F. However, once the Landau level is full, the Fermi level jumps to the next LL where the process begins over. We say that the Fermi

level is 'pinned' within the LL. The highest occupied LL is

$$M = \text{int}\left(\frac{hn}{2eB} + 1\right), \tag{5.5}$$

which obtained as the integer part of the number-density of electrons divided by the number-density $\mathcal{D}_0^{\text{LL}}$ of a single LL, plus one since we count the state centered around $\hbar\omega_c/2$ as the first (not the zeroth) LL. The jumps associated with the discrete values of M as the density is increased is what imparts the oscillatory behaviour on the magentoreisitance.

Whilst we have considered what happens with increasing electron densioty, the same arguments apply if we consider the density n to be fixed, and vary the magnetic field. In this case, Eq. (5.5) still holds, but now the Fermi level jumps between Landau levels with a frequency $\sim 1/B$.

Shubnikov-de Haas oscillations provide a useful tool for determining the carrier density, which can be extracted by plotting the positions of subsequent current maxima as a function of $1/B$ (Homework).

5.2 Edge channels

Naively, one might expect that the maxima in the longitudinal conductance occur when the Fermi level lies in the middle of a LL, where the density of states is high. This is, however, absolutely not what is actually happens! The reason is that the states described by the Landau levels are completely localised: from Eq. (5.1), their velocity is $v(n,k) = \hbar^{-1}\partial E_n/\partial k = 0$, and they thus carry no net current. Classically, the motion of cyclotron electrons is in simple closed orbits with no net translation and no transport.

The conductance maxima (resistance minima) actually occur when the Fermi energy lies *between* the LLs — but what states exist here? The answer is the so-called *edge states*. In our description up to now we have considered a bulk 2D sample, but to properly understand the magneto-resistance of Fig. 5.1, we must also take into account quantum confinement. As we now show, this confinement gives rise to a set of states near the edges of the conductor that extend the length of the sample and are current-carrying.

The properties of these edge states also explain the sequence of remarkably flat plateaus in the Hall resistance. Although the QPC, for example, shows conductance quantisation with steps of height $2e^2/h$, experimentally the height of these steps is constant only to within a few percent, since a conductor will never be perfectly ballistic. In contrast, the plateaus of the QHE are measured to be flat to some 1 part in 10^8 and this amazing degree

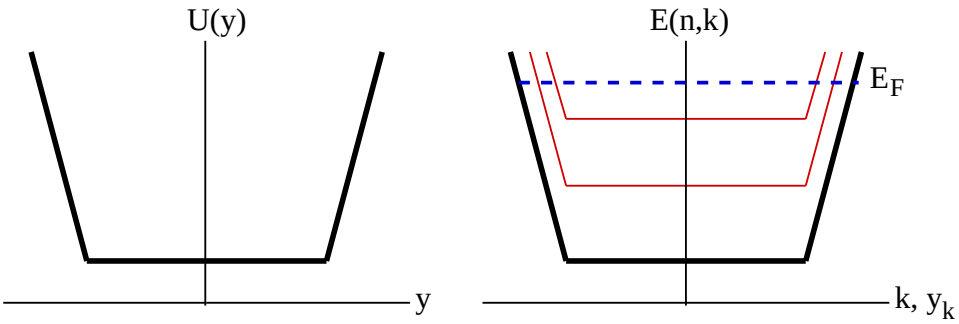

Figure 5.3: Formation of edge channels. Left: The confinement potential $U(y)$ is flat near the middle of the sample. Right: The dispersion $E(n,k)$ as a function of k or y_k the centre of wavefunction with wavenumber k. Near the centre, the spectrum is that of the unperturbed Landau levels. The lowest two are shown. Near the edges of the sample, the dispersion turns upwards due to the perturbation of the confinement. The Fermi energy E_F is shown lying two Landau levels. The only states in the vicinity of the Fermi energy are the two sets of edge channels two on either side of the conductor.

of flatness implies that the effect is not simply the result of good sample preparation, but rather something of a more fundamental nature, which we now outline. This flatness is what allows the QHE to be used as a resistance standard.

5.2.1 Origin of the edge states

In Section 3.4 we considered the exact eigenfunctions of a system with both magnetic field and transverse confinement. We chose parabolic confinement and obtained an exact analytic solution. Here we take a different approach and consider the potential sketched in Fig. 5.3. For most of the conductor width, the potential is flat; only near the edges do the electrons feel the effects of the confinement. Here we will treat the effects of the confinement as a perturbation of the Landau levels.

With confinement in y direction and gauge choice of Sec. 3.4, the effective mass equation reads

$$\left[E_s + \frac{1}{2m^*}\left(p_x + eBy\right)^2 + \frac{1}{2m^*}p_y^2 + U(y)\right]\psi(x,y) = E\psi(x,y). \qquad (5.6)$$

We first analyse the solutions with zero confinement by setting $U(y) = 0$. As discussed previously, the eigenfunctions of the system can be written as

$$\psi_{nk}(x, y) = \frac{1}{\sqrt{L}} e^{ikx} u_n(q + q_k) \tag{5.7}$$

with

$$u_n(q) = e^{-q^2/2} H_n(q); \qquad H_n(q) = n\text{th Hermite polynomial.} \tag{5.8}$$

We have introduced the two dimensionless distances

$$q = \sqrt{m\omega_c/\hbar}y \quad \text{and} \quad q_k = \sqrt{m\omega_c/\hbar}y_k \tag{5.9}$$

and the displacement

$$y_k = \frac{\hbar k}{eB}. \tag{5.10}$$

The Landau level wavefunction of Eq. (5.7) is extended in the x direction but localised to within a few times the magnetic length about the point y_k in the transverse direction.

As in Eq. (5.1), the energy of these states is given by

$$E(n, k) = E_n = E_s + \hbar\omega_c \left(n + \tfrac{1}{2}\right). \tag{5.11}$$

Consequently, the velocity of the electron with quantum numbers (n, k) is

$$v(n, k) = \frac{1}{\hbar}\frac{\partial E(n, k)}{\partial k} = 0 : \tag{5.12}$$

As discussed above, electrons in a LL carry no net current. [1]

Now let us include the effects of confinement through perturbation theory. Writing $|n, k\rangle$ as the ket corresponding to $\psi_{nk}(x, y)$, the change in energy of the LLs to lowest-order in the confinement potential is simply

$$E(n, k) \approx E_s + \hbar\omega_c \left(n + \tfrac{1}{2}\right) + \langle n, k|U(y)|n, k\rangle. \tag{5.13}$$

Assuming that the potential $U(y)$ is smooth on the scale of variation of the wavefunction $\psi_{nk}(x, y)$, we can write

$$E(n, k) \approx E_s + \hbar\omega_c \left(n + \tfrac{1}{2}\right) + U(y_k), \tag{5.14}$$

[1] This may seem strange given the plane-wave form of Eq. (5.6). However, this form actually depends on the gauge chosen for the vector potential. Each LL is highly degenerate, and these states can be combined to give a set of localised wave functions. Perturbation by e.g. the confinement removes this degeneracy and we obtain non-degenerate solutions with plane wave form.

where y_k is the centre of wave function in the transverse direction. We thus obtain a dispersion relation that is dependent on the location of the electron (strictly: the centre of the electronic wave function). This result is illustrated in Fig. 5.3: Near the centre of the conductor, the potential $U(y_k)$ is approximately zero, and the bulk Landau level dispersion applies. Only near the edges of the conductor does the perturbation term $U(y_k)$ contribute significantly, where it causes the energies to bend upwards. Near the edges there is a continuous distribution of energies.

The velocity of an electron with the dispersion of Eq. (5.14) is

$$v(n,k) = \frac{1}{\hbar}\frac{\partial E(n,k)}{\partial k} = \frac{1}{\hbar}\frac{\partial U(y_k)}{\partial k} = \frac{1}{\hbar}\frac{\partial U(y)}{\partial y}\frac{\partial y_k}{\partial k} = \frac{1}{eB}\frac{\partial U(y)}{\partial y} \qquad (5.15)$$

Electrons away from the edges are largely unperturbed and thus have $v(n,k) = 0$ and carry no current. In contrast, states near the edges will have finite $\partial U(y)/\partial y$ and thus be capable of carrying a current. Moreover, *states near the two edges of the conductor carry currents in different directions*, since $\partial U(y)/\partial y$ is of opposite sign at the two edges of the conductor.

This last observation has a remarkable consequence: since the wavefunctions of states with different momentum directions reside on opposite sides of the conductor, there can be virtually no back scattering, since this would involve scattering a carrier from one side of the conductor to the other and the overlap between these two wavefunctions is exponentially small. Thus, even in the presence of impurities, transport within an edge channel will be almost completely ballistic since the back-scattered states are inaccessible (and of course, elastic forward-scattering leaves momentum unchanged).

5.2.2 Transport in the edges channels

Now we understand the nature of the edge states, it is time to see how they effect transport. If, as in the plateau regions of Fig 5.1, the Fermi level lies between Landau levels, the only states in the vicinity of the Fermi level are the edge states, as Fig 5.3 makes clear, and we therefore we expect any current to be carried by the edge states.

A conductor in the Quantum Hall regime is shown in Fig. 5.4 connected between two reservoirs. Since there is an absence of backscattering, right-moving states, which are localised at the top of the conductor, originate solely from the left reservoir; left-moving carriers originate solely from the right. The electrons in each edge channel will therefore be in equilibrium with the reservoir from which they are sourced. It is then clear that two voltage probes on the same side on the sample will measure the same voltage

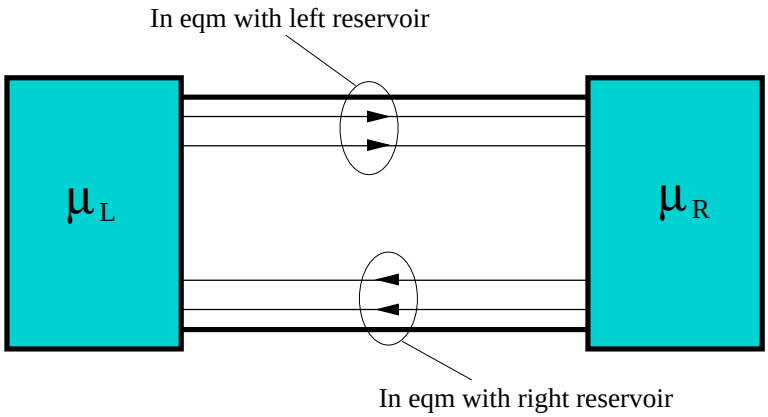

Figure 5.4: Two terminal conductor in Quantum Hall regime. Right moving channels are spatially separated from left moving channels. Left-moving channels can only be populated by electrons in the left reservoir, Left-moving channels from the right reservoir.

regardless of their position. Conversely, voltage probes on opposite sides of the sample will measure a voltage drop given by $\mu_L - \mu_R$. Whence

$$V_L = 0 \qquad \text{and} \quad eV_H = \mu_L - \mu_R. \tag{5.16}$$

A more comprehensive analysis suitable for complex Hall geometries can be undertaken by treating the individual edge channels in the exactly the same way as we did the the quantised conductance channels within the Landauer-Büttiker approach. Figure 5.5 shows a typical set up: a multi-probe experiment with a number of edge channels forming a set of discrete conductance channels between the probes. In such a set-up there is essentially no back-scattering and the transport is ballistic. Thus the transmission probability of a single edge channel connecting two terminals is approximately unity. The total conductance between two terminals connected by M edge states is therefore

$$G = \frac{2e^2}{m} M, \tag{5.17}$$

where M is the number of channels connecting the terminals, assumed to be spin-degenerate. Thus, whenever the Fermi level of the system lies between LLs, we expect the longitudinal resistance to be zero $R_L = V_L/I_L = 0$, and

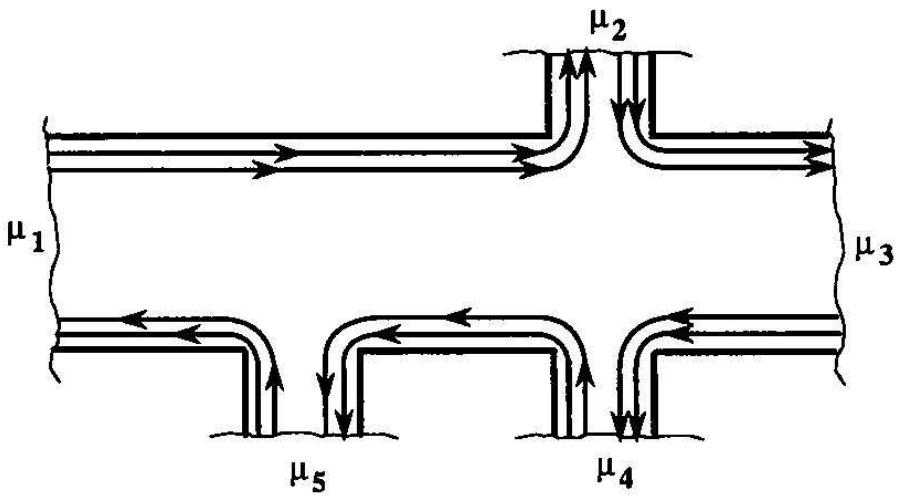

Figure 5.5: Hall bar with five terminals each with chemical potential μ_i. The Fermi energy is set in the Quantum Hall regime such that there are two edge-channels connecting the terminals. Picture from Ferry & Goodnick.

the Hall resistance to be given by

$$R_H = G^{-1} = \frac{h}{2e^2 M} = \frac{25.8128k\Omega}{2M}, \tag{5.18}$$

with M the number of edge channels at the Fermi energy. As is clear from Fig. 5.3, the number of edge channels is simply the number of LL below the Fermi level, and recalling Eq. (5.5) this is just

$$M = \text{int}\left(\frac{hn}{2eB} + 1\right). \tag{5.19}$$

Note that M can be used to index the plateaus, as in Fig. 5.1 and that this index decreases as the field increased.

5.2.3 Resistance in Hall bar geometry

Having established the connection between edge states and conductance channels, we may apply the approach of Büttiker to multi-terminal problems such as the five-terminal Hall bar geometry shown in Fig. 5.5. We assume that contacts 1 and 3 are current contacts, and that contacts 2,3, and 4 are

voltage probe contacts that draw no current. From Eq. (4.71) and Eq. (4.73), we have

$$\begin{pmatrix} I \\ 0 \\ -I \\ 0 \\ 0 \end{pmatrix} = \frac{2e^2}{h} \begin{pmatrix} M & 0 & 0 & 0 & -M \\ -M & M & 0 & 0 & 0 \\ 0 & -M & M & 0 & 0 \\ 0 & 0 & -M & M & 0 \\ 0 & 0 & 0 & -M & M \end{pmatrix} \begin{pmatrix} V_1 \\ V_2 \\ V_3 \\ V_4 \\ V_5 \end{pmatrix}. \quad (5.20)$$

The first two and last two lines gives

$$I = \frac{2e^2}{h}(V_1 - V_5); \quad V_1 = V_2; \quad V_3 = V_4; \quad V_4 = V_5. \quad (5.21)$$

The four-terminal Hall resistance in this set-up is then

$$R_H = R_{13,24} = \frac{V_4 - V_2}{I} = \frac{h}{2e^2}\frac{1}{M}, \quad (5.22)$$

where we have introduced the notation $R_{ii',vv'} = V_{vv'}/I_{ii'}$, and the longitudinal resistance is

$$R_L = R_{13,45} = \frac{V_4 - V_5}{I} = 0, \quad (5.23)$$

in line with expectations.

It should be noted that the above results only apply in the quantum Hall regime i.e. when the Fermi level is in between Landau levels. When this is not the case and the Fermi level lies within a Landau level, edge states still exist, but since a continuum of other non-edge states exist between the edge states at the same energy, back scattering will occur out of and between edge states. This increased backscattering (relative to QH regime) is why the longitudinal resistance reaches a maximum when the Fermi level is within the Landau level.

5.3 Back scattering

We can intentionally introduce back-scattering into the QH system by narrowing the conductor such that the left-moving and right moving channels come in close proximity to one another. This is typically accomplished through the addition of a split-gate QPC to the device, as shown in Fig. 5.6. As in the previous Chapter, we can describe the scattering that occurs at the junction with a scattering matrix containing amplitudes for scattering

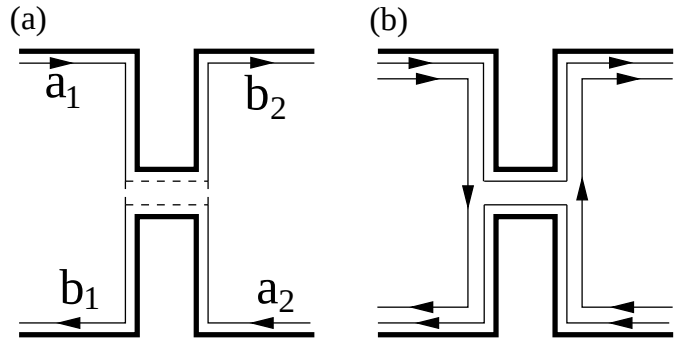

Figure 5.6: A QPC acting as a beam-splitter for electrons in QH edge-states. (a) The effect of the QPC can be modelled with a scattering matrix relating outgoing (b_i) to incoming states (a_i). (b) Special case in which one edge-channel is completely transmitted, whilst the other is completely reflected.

between all incoming and outgoing edge-channels. Figure 5.6 shows a single edge-channel being scattered, for which the scattering relation would be

$$\begin{pmatrix} \hat{b}_1(E) \\ \hat{b}_2(E) \end{pmatrix} = \begin{pmatrix} r(E) & t'(E) \\ t(E) & r'(E) \end{pmatrix} \begin{pmatrix} \hat{a}_1(E) \\ \hat{a}_2(E) \end{pmatrix}. \tag{5.24}$$

Such a set-up has a direct analogy to the beam-splitter in optics, with well defined input and output "beams"(here, edge-channels) and a scattering matrix between them.

Figure 5.6 shows a two-channel example in which one channel is perfectly transmitted through the QPC and the other is perfectly reflected. The consequences of this type of scattering for the Hall measurement are easily calculated within the Landauer-Büttiker approach. In the set-up of Fig. 5.7, a QPC has been inserted in the Hall bar set-up discussed previously. If M is again the total number of (spin-degenerate) edge-channels and K is the number of edge channels reflected at the QPC, then the current-voltage relation for the system is

$$\begin{pmatrix} I \\ 0 \\ -I \\ 0 \\ 0 \end{pmatrix} = \frac{2e^2}{h} \begin{pmatrix} M & 0 & 0 & 0 & -M \\ -(M-K) & M & 0 & -K & 0 \\ 0 & -M & M & 0 & 0 \\ 0 & 0 & -M & M & 0 \\ -K & 0 & 0 & -(M-K) & M \end{pmatrix} \begin{pmatrix} V_1 \\ V_2 \\ V_3 \\ V_4 \\ V_5 \end{pmatrix} \tag{5.25}$$

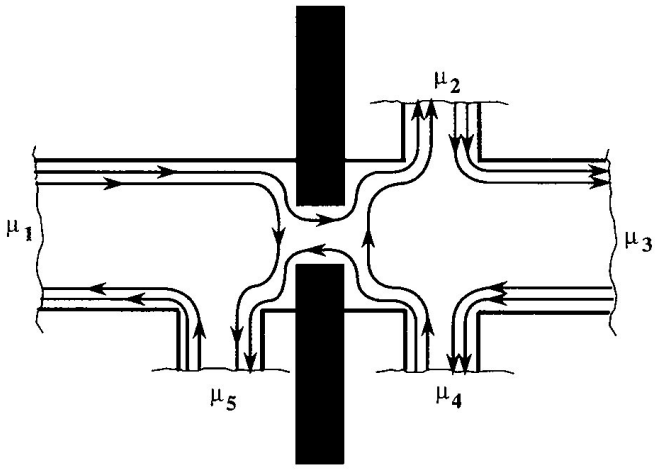

Figure 5.7: Five-terminal QH bar with QPC barrier (black) in middle. The QPC reflects K channels and transmits $M - K$. Picture from Ferry & Goodnick.

where we have assumed the same roles for the probes as previously. Inverting, we find the longitudinal resistance is now

$$R_L = R_{13,45} = \frac{h}{2e^2 M} \frac{K}{M-K}, \tag{5.26}$$

which is non-zero. If the Hall resistance is measured with both probes on one side of the scatterer, R_H is found to be the same as without the scatter. If, however, we measure on opposite sides of the scatterer (between terminals 2 and 5 in Fig. 5.7), we obtain

$$R_H = R_{13,52} = \frac{h}{2e^2} \frac{1}{M-K}, \tag{5.27}$$

which is increased with respect to the value without back-scattering.

We conclude by noting that in modern experiments, the edge states can be addressed individually, thus allowing selective population and current detection.

5.4 Fractional Quantum Hall effect

We have seen that the Hall resistance is given by

$$R_H = \frac{h}{e^2}\frac{1}{N} \tag{5.28}$$

where N is the total number of filled LLs which we previously wrote as $N = 2M$ for spin-degenerate levels. At high fields, the electrons are also Zeeman-split and if B is high enough, all the electrons will eventually be in a single spin-polarised LL. Based on the foregoing, we would then expect there to be no further plateaus in the Hall resistance. However, experimentally, just such plateaus are found, and these occur at Hall resistances of

$$R_H = \frac{h}{e^2}\frac{1}{p/q} \tag{5.29}$$

where p/q is a rational fraction, like $\frac{1}{3}$, $\frac{2}{5}$, etc, see Fig. 5.8. This effect is referred to as the fractional quantum Hall effect, with the "normal" QH effect referred to as the integer QHE. These plateaus arise due to the formation of many-body electronic states, far removed from the simple single-particle approach we have been discussing here. The wavefunctions of these states are named after Laughlin, who first postulated their form.

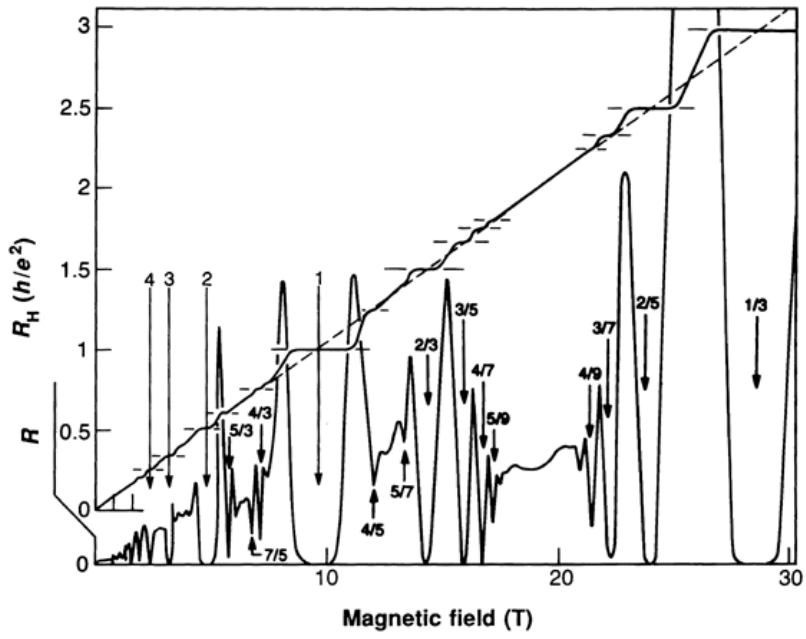

Figure 5.8: Fractional quantum Hall effect. The diagonal line (dashed) represents the "classical" Hall resistance and the full line with the steps are the observed quantum Hall effects. Magnetic fields at which the steps appear are marked with arrows. The step first discovered by Störmer and Tsui and Gossard was at 1/3. This picture from Störmer and Tsui

Chapter 6

Transport through Quantum Dots

We have encountered quantum dots (QDs) several times now in the lecture course. They are one of the most widely studied (and useful) of nanostructures and this level of interest shows no sign of waning. QDs have been defined in many different physical systems. Examples include

- lateral quantum dots defined by electrodes (top gates) in the 2DEG in a semiconductor heterostructure. This is an example of 'bottom up' QD construction.

- 2DEG patterned in other ways, e.g., etching, scratching, milling, local anodic oxidation.

- self-assembled quantum dots (SAQD) The lattice mismatch between two different semiconductors promote the spontaneous formation of QD 'islands' of e.g. InAs on a GaAs substrate. This is an example of 'top down' growth.

- kinks in nanotubes, nanowires: combination of top down and bottom up QD formation.

QDs of the first type are the most-often encountered type in transport experiments at the moment, as these allow a high degree of control and the formation of rather elaborate structures.

A useful classification of quantum dots, based not on their physical construtions but rather on their behaviour, is as being either *open* or *closed*:

- An open QD is connected to the bulk electron gas (reservoirs) via leads that carry several transverse modes $N_\alpha \gg 1$ for lead α. The conductance is correspondingly $G \gg e^2/h$.

- A closed QD is coupled to the reservoirs via narrow contractions: so narrow that just a single mode is supported in each lean. Furthermore, the transmission amplitudes of these modes is very low. The conductance is correspondingly $G \ll e/h$ and proceeds via the tunnelling of electrons between the bulk and the dot.

In this chapter and the next we will focus on closed dots,for which a tunnelling picture of transport is appropriate. For open dots, strongly-coupled to the reservoirs, scattering theory is more appropriate and we can directly employ the LB formalism. Open dots show many interesting features, such as providing a realisation of chaotic cavities (billiards) in quantum mechanical system. (I am not sure if we have time for this: If you are interested see C.W.J. Beenakker, Random-Matrix Theory of Quantum Transport, Rev.Mod.Phys. **69**, 731 (1997); cond-mat/9612179).

6.1 Single-electron tunnelling and charging effects

Given the results for the resonant tunnelling barrier of Section 4.4.2, we might conclude that the (linear) conductance through a QD should show a series of peaks whenever one of the dots single-particle energy levels lies within the transport window. As far as the dot potential can be modelled as being parabolic, sweeping a magnetic field would then yield conductance peaks at positions given by the Fock-Darwin (FD) spectrum of Fig. 3.5. Mapping the energy spectrum of a device (here, a QD) in this way is a process known as *tunnelling magneto-spectroscopy*.

However, whilst this analysis may hold for open QDs, for closed dots it is not the full story, as the experimental results of Fig. 6.1 show. Fig. 6.1b shows the relevant portion of the FD spectrum (in the first LL), and Fig. 6.1c shows the corresponding experimental results. Superficially, these two spectra look totally unrelated. We have clearly failed to take into account something very important here, and that something is single-electron charging effects, or the *Coulomb blockade*.

The measurements of Fig. 6.1 were obtained for a small semiconducting dot (width $\approx$ 500nm) weakly coupled to the leads, and both of these facts play a role in explaining the discrepancy between our simple FD theory and experiment. Since the dot is only weakly coupled to the leads, electrons

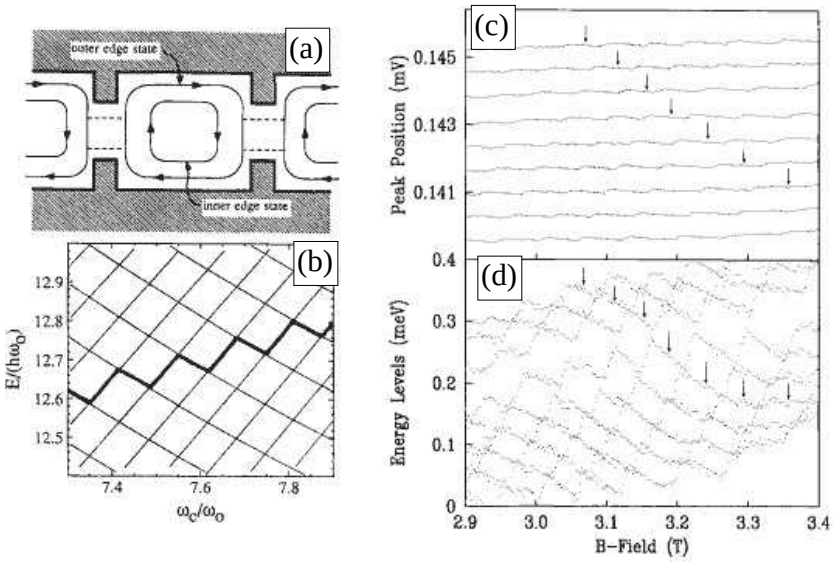

Figure 6.1: Tunnelling magneto-spectroscopy experiment reported by McEuen *et al.*, Phys. Rev. Lett. **66** 1926 (1991). **(a)** The system consists of a lateral QD connected to 2DEG leads. At high perpendicular magnetic field, edge channels are expected to form. **(b)** Revelant section of the Fock-Darwin spectrum. If a single-particle picture was appropriate here, the dot conductance should show peaks at the energies shown in this diagram. **(c)** Actual peak positions measured in the experiment. There appears to be little resemblance with the Fock-Darwin prediction. **(d)** However, if we subtract a constant charging energy from the peak positions, a very FD-like spectrum is recovered.

enter and exit via infrequent tunnelling events. Fluctuations in the number of electrons occupying the QD are suppressed and in this way, we arrive at a picture of the dot as an almost isolated island on which there resides a well-defined integer number of electrons $n = 0, \pm 1, \pm 2$. In this way, the discrete nature of charge on a microscopic scale is seen to enter our considerations.

What makes this discreteness able to play a role in transport is the second important characteristic of the QD, namely its small size. Moving even a small amount of charge (even just a single electron) to or from the dot will therefore result in a large redistribution of the electric field and hence the energy of the system. This can be described in terms of a (macroscopic)

capacitance. Modelling the QD as a disc of radius R, a distance d above a conducting gate electrode, a standard classical electrostatic calculation yields the capacitance of the dot to be $C \approx 8\epsilon R$ for $R \ll d$. The energy scale associated with moving a single electron to the dot is therefore

$$E_C = \frac{e^2}{2C}, \tag{6.1}$$

which sets the natural scale for charging effects. Typical values of this capacitance and single-electron charging energy (for dielectric constant $\epsilon_r = 13$ for GaAs) are

R (nm)	C (F)	E_C (meV)
1000	10^{-15}	0.09
250	2×10^{-16}	0.35
10	10^{-17}	8.7

We can now offer an explanation of the difference between parts (b) and (c) of Fig. 6.1. With QDs of size $R \sim 250$nm, the charging energy associated with adding an electron to the dot is, from the above table, $E_C \approx 0.35$meV, which compares well with the experimentally determined value of 0.274meV. This is significant compared with the typical energy scale associated with the single-particle spectrum $\Delta E \sim 0.05$meV. The peaks in the tunnelling spectra occur then, not at the single-particle energies as in part (a), but at these energies plus contributions from the single-electron charging, since we must also expend that extra energy to bring the electron onto the QD. This results in a conductance plot as in Fig. 6.1b, with traces spaced, by single-particle energies plus charging energies. If we assume that the charging energy is constant (the so-called *constant interaction method*, see later), then we should be able to obtain the FD spectrum by simply subtracting the charging energies. This was performed for the experimental data, Fig. 6.1d, where it is observed that we recover a spectrum very similar to the FD.

6.1.1 When is single-electron charging important?

In small, closed QDs, charging effects can be very important in determining transport properties. For charging effects to be visible, we require:

- First that quantum fluctuations do not smear out the discreteness of the electron charge. For this to be the case, the tunnel resistance of

the contacts, R_t, must be high:

$$R_t \gg \frac{h}{e^2}. \tag{6.2}$$

If the junction between dot and reservoir possesses this property, it is known as a *tunnel junction*.

- And secondly that thermal fluctuations are not able to overcome charging effects, which implies

$$\frac{e^2}{2C} \gg k_B T. \tag{6.3}$$

6.1.2 The constant interaction model

Finding the actual charging energy associated with the transferal of a single electron from the leads to the dot is a complicated many-body problem. Often we ignore this difficulty and assume that the *constant interaction model* provides a good description of the physics. In this model we assume that the energy required to transfer an electron to the dot is independent of the number of electrons on the dot, and that this process can be described by a single number C the total capacitance of the dot. Despite its simplicity, this model provides a reasonable description of experiments.

6.2 Single-electron box

To gain an appreciation of single-electron charging effects, lets consider the *single-electron box*, as illustrated in Fig. 6.2. We have a QD island connected to a ideal voltage source (V_G) through a tunnel junction on the left and a simple capacitor on the right. The tunnel junction may effectively thought of as tunnel resistance R_t in parallel with a capacitance C_J. This tunnel resistance is so large that, in the limit, the effects of the tunnel junction acts as an ideal capacitor through which charge is slowly leaked.

Tunnelling allows n excess electrons to accumulate on the island such that the net island charge is $-n|e|$. This charge will be divided between the two capacitor plates as

$$-n|e| = Q_L + Q_R. \tag{6.4}$$

From Kirchoff's law, the total voltage drop around the circuit is

$$V_G = \frac{Q_L}{C_L} - \frac{Q_R}{C_G},, \tag{6.5}$$

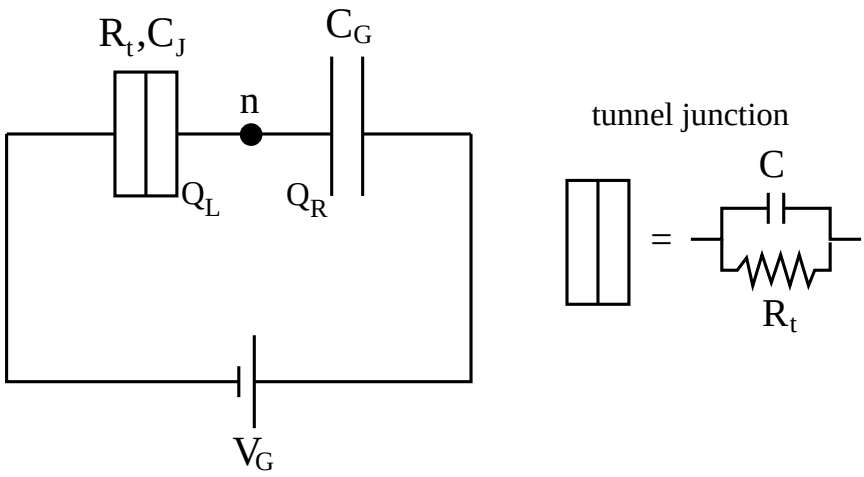

Figure 6.2: The effective circuit for a single-electron box, and for the tunnel junction it contains.

and the electrostatic energy stored by the capacitors is

$$E_{\rm s} = \frac{Q_L^2}{2C_J} + \frac{Q_R^2}{2C_G}. \tag{6.6}$$

The total energy to add n electrons to the box is called *the charging energy* and is given by the free energy

$$E_{\rm ch} = E_{\rm s} - L, \tag{6.7}$$

where L is the work done by external forces on the system; in this case it is the work done by the voltage source $L = -V_G Q_R$. Elimination of Q_L and Q_R gives

$$E_{\rm ch} = \frac{(n|e| - Q_G)^2}{2C} \tag{6.8}$$

where $C = C_G + C_J$ is the total capacitance of the island, $Q_G = C_G V_G$ is the so-called gate charge, and where we have dropped an unimportant constant independent of n.

This result is plotted in Fig. 6.3. In the interval $-e/2 < Q_G < e/2$, the lowest energy is obtained with no excess electrons on the dot. When $Q_G = e/2$, states with $n = 0$ and $n = 1$ electron becomes degenerate (and we can expect number fluctuations). Then for $e/2 < Q_G < 3e/2$, the

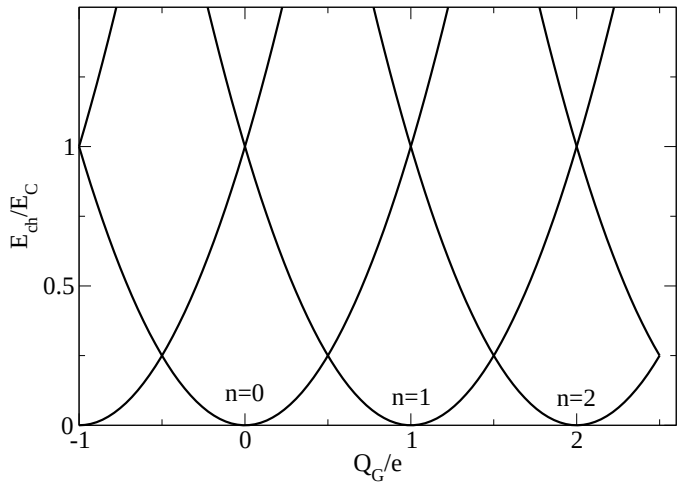

Figure 6.3: Charging energy of the single-electron box as a function of gate charge (gate voltage) for different numbers of excess electrons n on the island.

stability of the system changes, such that $n = 1$ electron is the lowset energy configuration. And so on. As Q_G increases then, the number of electrons on the dot increases in discrete steps.

6.3 Coulomb blockade in the single electron transistor

To see how this discreteness of charge can affect transport, we now consider the *single electron transistor* (SET), in which the island is connected to the external circuit through two tunnel junctions (left and right), and capacitatively coupled to a back gate voltage (V_G). The equivalent circuit diagram is shown in Fig. 6.4. We assume that the single-particle energy level spacing is much smaller that the charging energy, such that charging effects alone determine the behaviour of transport through the system. Note that this is the case when the island is a metallic grain instead of a quantum dot — since the Fermi wavelength in metals is much smaller than in semiconductors, size quantisation plays much less of a role.

Following a calculation similar to the above and defining the total island

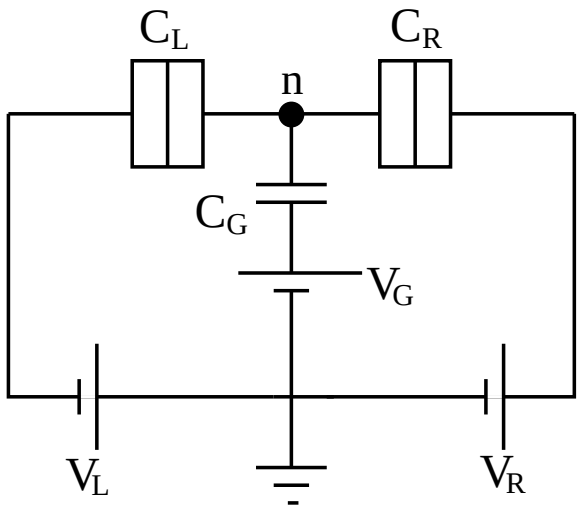

Figure 6.4: Equivalent circuit for the single-electron transistor.

capacitance,

$$C = C_G + C_L + C_R, \tag{6.9}$$

and the gate charge,

$$Q_G = C_G V_G + C_L V_L + C_R V_R, \tag{6.10}$$

the charging energy is found to be

$$E_{\mathrm{ch}}(n, Q_G) = \frac{(n|e| - Q_G)^2}{2C}, \tag{6.11}$$

which has the same form as for the box.

In a tunnelling event the number of electrons in the box changes by one, and the change in energy is accordingly

$$E_{\mathrm{ch}}(n+1, Q_G) - E_{\mathrm{ch}}(n, Q_G) = \left(n + \frac{1}{2} - \frac{Q_G}{e}\right)\frac{e^2}{C}. \tag{6.12}$$

This energy difference is known as the *addition energy* of the $n+1$th electron. Figure 6.5a shows these addition energies plotted alongside the chemical potentials of the reservoirs. Tunnelling can only occur when one of these energies lies within in the transport window, i.e. when the chemical potential of

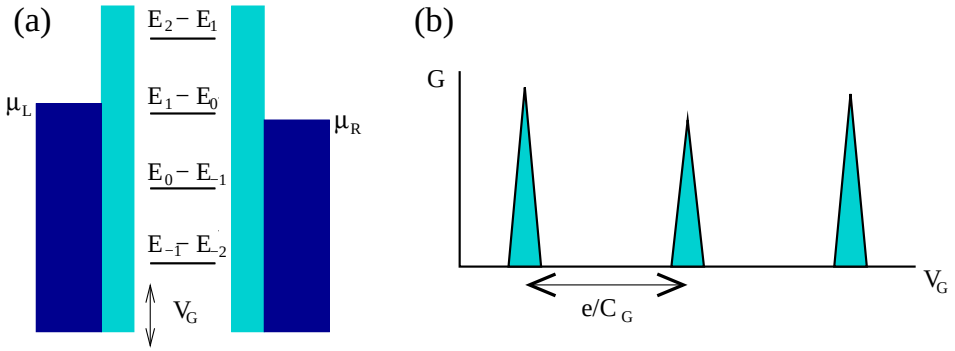

Figure 6.5: Linear transport through SET. **(a)** Transport can occur occur whenever the transport window contains the addition energy $E_{n+1} - E_n = E_{\rm ch}(n+1, Q_G) - E_{\rm ch}(n, Q_G)$. **(b)** As the gate voltage V_G is altered, transport levels enter and leave the bias window giving rise to *Coulomb oscillations* in the conductance.

the electrons in the leads is sufficiently high to overcome this charging energy. If the addition energy lies outside the bias window, transport through the dot is blocked — this is known as the *Coulomb blockade*.

In the linear regime, $\mu_L \approx \mu_R = \mu$, we will obtain a finite conductance when $E_{\rm ch}(n+1, Q_G) - E_{\rm ch}(n, Q_G) = \left(n + \frac{1}{2} - \frac{Q_G}{e}\right) \frac{e^2}{C} = \mu$. Choosing the energy axis such that $\mu = 0$, transport occurs whenever the state with n electrons is degenerate with the state with $n+1$. This situation is analogous to the single-electron box where, for specific choices of gate voltage, two state with different electron number became degenerate and the number of electrons in the box could fluctuate. Here, we have the same thing but in this case, fluctuating electron number yields transport through the dot.

Altering the gate voltage moves the 'ladder of states' up an down, bringing successive states into the bias window. As the addition energies are regularly spaced (see Eq. (6.12)), this results in oscillating in the current that is periodic in V_G as sketched in Fig. 6.5b. The spacing between the peaks is easily seen to be $\Delta V_G = e/C_G$.

6.3.1 Nonlinear transport and Coulomb diamonds

These results for the conductance through the QD can be extended to the non-linear transport regime, where we apply a finite source-drain voltage across the sample, $eV_{\rm SD} = \mu_L - \mu_R$. The standard method to investigate

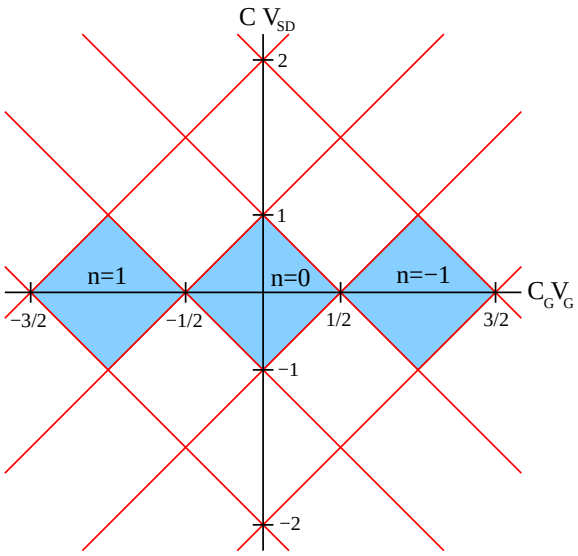

Figure 6.6: A stability diagram for a SET. The blue shaded regions are the Coulomb diamonds, where the number of electrons on the dot is fixed at n and transport through the dot is blocked. Red lines indicate voltages where the number of addition energies within the transport window changes by one. We have set $e = 1$ here for convenience.

such situation is with the help of a *stability diagram*, as shown in Fig. 6.6. The two axes are the gate and source-drain voltage and we then plot the differential conductance $G = dI/dV_{\rm SD}$ at each point using a colour scale (or some 3D representation). In Fig. 6.6, we just sketch the key features. For $V_{\rm SD} = 0$ we obtain the linear response results with finite conductance located only at $C_G V_G = n/2$. In between, the conductance is zero. As Fig. 6.6 shows, these regions of zero conductance extend for finite $V_{\rm SD}$ and close to form a sequence of so-called *Coulomb diamonds*. In these diamonds the number of electrons on the dot is fixed, and there is no transport through the dot. Increasing $V_{\rm SD}$ further increases the number of levels within the transport window, giving rise to the extended diamond pattern of Fig. 6.6.

A set of experimentally-determined stability diagrams is shown in Fig. 6.7 for several different experimental realisations of a single-electron transistor. The Coulomb diamonds are very pronounced. Note that in some cases, the Diamonds are not all the same size and that there is a lot more structure to these diagrams than expected from Fig. 6.6. This is because the quantum

dots themselves are far more intersting that the simple circuits we have been considering so far — in particular they have internal structure. In addition, the constant interaction model is also a huge simplification.

6.3.2 Single particle spectrum

So, what about the single particle spectrum? How does this affect these results? Well, in a non-interacting picture at zero temperature, and n electron state is obtained simply by filling up the single-particle states from the ground-state up, such that the total energy of an n-electron state in the dot is, from Eq. (6.11),

$$E_{\rm ch}(n, Q_G) = \frac{(n|e| - Q_G)^2}{2C} + \sum_{m=1}^{n} \epsilon_m, \tag{6.13}$$

where ϵ_m are the single-particle energies. The addition energy of the $n+1$th electron will therefore be

$$E_{\rm ch}(n+1, Q_G) - E_{\rm ch}(n, Q_G) = \left(n + \frac{1}{2} - \frac{Q_G}{e}\right)\frac{e^2}{C} + \epsilon_{n+1}. \tag{6.14}$$

This means that the conductance peaks will no longer be evenly spaced ($\Delta V_G = e/C_G$), but rather will have a spacing

$$\Delta V_G(n) = \frac{C}{eC_G}\left(\Delta\epsilon(n) + \frac{e^2}{C}\right), \tag{6.15}$$

where $\Delta\epsilon(n)$ is the difference in successive single-particle energies. Therefore, providing that the constant interaction model holds, we can indeed recover the single-particle energies from the stability diagram.

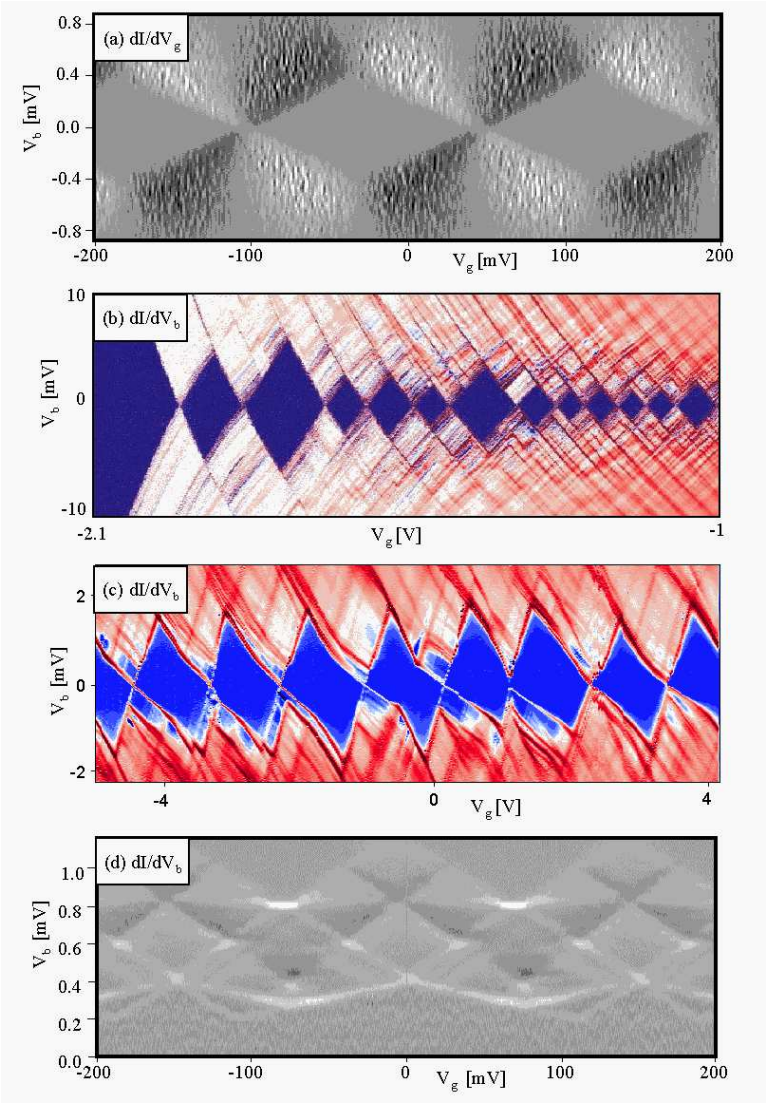

Figure 6.7: The low temperature conductances of (a) a metal single-electron transistor (SET), (b) a semiconducting SET, (c) a carbon nanotube SET, and (d) a superconducting SET are plotted as a function of gate voltage and bias voltage. The diamond shaped regions along the zero bias voltage axis are regions of Coulomb blockade. The conductance is a periodic function of gate voltage for the metal SET and the superconducting SET where the confinement energy is negligible. The conductance is not a periodic function of gate voltage for the semiconductor SET and the carbon nanotube SET where the confinement energy is important. From: P. Hadley and J.E. Mooij, Delft University of Technology, `http://qt.tn.tudelft.nl/publi/2000/quantumdev/qdevices.html`

Chapter 7

The quantum master equation in transport

Simple circuit models of devices like the SET give a reasonable account of the transport properties — but only up to a certain point. Although the circuit theory predicts well the positions of the conductance peaks, it says nothing about their heights, i.e. the conductances themselves. Furthermore, modern experimental techniques are sophisticated enough to allow the fabrication of rather complicated structures such as double, triple quantum dots, QD interferometers, etc., in which quantum effects play an important role. It is clear that the classical theory of the preceding chapter can not hope to give a full account of such systems.

To address these issues, we now introduce a more advanced theory of transport through quantum dots. — the quantum master equation (QME). This is a very powerful, flexible and popular method of handling transport through Coulomb blockade systems.

Master equation techniques have their origins in quantum optics. There are many good books on this topic, for example

- Howard Carmichael, *An Open Systems Approach to Quantum Optics* (Lecture Notes in Physics New Series M) (Springer 1993).
- Claude Cohen-Tannoudji, Jacques Dupont-Roc, and Gilbert Grynberg, *Atom-Photon Interactions: Basic Processes and Applications*, (Wiley-Interscience 1998).
- Karl Blum, *Density Matrix Theory and Applications*, (Springer 1996).

The presentation I follow here is somewhat different to the standard

approach — I employ here *perturbation theory in Liouville space*, a technique based on the references

- H. Schöller, Schladming lecture notes, `http://physik.uni-graz.at/itp/iutp/iutp_08/lecture_notes_part_1.pdf`
- M. Leijnse and M. R. Wegewijs, arXiv:0807.4027 .

These works themselves borrow on the *real-time diagrammatic approach* pioneered by Gerd Schön's group in Karlsruhe.

This Liouville perturbation approach has several advantages. Firstly, we work consistently in a language in which the description of current statistics is most conveniently expressed – this is one of the central areas of current mesoscopics research (inc. at the ITP Berlin). Flexibility — we will derive here expressions for completely arbitrary mesoscopic system which could be as simple as a single quantum dot or as complex as a large molecule (think: molecular electronics!). Furthermore, this approach offers possibilities to go beyond the standard QME — e.g. to include cotunnelling, resonant tunnelling approximation, or even renormalisation group approach. Again, this is a cutting-edge area of research.

7.1 A simple QME example

Before we get into the details of the QME derivation, let us begin by considering a simple example of a QME in practise. Let us consider a quantum dot with a single level in the bias window. This level is populated with an electron from the left lead and emptied to right (see Fig. 7.1a). We will assume that Coulomb blockade effect is strong enough to prevent double occupation on the level. Furthermore, we assume that spin is unimportant here and neglect it from our discussion. We then ask: what is the current through the dot?

To answer this, let us posit two rates Γ_L and Γ_R for hopping to and from the level. We can then immediately write down a set of coupled rate equations for the probabilities P_0 and P_1 of finding the level empty or occupied, respectively. These equations read

$$\begin{aligned} \dot{P}_0 &= -\Gamma_L P_0 + \Gamma_R P_1 \\ \dot{P}_1 &= -\Gamma_R P_1 + \Gamma_L P_0. \end{aligned} \tag{7.1}$$

It is convenient to write this is matrix form as

$$\frac{d}{dt}\begin{pmatrix} P_0 \\ P_1 \end{pmatrix} = \begin{pmatrix} -\Gamma_L & \Gamma_R \\ \Gamma_L & -\Gamma_R \end{pmatrix}\begin{pmatrix} P_0 \\ P_1 \end{pmatrix} \tag{7.2}$$

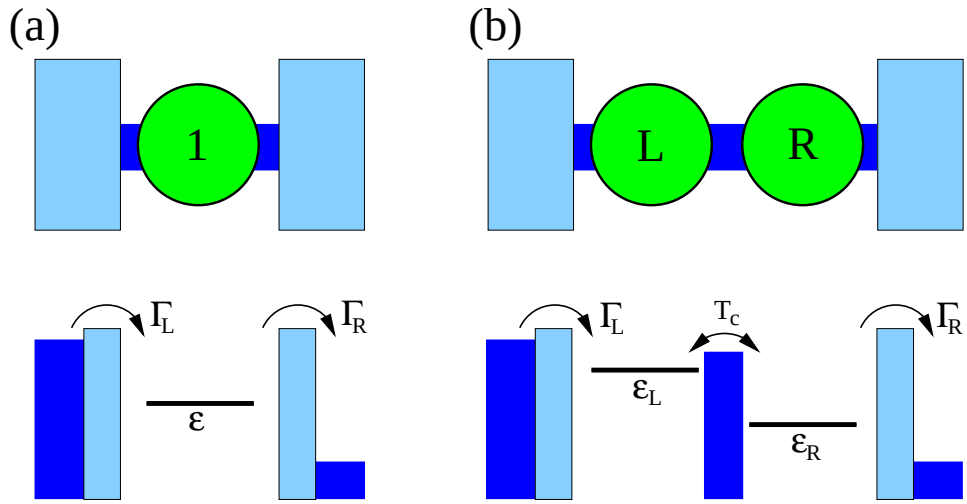

Figure 7.1: Two important quantum dot models discussed in the text **(a)** Single resonant level. **(b)** Double quantum dot. In both cases, strong Coulomb blockade is present which prevents more than one excess electron entering the dot system at any one time.

This is a rate equation, which is a particularly simple type of QME. To find the stationary solution we set

$$\frac{d}{dt}\begin{pmatrix} P_0 \\ P_1 \end{pmatrix}_{\text{stat}} = 0, \tag{7.3}$$

which admits the solution

$$\begin{pmatrix} P_0 \\ P_1 \end{pmatrix}_{\text{stat}} = \frac{1}{\Gamma_L + \Gamma_R}\begin{pmatrix} \Gamma_R \\ \Gamma_L \end{pmatrix}, \tag{7.4}$$

where we have taken into consideration the conservation of probability

$$P_0 + P_1 = 1. \tag{7.5}$$

The current through the level can simply be obtained by multiplying the probability of finding the dot occupied, P_1, with the rate at which a full dot transfers electrons to the right lead:

$$I = eP_1\Gamma_R = e\frac{\Gamma_L\Gamma_R}{\Gamma_L + \Gamma_R} \tag{7.6}$$

In the full quantum-mechanical treatment the populations P_i are obtained from the diagonal elements of the system density matrix $P_i = \rho_{ii}$. In this simple example the state of the dot is simply described by populations. However, for a more complicated system, there can be internal coherences, in which case we need also to take into account off-diagonal elements. A good example is the double quantum dot (DQD) in the strong Coulomb blockade regime, see Fig. 7.1b. Here, five numbers are required to describe the quantum state of the device: the three probabilities of finding the dot empty, of in the left or right dot, plus the two coherences between the left and right states. Coherences between states of different charge are not required, as we later show.

In general, the aim of the QME approach is to derive an equation similar to Eq. (7.2) for the reduced density matrix of the system in question. In the Markov approximation (see later), this equation will have the general form

$$\dot{\rho} \;=\; L\rho \tag{7.7}$$

where L is the Liouvillian of the system. Clearly ρ is a matrix, and the Liouvillian therefore maps matrices onto other matrices; or rather operators onto operators. For this reason L is known as a *superoperator*. Eq. (7.2) however suggests a useful way of looking at these superoperators: if we arrange the elements of the density matrix into a vector, superoperator L becomes a matrix mapping these "density matrix vectors" onto one another. This representation of L as a matrix is very useful, as we will see.

7.2 Generic Transport Model

We consider now a generic model of quantum transport specified by the Hamiltonian

$$H = H_{\mathrm{S}} + H_{\mathrm{res}} + V \tag{7.8}$$

where H_{S} describes the system, H_{res} the electron reservoirs (leads), and V the system-reservoir coupling.

7.2.1 System

Although we will mainly discuss quantum dot systems here, we will derive the maser equation in a general way, such that the system can be of arbitrary complexity. This formalism can therefore be directly applied to e.g. QD networks, molecules, nanomagnets.

Regardless of how complicated this system is, we assume that we can diagonalise its Hamiltonian exactly — let us write the eigenvectors as $|a\rangle$ where index a describes all quantum numbers necessary to specify the state uniquely. We write

$$H_{\mathrm{S}} = \sum_a E_a |a\rangle\langle a|, \tag{7.9}$$

where E_a is the energy of eigenstate. For transport through the system to be possible, the system itself must be capable of existing in a number of different charge states — recall the 'empty/filled' basis of our simple example. The eigenkets $|a\rangle$ are therefore defined in Fock space, with state $|a\rangle$ having N_a electrons. The states $|a\rangle$ form an orthonormal set in Fock space.

We normally consider a relatively small subsector of the full Fock space — typically an 'empty' state plus states with just a few excess electrons. This is permissible since the Coulomb blockade excludes states with higher electron numbers on energetic grounds. For example, in our single resonant-level model, we neglect the doubly-occupied level because the charging energy of this state is assumed high enough that this state lies well outside the transport window.

7.2.2 Reservoirs

We consider a set of N reservoirs that we label with α; if spin is important we can include the spin index in α. We assume the reservoirs can be described with a noninteracting Hamiltonian

$$H_{\mathrm{res}} = \sum_{k,\alpha} \omega_{k\alpha} a^\dagger_{k\alpha} a_{k\alpha}, \tag{7.10}$$

with $\omega_{k\alpha}$ the energy of the kth mode in lead α. In the absence of interaction with the system, the lead electrons are described by the equilibrium Fermi functions. We us define

$$f^{(+)}_\alpha(\omega) = \frac{1}{e^{(\omega-\mu_\alpha)/T_\alpha}+1} \tag{7.11}$$

as the Fermi-function of lead α with chemical potential μ_α and temperature T_α. For convenience, we also define

$$f^{(-)}_\alpha(\omega) = 1 - f^{(+)}_\alpha(\omega) = \frac{1}{e^{-(\omega-\mu_\alpha)/T_\alpha}+1}, \tag{7.12}$$

as well as the function without superscript:

$$f_\alpha(\omega) = \frac{1}{e^{\omega/T_\alpha}+1}, \tag{7.13}$$

which makes no reference to the chemical potential. We assume that the reservoir states lie within a band with band edges at $\pm D$.

7.2.3 Tunnel coupling

Tunnelling between system and reservoirs is described by the hopping Hamiltonian

$$V = \sum_{\alpha k m} t_{\alpha k m} a^\dagger_{k\alpha} d_m + t^*_{\alpha k m} d^\dagger_m a_{k\alpha}, \tag{7.14}$$

where $a_{k\alpha}$ is a lead operator, d_m is the annihilation operator for single-particle level m in the system and $t_{\alpha k m}$ is a tunnelling amplitude. To translate this Hamiltonian into the same many-body language of Eq. (7.9), we twice insert a complete set of many-body states to obtain

$$\begin{aligned} V &= \sum_{\alpha k m}\sum_{a a'} t_{\alpha k m} a^\dagger_{k\alpha} |a\rangle\langle a|d_m|a'\rangle\langle a'| + \text{h.c.} \\ &= \sum_{\alpha k m}\sum_{a a'} a^\dagger_{k\alpha} t_{\alpha k m} \langle a|d_m|a'\rangle |a\rangle\langle a'| + \text{h.c.} \\ &= \sum_{\alpha k} a^\dagger_{k\alpha} g_{k\alpha} + g^\dagger_{k\alpha} a_{k\alpha}, \end{aligned} \tag{7.15}$$

with the many-body system operator

$$g_{k\alpha} = \sum_{m a a'} t_{\alpha k m} \langle a|d_m|a'\rangle \delta\left(N_a - N_{a'} + 1\right) |a\rangle\langle a'|. \tag{7.16}$$

Here we have explicitly written in the delta-function since the action of d_m is to reduce the number of system electrons by one. It is convenient to write these system operators as

$$g_{k\alpha} = \sum_m t_{\alpha k m} j_m \tag{7.17}$$

with operator

$$j_m = \sum_{a a'} \langle a|d_m|a'\rangle \delta\left(N_a - N_{a'} + 1\right) |a\rangle\langle a'|, \tag{7.18}$$

which is just the annihilation operator d_m written is the many-body basis.

7.2.4 Notation

To ease the book-keeping here, we introduce an ultra-compact single index "1" to denote the triplet of indices (ξ_1, k_1, α_1). The first index $\xi_1 = \pm$ describes whether a reservoir operator is a creation or annihilation operator:

$$a_1 = a_{\xi_1 k_1 \alpha_1} = \begin{cases} a^\dagger_{k_1\alpha_1}, & \xi_1 = + \\ a_{k_1\alpha_1}, & \xi_1 = - \end{cases} . \tag{7.19}$$

The anti-commutation relation then reads

$$\{a_1, a_{1'}\} = \delta_{1,\overline{1'}} \tag{7.20}$$

with $\overline{1} = (-\xi_1, k_1, \alpha_1)$. We will leave all sums as implicit, such that the bath Hamiltonian becomes

$$H_{\rm res} = \omega_{k\alpha} a_{+k\alpha} a_{-k\alpha}. \tag{7.21}$$

In the compact notation, the interaction Hamiltonian becomes

$$\begin{aligned} V &= a_{+k\alpha} g_{+k\alpha} + g_{-k\alpha} a_{-k\alpha} \\ &= \xi_1 a_1 g_1. \end{aligned} \tag{7.22}$$

Note that whereas, in this convention, the "$\xi = +$" subscript corresponds to "$\dagger$" for the lead operators, "$\xi = +$" on a system operator denotes an annihilator. Starting from Eq. (7.17), the interaction can also be written as

$$V = \xi_1 t_{1m} a_1 j_{\xi_1 m} \tag{7.23}$$

with coefficients

$$t_{+k\alpha m} = t_{k\alpha m}; \quad t_{-k\alpha m} = t^*_{k\alpha m} \tag{7.24}$$

and operators

$$j_{+m} = j_m; \quad j_{-m} = j^\dagger_m \tag{7.25}$$

Note that although these operators only depend on ξ, we shall label them with the full "1" index for convenience: $j_{1m} = j_{\xi_1 m}$.

7.2.5 Example: single resonant level

In the single resonant level model, there are just two relevant many body states: "empty" $|0\rangle$ and "full" $|1\rangle$. Taking the energy of the empty state to be zero and the energy of the occupied dot to be ϵ, the system Hamiltonian is

$$H_S = \epsilon|1\rangle\langle 1|. \tag{7.26}$$

The tunnel coupling is simply

$$V = \sum_{\alpha k} t_{\alpha k} a^\dagger_{k\alpha} d + t^*_{\alpha k} d^\dagger a_{k\alpha}, \tag{7.27}$$

with d the annihilation operator for the single level. The corresponding jump operators are given by

$$\begin{aligned} j_+ &= j_\alpha = \sum_{aa'} \langle a|d|a'\rangle \delta\left(N_a - N_{a'} + 1\right)|a\rangle\langle a'| \\ &= \langle 0|d|1\rangle|0\rangle\langle 1| \\ &= |0\rangle\langle 1|; \\ j_- &= |1\rangle\langle 0|. \end{aligned} \tag{7.28}$$

7.2.6 Example: double quantum dot

Another important transport model is the double quantum dot model Fig. 7.1b with its internal quantum-mechanical degree of freedom (qubit). The system Hamiltonian is

$$H_S = \epsilon_L|L\rangle\langle L| + \epsilon_R|R\rangle\langle R| + T_c\left(|L\rangle\langle R| + |R\rangle\langle L|\right), \tag{7.29}$$

where we have chosen the energy of state $|0\rangle$ to be zero again. With single-electron levels arranged symmetrically about zero, we obtain

$$H_S = \frac{1}{2}\epsilon\left(|L\rangle\langle L| - |R\rangle\langle R|\right) + T_c\left(|L\rangle\langle R| + |R\rangle\langle L|\right). \tag{7.30}$$

Both ϵ and T_c are important in determining transport properties. However, for simplicity here, let's assume $\epsilon = 0$. Diagonalising, we find

$$H_S = T_c\left(|+\rangle\langle +| - |-\rangle\langle -|\right), \tag{7.31}$$

with

$$|\pm\rangle = 2^{-1/2}\left(|L\rangle \pm |R\rangle\right). \tag{7.32}$$

With the left dot coupled only to the left lead and similarly on the right, the tunnel coupling is

$$V = \sum_k t_{Lk} a_{kL}^\dagger d_L + t_{Lk}^* d_L^\dagger a_{kL} + \sum_k t_{Rk} a_{kR}^\dagger d_R + t_{Rk}^* d_R^\dagger a_{kR}, \tag{7.33}$$

with $d_L|L\rangle = |0\rangle$ and so on. This means that

$$\begin{aligned} j_{+L} &= \sum_{a'=\pm} \langle 0|d_L|a'\rangle|0\rangle\langle a'| = 2^{-1/2}\left(|0\rangle\langle +| + |0\rangle\langle -|\right) = |0\rangle\langle L| \\ j_{+R} &= \sum_{a'=\pm} \langle 0|d_R|a'\rangle|0\rangle\langle a'| = 2^{-1/2}\left(|0\rangle\langle +| - |0\rangle\langle -|\right) = |0\rangle\langle R| \end{aligned} \tag{7.34}$$

and thus we can write

$$V = \sum_k t_{Lk} a_{kL}^\dagger |0\rangle\langle L| + \sum_k t_{Rk} a_{kR}^\dagger |0\rangle\langle R| + \text{h.c.}. \tag{7.35}$$

This obviously holds true for $\epsilon \neq 0$ as well.

It might be said that the forms Eq. (7.28) and Eq. (7.35) are obvious and that the preceding discussion in terms of many-body states, etc, is superfluous. However, whilst this may be the case for simple models (0 and 1 electrons), it is not for more complex systems, where we have to be more careful.

7.3 Liouville space

Let $\rho(t)$ and $\rho_S(t)$ denote the density matrices of the full system and the dot only respectively at time t. At time $t = t_0$ let us posit a separable full density matrix with reservoirs in thermal equilibrium:

$$\rho(t_0) = \rho_S(t_0)\rho_{\text{res}}^{\text{eq}}, \tag{7.36}$$

with arbitrary initial state of the dot. Note that this form implies that at t_0 there are no charge-superpositions between system and reservoir.

The full density matrix evolves under the von Neumann equation:

$$\dot{\rho}(t) = -i\left[H, \rho(t)\right] \tag{7.37}$$

We rewrite this in terms of the total Liouvillian super-operator

$$\dot{\rho}(t) = L\rho(t). \tag{7.38}$$

The Liouvillian L is defined by its action on an arbitrary operator O: $LO = -i\,[H, O]$, which we write as

$$L = -i\,[H, \bullet]\,. \tag{7.39}$$

The matrix elements of a general super-operator are obtained by considering its action on arbitrary operator:

$$(LO)_{nm} = \sum_{n'm'} L_{nm,n'm'} O_{n'm'}. \tag{7.40}$$

With $L = -i\,[H, \bullet\,]$, we have

$$\begin{aligned} (LO)_{nm} &= -i\,[H, O]_{nm} \\ &= -i\left(\sum_{n'} H_{nn'}O_{n'm} - \sum_{m'} O_{nm'}H_{m'm}\right), \\ \Rightarrow L_{nm,n'm'} &= -i\,(H_{nn'}\delta_{mm'} - \delta_{nn'}H_{m'm})\,. \end{aligned} \tag{7.41}$$

With the Hamiltonian of Eq. (7.8), the full Liouvillian can be written as the sum of three parts

$$L = L_{\rm res} + L_{\rm S} + L_V, \tag{7.42}$$

with $L_{\rm res} = -i\,[H_{\rm res}, \bullet\,]$, $L_{\rm S} = -i\,[H_{\rm S}, \bullet\,]$, and the all-important interaction Liouvillian

$$L_V = -i\,[V, \bullet\,] = -i\xi_1\,[a_1 g_1, \bullet\,]\,. \tag{7.43}$$

7.3.1 Free system Liouvillian

Without coupling to the leads, the system evolves under the action of the free system Liouvillian $L_{\rm S} = -i\,[H_{\rm S}, \bullet\,]$.

At this point it makes sense to start thinking of the Liouvillian as a matrix that acts on vectors that correspond to density matrices. A density matrix is converted into a vector via a mapping of the double index aa' to a single index. The elements of the Liouvillian (or another superoperator) are then obtained via Eq. (7.41) and application of the index mapping.

A general system density matrix can be written $\rho_S = \sum_{aa'} \rho_{aa'}|a\rangle\langle a'|$. In vector notation, we will write this as $|\rho_S\rangle\!\rangle = \sum_{(aa')} \rho_{aa'}|aa'\rangle\!\rangle$ with "ket" $|aa'\rangle\!\rangle$ corresponding to $|a\rangle\langle a'|$.

The action of L_S on vector $|aa'\rangle\!\rangle$ is simply obtained as

$$L_S|aa'\rangle\!\rangle = -i\,\big[H_S, |a\rangle\langle a'|\,\big] = -i(E_a - E_{a'})|a\rangle\langle a'| = -i\Delta_{aa'}|aa'\rangle\!\rangle \tag{7.44}$$

which defines the Bohr frequencies $\Delta_{aa'}$. Vectors $|aa'\rangle\!\rangle$ are therefore the right eigenvectors of Liouvillian L_S. Let us denote the left eigenvectors of L_s as $\langle\!\langle aa'|$ such that

$$\langle\!\langle aa'|L_S = -i\Delta_{aa'}\langle\!\langle aa'| \tag{7.45}$$

with

$$\langle\!\langle aa'|bb'\rangle\!\rangle = \delta_{(aa'),(bb')}. \tag{7.46}$$

It is crucial to make the distinction between left and right eigenvectors because, in general, the Liouvillian will not be Hermitian, and the left and right eigenvectors are not adjoint. Computationally, the left eigenvectors are most easily found by first determining the right eigenvectors, forming a matrix of them and then inverting this matrix. We have the completeness relation in Liouvillian space

$$\mathbb{1} = \sum_{aa'} |aa'\rangle\!\rangle\langle\!\langle aa'|. \tag{7.47}$$

Example: single resonant level

With just two system states (0 and 1), the system density matrix is $\rho_S = \sum_{i,j=0,1}\rho_{ij}|i\rangle\langle j|$, which can be represented by a vector of length four: $|\rho\rangle\!\rangle = (\rho_{00},\rho_1,\rho_{01},\rho_{10})^T$, where, by convention, we list the populations first and then coherences. The action of the Liouvillian on the four right basis states in Liouville-space is $L_S|00\rangle\!\rangle = L_S|11\rangle\!\rangle = 0$, $L_S|01\rangle\!\rangle = i\epsilon|01\rangle\!\rangle$, and $L|10\rangle\!\rangle = -i\epsilon|10\rangle\!\rangle$.

7.3.2 Interaction Liouvillian

Define superoperators in Liouville space corresponding to the action of g and a on both Keldysh branches (i.e. both parts of the commutator):

$$L_V = -i\xi_1 \sum_p A_1^p G_1^p, \tag{7.48}$$

with $p = \pm$ are Keldysh indices and from now on, we leave the sum over them implicit. The actions of superoperators G and d are defined via

$$G_1^p O = \begin{cases} g_1 O, & p = + \\ O g_1, & p = - \end{cases}, \tag{7.49}$$

and

$$A_1^p O = \begin{cases} a_1 O, & p = + \\ O a_1, & p = - \end{cases} . \tag{7.50}$$

With these definitions, the action of L_V on O is simply

$$\begin{aligned} L_V O &= -i\xi_1 \left(a_1 g_1 O - O a_1 g_1 \right) \\ &= -i\xi_1 \left[a_1 g_1, O \right], \end{aligned} \tag{7.51}$$

which is as required.

It is also useful to define super-operators corresponding to Eq. (7.23)

$$G_1^p = t_{1m} J_{1m}^p, \tag{7.52}$$

with jump operator defined as

$$J_{1m}^p O = \begin{cases} j_{1m} O, & p = + \\ O j_{1m}, & p = - \end{cases} . \tag{7.53}$$

7.3.3 Example: single resonant level

In Fock space, the jump operators for the SRL model were found to be

$$j_+ = |0\rangle\langle 1|; \quad j_- = |1\rangle\langle 0|. \tag{7.54}$$

We can then write their Liouville-space counterparts as

$$\begin{aligned} J_+^+ &= |0\cdot\rangle\!\rangle\langle\!\langle 1\cdot|; \quad J_-^+ = |1\cdot\rangle\!\rangle\langle\!\langle 0\cdot| \\ J_+^- &= |\cdot 1\rangle\!\rangle\langle\!\langle \cdot 0|; \quad J_-^- = |\cdot 0\rangle\!\rangle\langle\!\langle \cdot 1| \end{aligned} \tag{7.55}$$

where the "$\cdot$" denotes that the index at that location is left unaltered (really a sum over all possible indices).

7.4 Perturbation theory in Liouville space

We now derive an effective Liouvillian which describes the time-evolution of the reduced system density matrix under the influence of the coupling to the leads. Our approach is to expand the propagator of full system+reservoir to second order in the coupling and then trace out the reservoirs.

7.4.1 Laplace transform

We will work in Laplace space defined through the transform

$$\rho(z) \equiv \int_{t_0}^{\infty} dt e^{-z(t-t_0)} \rho(t). \tag{7.56}$$

Our starting point is the full von Neumann equation, Eq. (7.38), which Laplace-transforms as

$$z\rho(z) - \rho(t_0) = L\rho(z), \tag{7.57}$$

which we solve as

$$\rho(z) = \frac{1}{z-L}\rho(t_0). \tag{7.58}$$

The object $(z-L)^{-1}$ is the full propagator in Laplace space.

7.4.2 Perturbative expansion

The reduced density matrix of the dot is given by

$$\rho_{\rm S}(z) = {\rm Tr}_{\rm res}\left\{ \rho(z)\right\}. \tag{7.59}$$

Inserting Eq. (7.58) and the initial condition Eq. (7.36), we have

$$\rho_{\rm S}(z) = {\rm Tr}_{\rm res}\left\{ \frac{1}{z-L}\rho_{\rm S}(t_0)\rho_{\rm res}^{\rm eq}\right\}. \tag{7.60}$$

Expand propagator, Dyson-like, in powers of L_V to obtain

$$\begin{aligned} \frac{1}{z-L} &= \frac{1}{z-L_{\rm res}-L_{\rm S}-L_V} \\ &= \Omega_0(z) + \Omega_0(z)L_V\Omega_0(z) + \Omega_0(z)L_V\Omega_0(z)L_V\Omega_0(z) + \ldots \end{aligned} \tag{7.61}$$

with free propagator

$$\Omega_0(z) = \frac{1}{z-L_{\rm res}-L_{\rm S}}. \tag{7.62}$$

Inserting this into Eq. (7.60) we see that terms with an odd number of L_V disappear under the trace. Furthermore, since the coupling with the reservoirs is assumed to be weak, we can truncate this series at second order

in L_V. This defines the so-called *sequential tunneling limit*. The RDM is therefore

$$\rho_{\rm S}(z) \approx {\rm Tr}_{\rm res}\left\{ \Big(\Omega_0(z) + \Omega_0(z) L_V \Omega_0(z) L_V \Omega_0(z) \Big) \rho_{\rm S}(t_0) \rho_{\rm res}^{\rm eq} \right\} \quad (7.63)$$

With substitution of L_V from Eq. (7.48), the second-order term, which we denote as $\widetilde{\Sigma}$, becomes

$$\widetilde{\Sigma} = (-i)^2 \xi_1 \xi_2 {\rm Tr}_{\rm res}\left\{ \Omega_0(z) A_2^{p_2} G_2^{p_2} \Omega_0(z) A_1^{p_1} G_1^{p_1} \Omega_0(z) \rho_{\rm S}(t_0) \rho_{\rm res}^{\rm eq} \right\}. \quad (7.64)$$

The next task is to separate dot and reservoir degrees of freedom so we can perform trace. For this we use the dot-reservoir superoperator commutation relation

$$A_1^p G_{1'}^{p'} = -pp' G_{1'}^{p'} A_1^p, \quad (7.65)$$

which may be verified by a translation back to normal operators or by noting that if the operators reside on different branches, they commute, whereas if they lie on the same branch, normal fermionic anti-commutation relations apply. We will also need the following easily verified rules:

$$\begin{aligned} {\rm Tr}_{\rm res} L_{\rm res} = -i {\rm Tr}_{\rm res}\left[H_{\rm res}, \bullet \right] &= 0 && (7.66) \\ L_{\rm res} \rho_{\rm res}^{\rm eq} &= 0 \\ A_1^p L_{\rm res} &= \left(L_{\rm res} - x_1 \right) A_1^p; \quad x_1 = -i\xi_1\omega_1. && (7.67) \end{aligned}$$

The commutation of the dot-operators through the free propagators therefore changes the argument of the propagator:

$$\begin{aligned} A_1^p \Omega_0(z) &= A_1^p \frac{1}{z - L_{\rm res} - L_{\rm S}} \\ &= \frac{1}{z + x_1 - L_{\rm res} - L_{\rm S}} A_1^p \\ &= \Omega_0(z + x_1) A_1^p. \end{aligned} \quad (7.68)$$

When these results are placed into Eq. (7.64) we obtain

$$\widetilde{\Sigma} = p_1 p_2 \xi_1 \xi_2 {\rm Tr}_{\rm res}\left\{ \Omega_{\rm S}(z) G_2^{p_2} \Omega_{\rm S}(z + x_2) G_1^{p_1} \Omega_{\rm S}(z) A_2^{p_2} A_1^{p_1} \rho_{\rm S}(t_0) \rho_{\rm res}^{\rm eq} \right\} \quad (7.69)$$

with $-p_1 p_2$ coming from commutation, and with free dot propagator

$$\Omega_{\rm S}(z) = \frac{1}{z - L_{\rm S}}. \quad (7.70)$$

We then take the trace over reservoir degrees of freedom to obtain

$$\widetilde{\Sigma} = p_1 p_2 \xi_1 \xi_2 \langle A_2^{p_2} A_1^{p_1} \rangle \Omega_{\rm S}(z) G_2^{p_2} \Omega_{\rm S}(z + x_2) G_1^{p_1} \Omega_{\rm S}(z) \rho_{\rm S}(t_0) \tag{7.71}$$

with

$$\langle A_2^{p_2} A_1^{p_1} \rangle = {\rm Tr}\left\{ A_2^{p_2} A_1^{p_1} \rho_{\rm res}^{\rm eq} \right\} \tag{7.72}$$

the equilibrium reservoir correlation function. It is then straightforward to show that

$$\langle A_2^{p_2} A_1^{p_1} \rangle = \gamma_{21}^{p_2 p_1} = \delta_{2\overline{1}} f_{\alpha_1}^{(-\xi_1 p_1)}(\omega_1), \tag{7.73}$$

which sees the introduction of the Fermi-function of lead α. Summing over index 2 and using the delta function we have

$$\widetilde{\Sigma} = -p_1 p_2 f_{\alpha_1}^{(-\xi_1 p_1)}(\omega_1) \Omega_{\rm S}(z) G_2^{p_2} \Omega_{\rm S}(z - x_1) G_1^{p_1} \Omega_{\rm S}(z) \rho_{\rm S}(t_0). \tag{7.74}$$

7.5 Effective system Liouvillian

Quite generally, we can consider the dot RDM as evolving under the action of an effective Liouvillian. The RDM is then

$$\rho_{\rm S}(z) = \frac{1}{z - L_{\rm eff}(z)} \rho_{\rm S}(t_0), \tag{7.75}$$

where the effective Liouvillian is a function of Laplace variable z. This is quite generally the case when degrees of freedom have been traced out.

Such a Liouvillian is called nonMarkovian in the sense that, if we consider the equation of motion for the RDM in time-domain (inverse Laplace transform of Eq. (7.75)), we have

$$\dot{\rho}_S(t) = \int_{t_0}^{t} dt' L_{\rm eff}(t - t') \rho_S(t') \tag{7.76}$$

where it is clear that the evolution of the system at time t depends on all previous times (NB: we have assume no correlations at $t = t_0$). This stands in comparison with the Markovian evolution of Eq. (7.38) in which the Liouvillian itself is independent of time and thus the evolution depends only on the state of the system at time t.

Let us rewrite Eq. (7.75) as

$$\rho_{\rm S}(z) = \frac{1}{z - L_{\rm S} - \Sigma(z)} \rho_{\rm S}(t_0), \tag{7.77}$$

with $\Sigma(z)$ is the the memory kernel or "self-energy" The effective dot Liouvillian is thus

$$L_D^{\rm eff}(z) = L_{\rm S} + \Sigma(z). \tag{7.78}$$

Expanding Eq. (7.77) to first order in $\Sigma(z)$ (which will be second-order in the tunnel couplings) we obtain

$$\rho_{\rm S}(z) = \left(\Omega_{\rm S}(z) + \Omega_{\rm S}(z)\Sigma(z)\Omega_{\rm S}(z)\right)\rho_{\rm S}(t_0). \tag{7.79}$$

Comparing this result with Eq. (7.64) we can identify $\widetilde{\Sigma}(z) = \Omega_{\rm S}(z)\Sigma(z)\Omega_{\rm S}(z)$, such that the memory kernel is [1]

$$\Sigma(z) = -p_1 p_2 G_2^{p_2}\Omega_{\rm S}(z + i\xi_1\omega_1)G_1^{p_1} f_{\alpha_1}^{(-\xi_1 p_1)}(\omega_1). \tag{7.80}$$

We now write out the free system propagator to obtain

$$\Sigma(z) \;=\; -p_1 p_2 G_{\bar{1}}^{p_2}\frac{1}{z + i\xi_1\omega_1 - L_S}G_1^{p_1} f_{\alpha_1}^{(-\xi_1 p_1)}(\omega_1). \tag{7.81}$$

We then insert a complete set of states in Liouvillian space (see Eq. (7.47)) and substitute in for G from Eq. (7.52) to find

$$\Sigma(z) \;=\; -p_1 p_2 J_{-\xi_1 m}^{p_2}|aa'\rangle\rangle\langle\langle aa'|J_{\xi_1 m'}^{p_1}\left(t_{\bar{1}m}t_{1m'}\frac{f_{\alpha_1}^{(-\xi_1 p_1)}(\omega_1)}{z + i\xi_1\omega_1 + i\Delta_{aa'}}\right) \tag{7.82}$$

The term in brackets in essentially a number; The term before the brackets is a super-operator, which is independent of k. We therefore define

$$I_{aa'}(z;\xi_1,\alpha_1,p_1) = \sum_k t_{\bar{\xi}k\alpha_1 m}t_{\xi k\alpha_1 m'}\frac{f_{\alpha_1}^{(-\xi_1 p_1)}(\omega_{k\alpha})}{z + i\xi_1\omega_{k\alpha} + i\Delta_{aa'}}, \tag{7.83}$$

in which we have made explicit the sum over k, such that the memory kernel can be written

$$\boxed{\Sigma^{(2)}(z) = -p_1 p_2 J_{-\xi_1 m}^{p_2}|aa'\rangle\rangle\langle\langle aa'|J_{\xi_1 m'}^{p_1}I_{aa'}(z;\xi_1,\alpha_1,p_1)} \tag{7.84}$$

[1] We have obtained $\Sigma(z)$ in a simplified manner here, relevant to 2nd order only. More rigorously, $\Sigma(z)$ can be obtained as the sum over all irreducible diagrams in the expansion of $\mathrm{Tr}_{\rm res}\rho(z)$

Now perform a trick for going to continuum limit for reservoir: insert $1 = \int_{-D}^{D} d\omega \delta(\omega - \omega_{k\alpha})$ where D is the bandwidth of the leads (assumed to be the same for all leads). We have then

$$I_{aa'}(z;\xi_1,\alpha_1,p_1) = \int_{-D}^{D} d\omega \left(\sum_k t_{\bar{\xi}_1 k\alpha_1 m} t_{\xi_1 k\alpha_1 m'} \delta(\omega - \omega_{k\alpha}) \right) \frac{f_{\alpha_1}^{(-\xi_1 p_1)}(\omega_{k\alpha})}{z + i\xi_1\omega_{k\alpha} + i\Delta_{aa'}}. \tag{7.85}$$

Then let us define

$$\Gamma_{mm'\xi\alpha}(\omega) = 2\pi \sum_k t_{\bar{\xi}k\alpha m} t_{\xi k\alpha m'} \delta(\omega - \omega_{k\alpha}). \tag{7.86}$$

The diagonal elements

$$\Gamma_{mm\alpha}(\omega) = 2\pi \sum_k |t_{k\alpha m}|^2 \delta(\omega - \omega_{k\alpha}) \tag{7.87}$$

are the familiar Fermi golden rule rates. We can then write Eq. (7.85) as

$$I_{aa'}(z;\xi_1,\alpha_1,p_1) = \frac{1}{2\pi} \int_{-D}^{D} d\omega \Gamma_{mm'\xi_1\alpha_1}(\omega) \frac{f_{\alpha_1}^{(-\xi_1 p_1)}(\omega)}{z + i\xi_1\omega + i\Delta_{aa'}}. \tag{7.88}$$

It is then convenient to introduce a change of integration variable $x = -\xi_1 p_1(\omega - \mu_\alpha)$. With $D \gg \mu_\alpha$ such that $D \pm \mu_\alpha \approx D$ we obtain the integral

$$\boxed{I_{aa'}(z;\xi_1,\alpha_1,p_1) = \frac{i}{2\pi} \int_{-D}^{D} dx \frac{\Gamma_{mm'\xi_1\alpha_1}(\mu_\alpha - \xi_1 p_1 x) f_{\alpha_1}(x)}{iz + p_1[x - p_1(\xi_1\mu_\alpha + \Delta_{aa'})]}}. \tag{7.89}$$

Flat band approximation

Integrating Eq. (7.89) for reservoirs showing structure can be tricky. Normally however, we can approximate the rates as flat within the region of interest, and take Γ outside the integral.

$$I_{aa'}(z;\xi_1,\alpha_1,p_1) = \frac{i}{2\pi} \Gamma_{mm'\xi_1\alpha_1} \int_{-D}^{D} dx \frac{f_\alpha(x)}{iz + p_1[x - p_1(\xi_1\mu_\alpha + \Delta_{aa'})]} \tag{7.90}$$

Markov approximation

As it stands, this integral is a function of z, and hence Σ is nonMarkovian. If we are interested in the behaviour of the system on time scales much

greater than the dynamics of the bath (e.g. the stationary current) then we can take the long-time limit of the integral by replacing $z \to 0^+$ where 0^+ is a positive infinitesimal. This regularises the integral as

$$\begin{aligned} I_{aa'}(z;\xi_1,\alpha_1,p_1) &\approx I_{aa'}(0^+;\xi_1,\alpha_1,p_1) \\ &= \frac{i}{2\pi}\Gamma_{mm'\xi_1\alpha_1}\int_{-D}^{D} dx \frac{f_\alpha(x)}{i0^+ + p_1[x - p_1(\xi\mu_\alpha + \Delta_{aa'})]} \end{aligned} \tag{7.91}$$

Use of Dirac's identity

$$(i0^+ + x)^{-1} = -i\pi\delta(x) + \mathcal{P}\frac{1}{x} \tag{7.92}$$

where $\mathcal{P}$ denotes the principal part, allows us to write

$$\begin{aligned} I^{(2)}_{aa'}(z;\xi_1,p_1,\mu_1) &= \Gamma_{mm'\xi_1\alpha_1}\left\{\frac{1}{2}f_{\alpha_1}(p_1(\Delta_{aa'} + \xi_1\mu_{\alpha_1})) \right. \\ &\qquad \left. + \frac{ip_1}{2\pi}\phi_{\alpha_1}(p_1(\Delta_{aa'} + \xi_1\mu_{\alpha_1}))\right\} \end{aligned} \tag{7.93}$$

in terms of the function

$$\begin{aligned} \phi(\lambda) &= \int_{-D}^{D} d\omega \frac{f(\omega)}{\omega - \lambda} \\ &= \mathrm{Re}\Psi\left(\frac{1}{2} + i\frac{\lambda}{2\pi k_B T}\right) - \ln\frac{D}{2\pi k_B T} \end{aligned} \tag{7.94}$$

with Ψ the digamma function. This is a standard and useful integral (this is result is correct to order $1/D$ as we made a large D approximation in obtaining Eq. (7.89)). The real part of the integral $I^{(2)}_{aa'}$ are rates describing the transfer of population between system states, whereas the imaginary parts lead to renormalisation of the system energies.

Rate equation

In general, the reduced density matrix ρ_S contains both diagonal and off-diagonal elements — populations as well as coherences. If, however, the coupling to the leads is weak compared with the free evolution frequencies of the isolated dot Hamiltonian, $\Gamma \ll \Delta_{aa'}$, it is valid to consider just the (eigenstate) populations of the system, since the coherences will 'self-average

to zero' on the time-scale of the tunnelling processes in which we are interested [2]. Since the Liouvillian then maps populations onto populations it must be wholly real and we need not calculate the renormalisation parts, as they must cancel.

7.5.1 Example: single resonant level

We now derive the (second-order) memory kernel for the SRL in Markov and flat-band approximations. For each lead $\alpha = L, R$, expression Eq. (7.84) has eight terms, given by the various combinations of p_1, p_2 and ξ_1. We explicitly evaluate just a single term here to illustrate the procedure. Writing in for the jump operators of Eq. (7.55), the term in Σ corresponding to $(p_1, p_2, \xi_1) = (+, +, +)$ is

$$-\frac{1}{2}\Gamma_\alpha |1\cdot\rangle\!\rangle\langle\!\langle 0\cdot||aa'\rangle\!\rangle\langle\!\langle aa'||0\cdot\rangle\!\rangle\langle\!\langle 1\cdot| f_\alpha(\Delta_{aa'}+\mu)$$
$$= -\frac{1}{2}\Gamma_\alpha |1a'\rangle\!\rangle\langle\!\langle 1a'| f_\alpha(\Delta_{0a'}+\mu). \tag{7.95}$$

Other terms are evaluated similarly and from these we can directly build the Liouvillian. We can also build the Liouvillian by considering the action of Σ on an arbitrary vector $|\rho\rangle\!\rangle$ and taking elements. We obtain

$$\begin{aligned}
\langle\!\langle 00|\Sigma|\rho\rangle\!\rangle &= \Gamma_\alpha \Big\{ \langle\!\langle 11|\rho\rangle\!\rangle f^{(+)}(\mu_\alpha - \epsilon) - \langle\!\langle 00|\rho\rangle\!\rangle f^{(-)}(\mu_\alpha - \epsilon) \Big\} \\
\langle\!\langle 11|\Sigma|\rho\rangle\!\rangle &= \Gamma_\alpha \Big\{ \langle\!\langle 00|\rho\rangle\!\rangle f^{(-)}(\mu_\alpha - \epsilon) - \langle\!\langle 11|\rho\rangle\!\rangle f^{(+)}(\mu_\alpha - \epsilon) \Big\} .
\end{aligned} \tag{7.96}$$

Note that the equations for the populations do not couple to matrix elements in which there is charge-superposition. This is a general feature. Since, for the diagonal elements, the free system Liouvillian is zero, the total effective Liouvillian of the system is

$$L_{\text{eff}} = \Gamma_\alpha \begin{pmatrix} -f^{(-)}(\mu_\alpha - \epsilon) & f^{(+)}(\mu_\alpha - \epsilon) \\ f^{(-)}(\mu_\alpha - \epsilon) & -f^{(+)}(\mu_\alpha - \epsilon) \end{pmatrix} \tag{7.97}$$

This should be compared with Eq. (7.2) — it is similar but now we have precise prescription for the rates Γ_α and incorporate finite bias and temperature effects through the inclusion of the Fermi functions.

Note that since the SRL model has no internal quantum degrees of freedom, the effective Liouvillian is already of rate equation form without further approximation.

[2] This approximation is no longer good if one is interested in the high-frequency noise

7.6 Infinite bias limit

A very useful limit of the QME is obtained when we assume that biases applied are large enough that all relevant energy scales lie well within the transport window, i.e.

$$|\mu_\alpha| \gg \Delta_{aa'}, k_B T, D. \tag{7.98}$$

Let us consider a two lead set-up ($\alpha = L, R$) in the limit $\mu_L \to +\infty$ and $\mu_R \to -\infty$. In this case all arguments, including $\Delta_{aa'}$, can be neglected in Eq. (7.93). The level renormalisation parts then require the evaluation of integrals of the form

$$\mathcal{P}\int_{-D}^{D} d\omega \frac{f(\omega)}{\omega \pm |\mu|} \sim \log \frac{\mu + D}{\mu - D}, \tag{7.99}$$

which in the infinite bias limit, vanish. Furthermore, the rate parts become particularly simple since the temperature dependence of the Fermi functions is now irrelevant, reducing to step-functions. The Fermi function $f^{(+)}$ then evaluates to unity on the left and zero on the right and Eq. (7.93) therefore becomes

$$I^{(2)}_{aa'}(z; \xi_1, p_1, \alpha_1) \;=\; \frac{1}{2}\Gamma_{mm'\xi_1\alpha_1}\left(\delta_{\alpha_1,L}\delta_{p_1\xi_1,-1} + \delta_{\alpha_1,R}\delta_{p_1\xi_1,+1}\right) \tag{7.100}$$

This can be placed back into Eq. (7.84) to give

$$\Sigma = -p_1 p_2 J^{p_2}_{-\xi_1 m}|aa'\rangle\!\rangle\langle\!\langle aa'|J^{p_1}_{\xi_1 m'}\frac{1}{2}\Gamma_{mm'\xi_1\alpha_1}\left(\delta_{\alpha_1,L}\delta_{p_1\xi_1,-1} + \delta_{\alpha_1,R}\delta_{p_1\xi_1,+1}\right) \tag{7.101}$$

Then since there is no further dependence on indices aa', the sum over projection operators reverts back to the unit operator, whence

$$\Sigma = -p_1 p_2 J^{p_2}_{-\xi_1 m} J^{p_1}_{\xi_1 m'}\frac{1}{2}\Gamma_{mm'\xi_1\alpha_1}\left(\delta_{\alpha_1,L}\delta_{p_1\xi_1,-1} + \delta_{\alpha_1,R}\delta_{p_1\xi_1,+1}\right) \tag{7.102}$$

Summing over ξ_1 and α, we obtain

$$\Sigma = -\frac{1}{2}p_1 p_2 \left\{\Gamma_{mm'\bar{p}_1 L} J^{p_2}_{p_1 m} J^{p_1}_{-p_1 m'} + \Gamma_{mm' p_1 R} J^{p_2}_{-p_1 m} J^{p_1}_{p_1 m' R}\right\}. \tag{7.103}$$

We can then regeneralise this result to a situation where we have a set of source leads, labelled with α_S with $\mu_{\alpha_S} = +\infty$, and a set of drain leads,

labelled with α_D with $\mu_{\alpha_D} = -\infty$. The memory kernel is then

$$\boxed{\Sigma = -\frac{1}{2} p_1 p_2 \left\{ \Gamma_{mm'\bar{p}_1\alpha_S} J^{p_2}_{p_1 m} J^{p_1}_{-p_1 m'} + \Gamma_{mm' p_1 \alpha_D} J^{p_2}_{-p_1 m} J^{p_1}_{p_1 m'} \right\}} \quad . \tag{7.104}$$

A particularly simple form emerges if each reservoir operator is coupled to just a single transition in the system. Both examples we have considered have been of this kind. In the DQD for example, the left lead couples to the transition $|0\rangle \leftrightarrow |L\rangle$ only, and the right lead couples only to $|0\rangle \leftrightarrow |R\rangle$. Formally, this means that the m and m' indices are specified by the revelant lead index. In this case, we have

$$\Sigma = -\frac{1}{2} p_1 p_2 \left\{ \Gamma_{\alpha_S} J^{p_2}_{p_1 \alpha_S} J^{p_1}_{-p_1 \alpha_S} + \Gamma_{\alpha_D} J^{p_2}_{-p_1 \alpha_D} J^{p_1}_{p_1 \alpha_D} \right\}. \tag{7.105}$$

We can translate this back into Fock space by considering the action of Σ on density matrix ρ. Substituting in for super-operators J in terms of operators j acting to the left and to the right, we obtain

$$\begin{aligned} \Sigma\rho &= -\frac{1}{2}\Gamma_{\alpha_S} \left\{ j_{\alpha_S} j^\dagger_{\alpha_S} \rho + \rho j_{\alpha_S} j^\dagger_{\alpha_S} - 2 j^\dagger_{\alpha_S} \rho j_{\alpha_S} \right\} \\ &\quad -\frac{1}{2}\Gamma_{\alpha_D} \left\{ j^\dagger_{\alpha_D} j_{\alpha_D} \rho + \rho j^\dagger_{\alpha_D} j_{\alpha_D} - 2 j_{\alpha_D} \rho j^\dagger_{\alpha_D} \right\} \end{aligned} \tag{7.106}$$

Defining

$$s_{\alpha_S} = j^\dagger_{\alpha_S}; \quad s_{\alpha_D} = j_{\alpha_D} \tag{7.107}$$

we can write this result the action of the full effective Liouvillian as

$$L_{\text{eff}}\rho = -i\left[H_{\text{S}}, \rho\right] - \frac{1}{2}\sum_\alpha \Gamma_\alpha \left\{ s^\dagger_\alpha s_\alpha \rho + \rho s^\dagger_\alpha s_\alpha - 2 s_\alpha \rho s^\dagger_\alpha \right\}. \tag{7.108}$$

This is straightforwardly recognised as having *Lindblad* form, meaning that ρ retains its positivity (and hence interpretation as a density matrix) under time evolution due to L_{eff}.

7.7 Stationary state and average current

The Markovian master equation for the system density matrix reads

$$\dot{\rho} = L\rho, \tag{7.109}$$

where we have dropped any now-superfluous indices. The stationary density matrix $\rho_{\rm stat}$ is found by taking the limit $t \to \infty$, such that $\dot{\rho}_{\rm stat} = 0$, and the stationary density matrix can be obtained as the null-vector of Liouvillian [3]:

$$L\rho_{\rm stat} = 0. \tag{7.110}$$

7.7.1 Current

The average current through the system can be obtained in a number of ways — in the next chapter we will discuss the current in the context of electron counting statistics; here, we take a more standard quantum-mechanical operator approach.

Classically, the current in lead α is defined as being proportionally to the rate-of-change of the charge in the lead. Quantum-mechanically, this gives us the current operator

$$I_\alpha \equiv e\dot{n}_\alpha, \tag{7.111}$$

in terms of

$$n_\alpha = \sum_k a_{+k\alpha} a_{-k\alpha}, \tag{7.112}$$

the number operator of electrons in lead α. Employing Heisenberg's equation of motion, we can rewrite this as

$$\begin{aligned} I_\alpha &= \frac{e}{i\hbar}\left[n_\alpha, H\right] = \frac{e}{i\hbar}\left[n_\alpha, \xi_1 a_1 g_1\right] \\ &= \frac{e}{i\hbar} a_1 g_1, \end{aligned} \tag{7.113}$$

which is identical to the tunnel coupling operator V except for the forefactor and the absence of the sign ξ_1. The super-operator corresponding to I_α is

$$L_I^\alpha = \frac{-ie}{\hbar} A_1^+ G_1^+, \tag{7.114}$$

which has a definite $p = +$ Keldysh index, since the operator acts to the right (actually, irrelevant for calculating the average current, but important for higher statistics).

[3] The stationary state need not, in fact, be unique, and we would then talk of a null-space, rather than a single null-vector. However, in most transport models, including those we will consider here, this is not the case and $\rho_{\rm stat}$ is unique

The average current flowing into lead α at time t is simply obtained from the inverse Laplace transform of the expectation value

$$\langle I\rangle(z) = \mathrm{Tr}\left\{I_\alpha \rho(z)\right\}, \tag{7.115}$$

where both trace and ρ refer to full system+reservoir quantities. Procedding in Liouville-space as before, we have

$$\begin{aligned}\langle I\rangle(z) &= \mathrm{Tr}\left\{L_I^\alpha \frac{1}{z-L}\rho_D\rho_{\mathrm{res}}^{\mathrm{eq}}\right\} \\ &= \mathrm{Tr}\left\{L_I^\alpha\left(\Omega_0(z)+\Omega_0(z)L_V\Omega_0(z)+\ldots\right)\rho_D\rho_{\mathrm{res}}^{\mathrm{eq}}\right\}. \end{aligned}\tag{7.116}$$

Taking the trace over reservoir degrees of freedom and arranging tunnelling contributions into an effective Liouvillian, we obtain [4]

$$\langle I\rangle(z) = \mathrm{Tr}_D\left\{\Sigma_I^\alpha(z)\frac{1}{z-L_{\mathrm{eff}}(z)}\rho_D\right\}, \tag{7.117}$$

with L_{eff} as before and $\Sigma_I^\alpha(z)$, the same as the irreducible memory kernel derived before, but with the left-most tunnel-vertex replaced with the similar current vertex as from Eq. (7.114). In effect, this means we can simply take $\Sigma(z)$ of Eq. (7.84), replace p_2 with $+$, drop the p_2-sum and add the relevant forefactor from Eq. (7.114). Making these changes to Eq. (7.84) we obtain

$$\Sigma_I^\alpha(z) = -\frac{e}{\hbar}\xi_1 p_1 J^+_{-\xi_1 m}|aa'\rangle\!\rangle\langle\!\langle aa'|J^{p_1}_{\xi_1 m'}I_{aa'}(z;\xi_1,\alpha_1,p_1). \tag{7.118}$$

We are normally interested in the stationary current, which we obtain from

$$\langle I_\alpha\rangle = \langle I_\alpha\rangle_{\mathrm{stat}} = \langle I_\alpha\rangle(z\to 0^+) = \mathrm{Tr}_D\left\{\Sigma_I^\alpha(0^+)\rho_{\mathrm{stat}}\right\}. \tag{7.119}$$

7.7.2 Example: single resonant level in infinite bias limit

The effective Liouvillian of the single resonant level in infinite bias limit reads

$$L_{\mathrm{eff}} = \begin{pmatrix} -\Gamma_L & \Gamma_R \\ \Gamma_L & -\Gamma_R \end{pmatrix}, \tag{7.120}$$

the null-space of which is

$$\rho_{\mathrm{stat}} = \begin{pmatrix} \rho_{00} \\ \rho_{11} \end{pmatrix}_{\mathrm{stat}} = \frac{1}{\Gamma_L+\Gamma_R}\begin{pmatrix} \Gamma_R \\ \Gamma_L \end{pmatrix}. \tag{7.121}$$

[4] see H. Schöller, Schladming lecture notes, `http://physik.uni-graz.at/itp/iutp/iutp_08/lecture_notes_part_1.pdf` and M. Leijnse and M. R. Wegewijs, arXiv:0807.4027

The current super-operator of the left and right leads are

$$\Sigma_I^L = \begin{pmatrix} 0 & 0 \\ \Gamma_L & 0 \end{pmatrix}; \quad \Sigma_I^R = \begin{pmatrix} 0 & \Gamma_R \\ 0 & 0 \end{pmatrix}. \tag{7.122}$$

And evaluating the current as in Eq. (7.119) with either of these operators gives

$$I = e\frac{\Gamma_L\Gamma_R}{\Gamma_L + \Gamma_R}. \tag{7.123}$$

We therefore simply recover the results of the example presented in 7.1.

7.8 The Anderson model

The Anderson model (P. W. Anderson, Phys. Rev. **124**, 41 (1961)) was originally conceived to describe scattering of electrons by a magnetic impurity within a band of conduction electron states. This same model also serves to describe the transport through a single-level in a quantum dot. The critical feature is that electron-electron interactions mean that the doubly-charged configuration possesses an additional energy U over and above the non-interacting energy of the system.

The Anderson Hamiltonian (as relevant to dots) reads

$$H = \sum_\sigma \epsilon_\sigma d_\sigma^\dagger d_\sigma + U n_\uparrow n_\downarrow + H_{\rm res} + V, \tag{7.124}$$

where ϵ_σ is the energy of a spin-σ electron in the dot, U is the additional interaction energy. In addition we define, as before,

$$H_{\rm res} = \sum_{k,\alpha,\sigma} \omega_{k\alpha,\sigma} a_{k\alpha\sigma}^\dagger a_{k\alpha\sigma}, \tag{7.125}$$

and tunnelling term

$$V = \sum_{\alpha k\sigma} t_{\alpha k\sigma} a_{k\alpha\sigma}^\dagger d_\sigma + t_{\alpha k\sigma}^* d_\sigma^\dagger a_{k\alpha\sigma}, \tag{7.126}$$

where we have made explicit the spin index. Applying the machinery of the previous section, we find that the effective system Liouvillian can be written

$$L = \sum_{\alpha=L,R} L_\alpha^{\rm in} + L_\alpha^{\rm out} \tag{7.127}$$

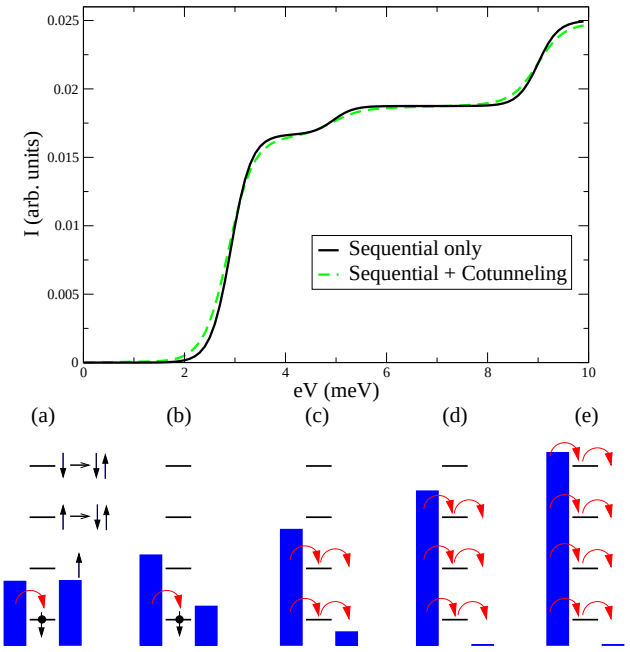

Figure 7.2: Current through the Anderson model with parameters $\epsilon_\downarrow = -1.5$meV, $\epsilon_\uparrow = 0.5$meV, $U = 4$meV, $\Gamma_L = \Gamma_R$ $\Gamma_L/k_BT = 1/4$. The levels involved in transport at various points are sketched below: (a) equillibrium and (b) small bias — Coulomb blockade; (c) parallel transport through both single-electron levels; (d) and (e) transport through 1 and then 2 of the transitions to the doubly occupied state. (After Thielmann *et al*, Phys. Rev. Lett. **95**, 146806 (2005)).

with (in the basis of $(0, \uparrow, \downarrow, \uparrow\downarrow)$ populations)

$$L_\alpha^{\rm in} = \Gamma_\alpha \begin{pmatrix} -f_\alpha^{(+)}(\epsilon_\uparrow) - f_\alpha^{(+)}(\epsilon_\downarrow) & 0 & 0 & 0 \\ f_\alpha^{(+)}(\epsilon_\uparrow) & -f_\alpha^{(+)}(U+\epsilon_\downarrow) & 0 & 0 \\ f_\alpha^{(+)}(\epsilon_\downarrow) & 0 & -f_\alpha^{(+)}(U+\epsilon_\uparrow) & 0 \\ 0 & f_\alpha^{(+)}(U+\epsilon_\downarrow) & f_\alpha^{(+)}(U+\epsilon_\uparrow) & 0 \end{pmatrix}$$

$$L_\alpha^{\rm out} = \Gamma_\alpha \begin{pmatrix} 0 & f_\alpha^{(-)}(\epsilon_\uparrow) & f_\alpha^{(-)}(\epsilon_\downarrow) & 0 \\ 0 & -f_\alpha^{(-)}(\epsilon_\uparrow) & 0 & f_\alpha^{(-)}(U+\epsilon_\downarrow) \\ 0 & 0 & -f_\alpha^{(-)}(\epsilon_\downarrow) & f_\alpha^{(-)}(U+\epsilon_\uparrow) \\ 0 & 0 & 0 & -f_\alpha^{(-)}(U+\epsilon_\downarrow) - f_\alpha^{(-)}(U+\epsilon_\uparrow) \end{pmatrix} \tag{7.128}$$

The current calculated from this theory is plotted in Fig. 7.2 for illustrative parameters.

7.9 Other current blockade mechanisms

We have seen that the Coulomb blockade provides an extremely important organising principle for understanding the transport through quantum dots, describing as it does, regions in which transport is blocked on energetic grounds. However, additional mechanisms also exist that can block the current through quantum dot systems, which are very different in nature. We consider two here.

7.9.1 Spin blockade

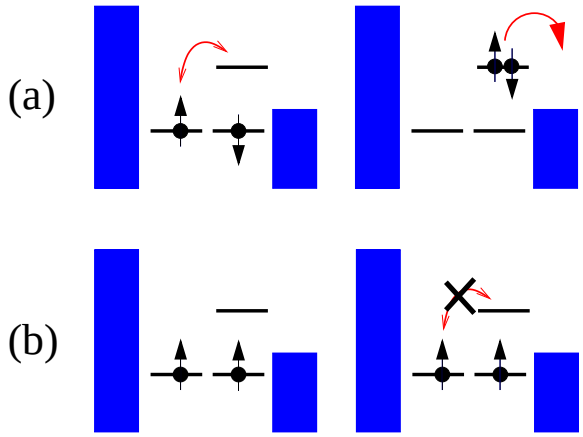

Figure 7.3: Spin blockade in a DQD. With two electrons in a singlet state in the dots, tunnelling can occur. With the spins in a triplet state, however, the Pauli principle prevents tunnelling and blocks the current through the dots.

Current through a double quantum dot can be blocked through a mechanism known as *spin blockade*, which arises from the Pauli exclusion principle. The situation is illustrated in Fig. 7.3. The chemical potentials are arranged such that singly-occupied states and states with one electron in each dot lie below the transport window, but the states with two electrons in one dot lie within the window. On energetic (Coulomb blockade) grounds, one would

therefore expect transport to proceed through these latter levels. However, this picture neglects the spin of the electrons. If the system starts occupied with two electrons of different spin in a singlet state (Fig. 7.3a), then tunnelling can occur between the two dots, making the formation of the doubly-occupied single-dot state possible. In this case electrons will tunnel out of the DQD system. Eventually, however, the stochastic nature of tunnelling means we will arrive at a situation where the electrons in the dots have the same spin (or rather, are in one of the three triplet states) (Fig. 7.3b). In this case, the Pauli principle prevents tunnelling between the two dots and these two electrons are trapped, since the states in the transport window are inaccessible. This is the spin-blockade. Note that its existence relies on the Coulomb blockade, since, if there were no Coulomb blockade, higher energy, multiple-electron states would become accessible, enabling transport.

7.9.2 Dark states

Current flow through a QD device may also be blocked by the destructive interference between quantum-mechanical paths through it (B. Michaelis, C. Emary, and C. W. J. Beenakker, Europhys. Lett. **73**, 677 (2006).) One example is the triple quantum dot shown in Fig. 7.4. The device is biased from left to right, and the Coulomb blockade regime is assumed, such that just a single excess electron can be in the triple-dot-system at any one time.

Essentially, interefence between electron paths through the upper and lower dots leads to a state in which the electron wave function destructively interferes at the dot coupled to the collector. With the correct parameters, this intereference is complete and no current can flow. Formally this effect is similar to coherent population trapping encountered in quantum optics, where the state in which the electron is trapped is known as a *dark state*. Figure 7.4 shows the current through the device as a function of the detuning between levels in the dots — the current profile is the transport analogue of the optical dark resonance. If the system is biased in the other direction, then the paths no longer interfere and the system conducts. In this way, quantum interference diodes and transistors can be conceived.

Whilst these blockade mechanisms have been presented here as leading to a complete suppression of current flow, this is just an idealisation. Additional interactions, in particular those with the environmentof teh dots, which were not included in these simple models can partially remove the blockade effects,. For example, any interaction which dimishes the phase coherence of the trapped electron in the triple dot will disrupt the dark

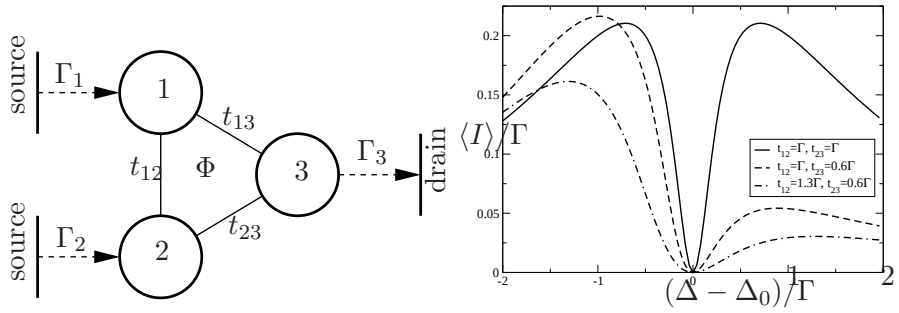

Figure 7.4: LEFT: Three quantum dots are coupled coherently to one another via tunnel couplings t_{ij}, and incoherently to source and drain leads with rates Γ_i. Each dot contains a single level and by adjusting the relative positions of these levels, the system can be prepared in a dark state where no current flows despite the applied bias. RIGHT: The stationary current $\langle I \rangle$ through the three-dot system shows a pronounced anti-resonance with complete current blocking at a detuning of $\Delta = \Delta_0$ where the dark-state forms. (from Emary Phys. Rev. B **76**, 245319 (2007))

state and lead to current flow. This residual current therefore gives us a method in which to probe electron-environment interactions in quantum dots.

7.10 Beyond the second-order master equation

The master equation we have described in this chpater is second-order in the tunnelling amplitude t and therefore first-order in the rates Γ. This corresponds to the so-called *sequential tunnelling* limit since it assumes that the temperature is high enough that the electron's phase coherence is destroying in between tunnelling events. Electron hops in. Electron hops out. As temperature is decreased, a certain degree of phase coherence may be maintained between electron tunnellings, which can lead to new transport possibilities.

7.10.1 Cotunneling

If, in performing our perturbative derivation of the master equation, we truncate, not after order Γ, but after order Γ^2, we include cotunneling processes in the effective Liouvillian. Such processes enable the tunnelling of

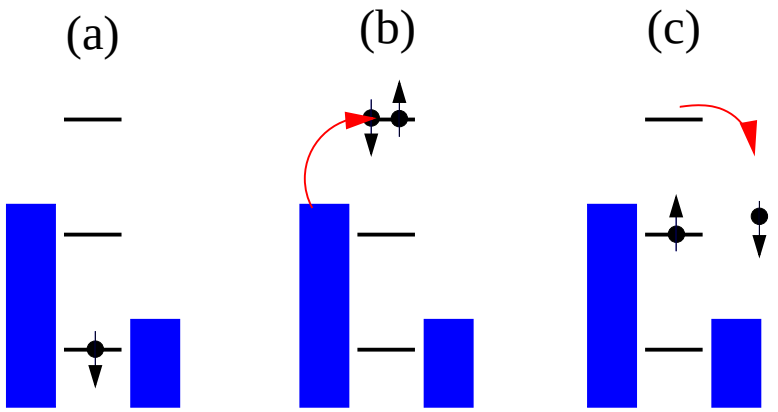

Figure 7.5: An inelastic cotunneling process. (a) With the bias as shown, current through the dot is blocked for sequential tunnelling processes. However, (b) an electron from the left lead can tunnel into the dot to 'virtually populate' the doubly-charged state. Then (c) one of these electrons can then tunnel out to the right. Either spin can tunnel out and here we have shown a spin-flip process in which in final state of the electron has opposite spin to its initial state. Due to the Zeeman splitting, these states have different energy and the process is therefore also inelastic.

electrons to/from the system via intermediate virtual states. An example of an inelastic cotunneling process is shown in Fig. 7.5.

Cotunneling is particularly important in regimes where sequential transport is suppressed due to the Coulomb blockade. In such regimes, cotunneling transport is dominant as these processes are only algebraically suppressed, compared with the exponential suppression of the sequential ones. Figure 7.2 shows results for both sequential and sequential+cotunneling master equation for the Anderson model. In the region of the first current step, especially, cotunneling plays a significant role.

7.10.2 The Kondo effect

What happens if we decrease temperature further? If we proceed as above and expand our perturbation series to third order in Γ, we obtain an indication that something very interesting is happening, as this third-order contribution causes the conductance of the dot to diverge logarithmically as temperature is decreased. This divergence was discovered by Kondo whilst

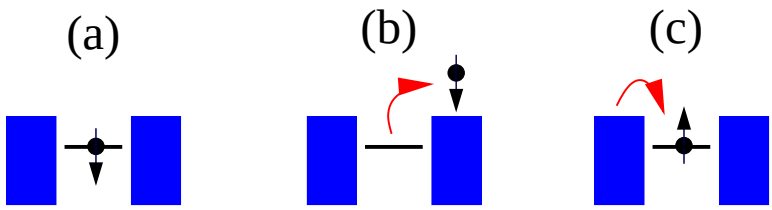

Figure 7.6: A Kondo spin-flip process. This is an elastic process

studying the theory of transport in metals (where it leads to a divergence in the resistivity, not the conductnace!). See Bruus and Flensberg for details.

This effect is known as the *Kondo effect* and it arises arises from virtual processes such as that depicted in Fig. 7.6, in which the spin of the dot electron is flipped. To fully describe the Kondo effect requires a nonperturbative approach; the divergence of our power series signals a break-down of the perturbative reasoning. Kondo physics is an important area of many-body invesitagation and a full understanding requires sophisticated many-body techniques (e.g. numerical RG: Wilson 1975, Bethe Ansatz, Tsvelik and Wiegmann 1983, or see book by Hewson, 1997). The master equation expansion may also be extended to describe the Kondo effect within the so-called resonant-tunnelling approximation (J. König 1999/2000). The Kondo effect in quantum dots is also an active area of experimental investigation (see Fig. 7.7).

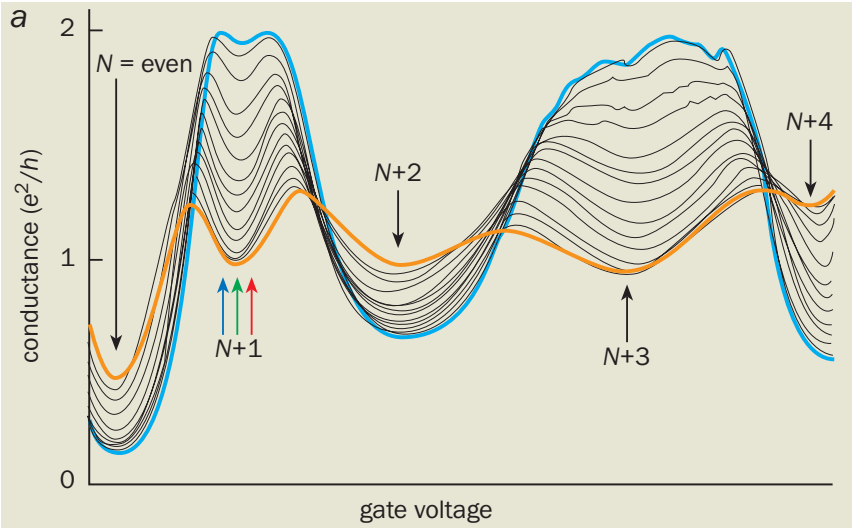

Figure 7.7: Conductance of single quantum dot in Kondo regime. With an even number of electrons in the dot, there is no Kondo effect and the conductance decreases with decreasing temperature. With N odd, the Kondo resonance comes into play and the conductance increases with decreasing temperature. Experimental data from W. G. van der Wiel *et al*, Science **289**, 2105 (2000).

Chapter 8

Shotnoise

Up to now, our considerations have only extended to the average current (or conductance) of mesoscopic devices. However, transport is stochastic process and the current will show fluctuations around this average value as a function of time, something like this:

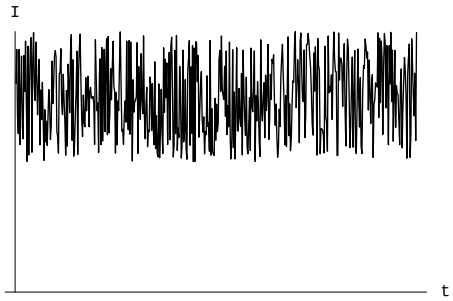

The size of these current fluctuations is termed the *noise*. If we were designing a stereo system, the (instantaneous) mean current would be the signal, the important part, and the noise would be seen as an unwelcome influence and we would try to eliminate it as far as possible.

In mesoscopic transport, however, this negative view of noise has subsided, with the increasing realisation that we can actually learn a lot about what is happening inside a mesoscopic device by looking at the noise, much more in fact than can be gleaned by considering the average current alone. R. Landauer, one of the founding fathers of mesoscopics, has stated that "the noise is the signal" to reflect the importance of the study of noise.

In this chapter we will introduce key noise concepts and learn how to calculate noise within the scattering theory of transport. Most of the details of this chapter can be found in the review by Blanter and Büttiker. A

nice introduction is to be found in *Quantum Shot Noise* by Beenakker and Schönenberger, http://arxiv.org/abs/cond-mat/0605025.

8.1 Sources of Noise

The two sources of noise in which we will be most interested are *thermal noise* (also known as Nyquist-Johnson noise) and *shotnoise* (or partition noise). We first introduce these concepts through a simple example.

Let us consider a single electron channel that impinges on a barrier such that the electron is transmitted with probability T and reflected with probability R. Ignoring an irrelevant phase factor, the wave function of an electron scattering at the barrier will be $|\psi\rangle = \sqrt{T}|T\rangle + \sqrt{R}|R\rangle$ where the kets denote transmitted and reflected states respectively, and $R+T = 1$. Let us populate the incoming channel with an electron from a thermal reservoir with Fermi function f. The input density matrix of the system is then

$$\rho_{\text{in}} = f|i\rangle\langle i| + (1-f)|0\rangle\langle 0|, \tag{8.1}$$

where $|i\rangle$ and $|0\rangle$ denote filled and empty input channel respectively. The density matrix after scattering will then be

$$\rho = f|\psi\rangle\langle\psi| + (1-f)|0\rangle\langle 0|. \tag{8.2}$$

Average occupancies of the transmitted and reflected channels are easily calculated to be

$$\begin{aligned} \langle n_T\rangle &= f\langle\psi|n_T|\psi\rangle = fT \\ \langle n_R\rangle &= f\langle\psi|n_R|\psi\rangle = fR. \end{aligned} \tag{8.3}$$

We are here interested in the fluctuations of the number of particles in each channel; to quantify their size, we calculate the variance $\langle(\delta n)^2\rangle$ with $\delta n = n - \langle n\rangle$, the difference between the number operator and its average. We obtain

$$\begin{aligned} \langle(\delta n_T)^2\rangle &= fT(1-fT) \\ \langle(\delta n_R)^2\rangle &= fR(1-fR). \end{aligned} \tag{8.4}$$

We can also calculate the cross-correlator between transmitted and reflected channels:

$$\langle\delta n_T \delta n_R\rangle = -f^2TR \tag{8.5}$$

These variances characterise the total noise in the system which contains both thermal and partition contributions.

We can separate these two contributions by analysing to limiting cases. First, we set $T = 1$ such that we only have thermal fluctuations. The noise in the transmitted channel is $\langle(\delta n_T)^2\rangle = f(1-f)$, which is equal to the thermal noise of the input channel.

We then consider the zero-temperature limit such that $f = 1$ such that the input channel is definitely occupied. We obtain

$$\langle(\delta n_T)^2\rangle = \langle(\delta n_R)^2\rangle = -\langle\delta n_T \delta n_R\rangle = TR = T(1-T) \tag{8.6}$$

This is *shotnoise* or partition noise — its source is the partitioning of the incoming electron stream into transmitted and reflected components and ultimately the discrete nature of charge. The shotnoise vanishes if either $T = 1$ or $R = 1$ and is maximal when $T = R = 1/2$.

As we will see shortly, the thermal noise is simply related to the conductance of the sample and tells us nothing new. The shotnoise, however, provides new information about the intrinsic properties of the device.

A third source of noise is the so-called $1/f$ (or flicker) noise, which has its origins in the random motion of impurities. The characteristic $1/f$ frequency dependence means that this noise-source becomes important at low frequencies $\lesssim$ 10kHz. Nowadays, mesoscopic measurements can be made at high enough frequency as to avoid these $1/f$ contributions and thus, we will not consider it any further. $1/f$ noise is, however, of great importance to attempts at realising quantum computation in the solid state, since in that setting, it is a significant form of environmental perturbation.

8.2 Noise and quantum statistics

One reason why noise is interesting is that it reflects the quantum statistics of the particles producing the noise. Consider three types of particle: classical, fermion, and boson, described by Boltzmann, Fermi-Dirac, and Bose-Einstein statistics respectively. The average occupation of single state in equilibrium is

$$\langle n\rangle = \frac{1}{e^{E/k_BT} + a}; \quad \text{where} \quad a = \begin{cases} 0 & \text{classical} \\ 1 & \text{fermions} \\ -1 & \text{bosons} \end{cases} \tag{8.7}$$

Correspondingly, the variance in the occupancy is

$$\langle(\delta n)^2\rangle = \langle n\rangle\left(1 - a\langle n\rangle\right). \tag{8.8}$$

For classical particles ($a = 0$), $\langle(\delta n)^2\rangle = \langle n\rangle$ which is the *Poissonian* value, indicative of uncorrelated events (see later). When quantum statistics are important, deviations from this Poissonian case are observed. For bosons we typically have $\langle(\delta n)^2\rangle > \langle n\rangle$; the particles are 'bunched together' and the situation is described as *super-Poissonian*. Conversely, fermions tend to have $\langle(\delta n)^2\rangle < \langle n\rangle$ and we say the fluctuations are anti-bunched or *sub-Poissonian*. An extreme example of the anti-bunching of fermions is a zero-temperature channel — this is occupied with certainty, and the corresponding noise is zero.

Note that these considerations just provide us with an idea of 'typical' behaviours — photons can be anti-bunched (i.e. behave like fermions) and electrons can be bunched (i.e. behave like bosons). However, this requires additional sources of correlation in the system, which implies interesting physics. For example, anti-bunched photons are encountered in resonance fluorescence in optics, and bunched electron flows can be caused by current-blockade mechanisms.

8.3 Shotnoise in the scattering approach

We begin by defining the current fluctuation operator in lead α:

$$\delta\hat{I}_\alpha(t) = \hat{I}_\alpha(t) - \langle\hat{I}_\alpha\rangle, \tag{8.9}$$

and the time-domain correlation function between currents in leads α and β as

$$S_{\alpha\beta}(t'-t) \equiv \frac{1}{2}\langle\delta\hat{I}_\alpha(t)\delta\hat{I}_\beta(t') + \delta\hat{I}_\beta(t')\delta\hat{I}_\alpha(t)\rangle. \tag{8.10}$$

Without time-dependent external fields, the correlation function must be translationally invariant and thus a function of $\tau = t - t'$ only. We then Fourier transform with respect to τ to give

$$S_{\alpha\beta}(\omega) \equiv \int_{-\infty}^{\infty} d\tau e^{i\omega t}\langle\delta\hat{I}_\alpha(t)\delta\hat{I}_\beta(t') + \delta\hat{I}_\beta(t')\delta\hat{I}_\alpha(t)\rangle \tag{8.11}$$

This is sometimes referred to as the noise power. Note that we have used an 'engineering convention' in this definition of the Fourier transform which brings in an extra factor of two. This is in accordance with Büttiker and gives the familiar thermal noise value.

Since we already have an expression for the current operator (Eq. (4.36)) and know how to take expectation values, we can directly evaluate Eq. (8.11)

$$\begin{aligned} S_{\alpha\beta}(\omega) &= \frac{e^2}{2\pi\hbar}\sum_{\gamma\delta}\sum_{mn}\int dE A^{mn}_{\gamma\delta}(\alpha;E,E+\hbar\omega)A^{nm}_{\delta\gamma}(\beta;E+\hbar\omega,E) \\ &\quad\times\{f_\gamma(E)[1-f_\delta(E+\hbar\omega)]+[1-f_\gamma(E)]f_\delta(E+\hbar\omega)\} \quad (8.12) \end{aligned}$$

We are interested here in the *zero-frequency noise*:

$$\begin{aligned} S_{\alpha\beta} &= S_{\alpha\beta}(0)=\frac{e^2}{2\pi\hbar}\sum_{\gamma\delta}\sum_{mn}\int dE A^{mn}_{\gamma\delta}(\alpha;E,E)A^{nm}_{\delta\gamma}(\beta;E,E) \\ &\quad\times\{f_\gamma(E)[1-f_\delta(E)]+[1-f_\gamma(E)]f_\delta(E)\} \quad (8.13) \end{aligned}$$

This expression is current-conserving and gauge-invariant (unlike the finite-frequency result of Eq. (8.12) [1])

Let us concentrate on the two-terminal case. Current conservation implies that we have $S = S_{LL} = S_{RR} = -S_{LR} = -S_{RL}$. Utilizing the eigenchannel representation of section 4.3.6 and some lengthy algebra, we can write the noise as

$$\begin{aligned} S &= \frac{e^2}{\pi\hbar}\sum_n\int dE\Big\{T_n(E)[f_L(1-f_L)+f_R(1-f_R)] \\ &\qquad +T_n(E)\left(1-T_n(E)\right)\left(f_L-f_R\right)^2\Big\} \quad (8.14) \end{aligned}$$

For slowly-varying transmission probabilities, which we evaluate at the Fermi-level, we obtain

$$S=\frac{e^2}{\pi\hbar}\left[2k_BT\sum_n T_n^2+eV\coth\left(\frac{eV}{2k_BT}\right)\sum_n T_n(1-T_n)\right] \quad (8.15)$$

8.3.1 Equilibrium noise

In equilibrium, $f_L = f_R$ and the second contribution in Eq. (8.14) vanishes. Furthermore, we may use the property $f(1-f) = -k_BT\partial f/\partial E$ to write the equilibrium noise as

$$S^{\rm eq} = \frac{2e^2k_BT}{\pi\hbar}\sum_n\int dE\left(-\frac{\partial f}{\partial E}\right)T_n(E) \quad (8.16)$$

[1] Eq. (8.12) fails to take into account displacement currents. See section 9.5 for more details.

Comparison with Eq. (4.46),yields the important relation

$$\boxed{S^{\text{eq}} = 4k_B TG} \tag{8.17}$$

such that the noise is proportional to both the conductance and the temperature. This is the Nyquist-Johnson noise and it is a manifestation of the fluctuation-dissipation theorem — equilibrium fluctuations are proportional to the corresponding susceptibility.

The important point here is that the equilibrium noise tells us nothing that we don't already know from conductance measurements.

8.3.2 Zero-temperature — shot noise

At zero temperature the product $f(1-f)$ is zero and the noise of Eq. (8.14) becomes

$$S = \frac{e^2}{\pi\hbar} \sum_n \int_{\mu_R}^{\mu_L} dE\ T_n(E)\,(1 - T_n(E)) \tag{8.18}$$

where we assumed $\mu_L > \mu_R$. Assuming that the tunnel probabilities are constant within the transport window, we obtain

$$S = \frac{e^3|V|}{\pi\hbar} \sum_n T_n\,(1 - T_n) \tag{8.19}$$

This is the shotnoise – it arises in nonequillibrium and is not simply determined by the conductance.

8.4 Poissonian noise and the Fano factor

A Poissonian process is a the stochastic process in which events occur continuously and independently of one another. A well-known example is radioactive decay of atoms. The noise associated with a Poissonian process swerves as an important benchmark — we have already seen in section 8.2 how having fluctuations greater or lesser than the Poissonian value is indicative of quantum statistics.

A (classical) current can be written as a string of electron-tunnel events

$$I(t) = e \sum_k \delta(t - t_k) \tag{8.20}$$

and for a Poisson process, the times t_k are distributed such the probability of there being n electrons in a time-interval τ is

$$P(N;t) = \frac{e^{-\gamma\tau}(\gamma\tau)^n}{n!}; \quad n = 0, 1, 2, \ldots, \tag{8.21}$$

with γ the characteristic rate of the process. The mean and the variance of electron number in interval τ are then $\langle n\rangle = \lambda\tau$ and $\langle(\delta n)^2\rangle = \lambda\tau$; in fact, all cumulants of the distribution are the same and equal to $\lambda\tau$. The corresponding current is $\langle I\rangle = -e/\tau\langle n\rangle = e\gamma$ and the shotnoise $S_P = 2e/\tau\langle(\delta n)^2\rangle = 2e^2\gamma$. For a Poisson process, therefore noise is proportional to the current

$$S_P = 2e\langle I\rangle. \tag{8.22}$$

The Fano factor is defined as

$$F = \frac{S}{S_P} = \frac{S}{2e\langle I\rangle}, \tag{8.23}$$

which allows us to easily see whether the current exhibits bunching ($F > 1$), anti-bunching ($F < 1$), or is Poissonian ($F = 1$).

If we now return to the expression for the shotnoise form Eq. (8.19), we see that, in the limit of small T_n, we may neglect quadratic terms and the noise becomes

$$S \sim \frac{e^3|V|}{\pi\hbar}\sum_n T_n. \tag{8.24}$$

From Eq. (4.47), the current is

$$I = \frac{e^2|V|}{2\pi\hbar}\sum_n T_n, \tag{8.25}$$

such that the Fano factor is equal to one and the noise Poissonian. Furthermore, this is the maximum value achievable by the shotnoise of Eq. (8.19) since the inclusion of the $(1 - T_n)$ factors always reduce the contribution from each channel. In general then, we can say that the shotnoise of non-interacting electrons (as described by this scattering theory) will be *sub-Poissonian* with $F \leq 1$. This is in accord with typical fermionic behaviour as mentioned previously. [2]

[2]Note that this statement about subPoissonian noise applies to the shotnoise contribution to the noise, and excludes the thermal contributions. Values of $F > 1$ are easily obtainable with thermal fluctuations since, as we reduce the voltage across the device, the current will vanish but the shotnoise tends towards the constant Johnson-Nyquist value. The resultant Fano factor then diverges.

8.5 Multi-lead formulae

The corresponding multi-lead results are

$$S^{\rm eq}_{\alpha\beta} = 2k_BT(G_{\alpha\beta} + G_{\beta\alpha}) \tag{8.26}$$

for the Nyquist-Johnson noise, and

$$\begin{aligned} S_{\alpha\beta} &= \frac{e^2}{2\pi\hbar}\sum_{\gamma\neq\delta}\int dE\ {\rm Tr}\left[s^\dagger_{\alpha\gamma}s_{\alpha\delta}s^\dagger_{\beta\delta}s_{\beta\gamma}\right] \\ &\qquad \{f_\gamma(E)(1-f_\delta(E)) + f_\delta(E)(1-f_\gamma(E))\} \end{aligned} \tag{8.27}$$

Shotnoise correlators in the same lead are always positive, whereas those between different leads are always negative.

8.6 Examples

8.6.1 Hanbury-Brown Twiss

Quantum Hall edge channels can be used to realise a beam-splitter geometry for which we can now calculate the noise (Fig. 8.1). At zero temperature the various noise components are $S_{11} = S_{33} = -S_{13} = -S_{31}$ with

$$S_{13} = -\frac{e^3V}{\pi\hbar}T(1-T) \tag{8.28}$$

with T the transmission of the barrier. The experimental results of Fig. 8.1 bare out the theoretical predictions, in particular the negative cross-correlator.

8.6.2 Single Tunnel barrier

A single tunnel barrier has all transmission probabilities $T_n \ll 1$. From Eq. (8.15) we have then

$$S = \frac{e^3V}{\pi\hbar}\coth\left(\frac{eV}{2k_BT}\right)\sum_n T_n = \coth\left(\frac{eV}{2k_BT}\right)S_P. \tag{8.29}$$

This result illustrates the cross-over between thermal noise for $e|V| \ll k_BT$ to shotnoise at voltages $e|V| \gg k_BT$ independent of the details of the tunnel junction. Very good agreement with this result was observed in the experiment of Fig. 8.2.

8.6.3 Units of transferred charge

In a tunnel junction between a normal metal and a superconductor, the granularity of the current transferred across the junction is not equal to the elementary charge e, but rather $2e$ due to the formation of Cooper pairs in the superconductor. In this case, it can be shown that the shotnoise is $S = 2S_P$, and the Fano Factor is twice the normal-metal value. This can be generalised such that if charge is transferred in independent units of q, the Fano factor will be $F = q$.

Surprisingly, q need not be integer-valued. For example, tunnelling between edges states in the FQHE is mediated by quasi-particles with a fraction $q = e/(2p + 1)$ of the elementary charge.

8.6.4 Point Contact

For a detailed calculation of the properties of a quantum point contact, we require an electrostatic potential of the constriction. An obvious model is the saddle

$$V(x, y) = V_0 - \frac{1}{2}m\omega_x^2 x^2 + \frac{1}{2}m\omega_y^2 y^2, \tag{8.30}$$

for which the transmission probability is (Büttiker 1990)

$$\begin{aligned} T_n(E) &= \frac{1}{1 + e^{-\pi\epsilon_n}}; \\ \epsilon_n &\equiv 2\left[E - \hbar\omega_y\left(n + \frac{1}{2}\right) - V_0\right]/\hbar\omega_x. \end{aligned} \tag{8.31}$$

This can be substituted into Eq. (8.19) and the noise calculated. The results are shown in Fig. 8.3. At each current step, the shotnoise exhibits a pronounced peak of height $S_{\max} = e^3|V|/4\pi\hbar$. Within the plateaus, the noise is exponentially suppressed.

8.6.5 Resonant Tunnel Barrier

If we consider the resonant tunnel barrier of section 4.4.2 in the non-linear regime, such that a set of N_V levels are well within the transport window, the current and noise integrals (Eq. (8.14)) with the RTB transmission co-

efficient of Eq. (4.55) can be evaluated analytically. The results are

$$I = \frac{e}{\hbar}\sum_{n=1}^{N_V}\frac{\Gamma_{Ln}\Gamma_{Rn}}{\Gamma_n} \tag{8.32}$$

$$S = \frac{2e^2}{\hbar}\sum_{n=1}^{N_V}\frac{\Gamma_{Ln}\Gamma_{Rn}(\Gamma_{Ln}^2+\Gamma_{Rn}^2)}{\Gamma_n^3} \tag{8.33}$$

For a single resonance, we have the Fano factor

$$F = \frac{\Gamma_L^2+\Gamma_R^2}{\Gamma^2} \tag{8.34}$$

which is equal to 1/2 (sub-Poissonian) for symmetric barriers, and is Poissonian for highly asymmetric barriers.

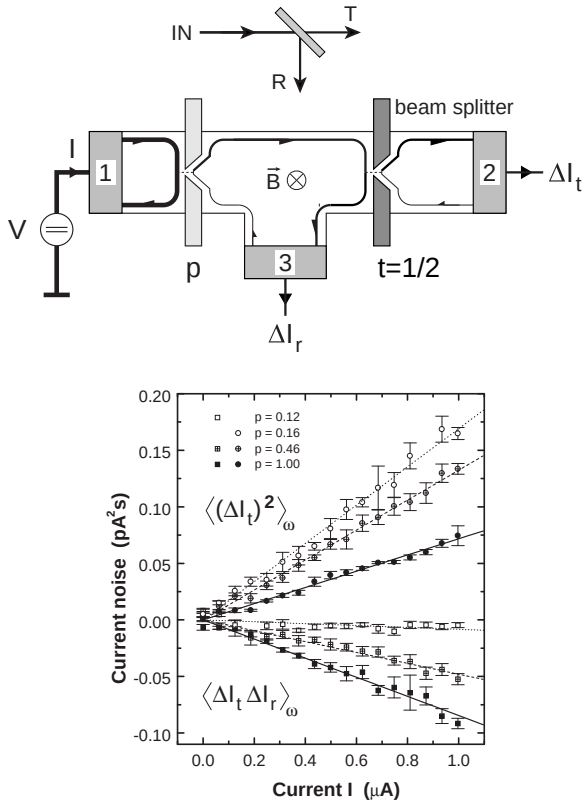

Figure 8.1: M. Henny, Science, **284**, 296, (1999).

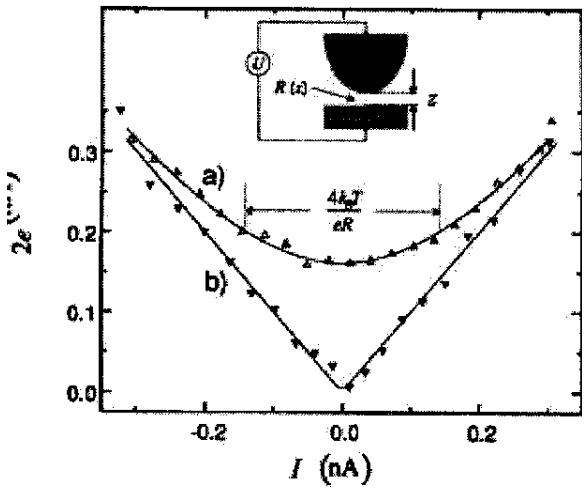

Figure 8.2: Shotnoise as a function of average current for a tunnel junction realised by an STM tip in proximity of a metal surface. Birk, de Jong and Schönengerger, 1995.

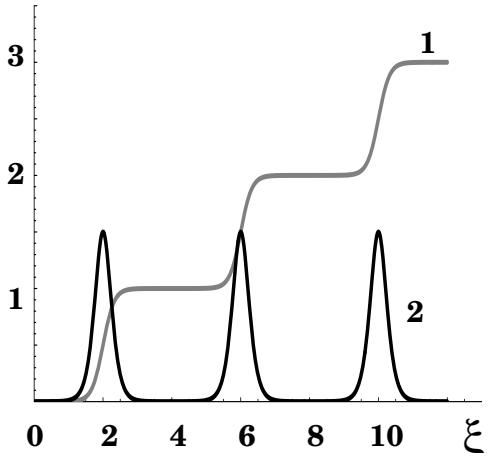

Figure 8.3: Current (1) and shotnoise (2) of QPC (from Blanter and Büttiker)

Chapter 9

Full counting statistics

As described in the previous chapter, the noise correlator S gives us a measure of the fluctuations in a current away from its mean value. However. there is more to the current that just its mean and variance — if we could count individual electrons passing through a device, we could a plot a histogram like that of part (d) of Fig. 9.1. We could then infer $P(n;t)$ — the probability of having n electrons passed to the collector in time t. From this quantity we could go on to calculate, not just the mean $\langle n \rangle$ and variance $\langle (\delta n)^2 \rangle$ of the number of electrons passed (and hence the current and shotnoise), but in principle, all the higher cumulants of the distribution. Knowledge of $P(n;t)$ therefore constitutes complete knowledge of the (zero-frequency) properties of the current fluctuations, and is thus known as the *full counting statics* (FCS) of the current. Just as there is more information contained in the noise than in the mean current alone, so we hope to learn more about the system from the FCS than from just the noise.

FCS began as a theoretical investigation (in the scattering approach, Levitov 1996; in the master equation approach, Bagrets and Nazarov, 2003). Although there had been a few measurements of the third current cumulant (or *skewness*) (Reulet 2003), it is only recently that experimentalists have been able to determine the FCS through a process of electron counting (Gustavsson 2006, Fujisawa 2006, Fricke 2007). The breakthrough that makes this possible is to use a QPC as an extremely sensitive electrometer — sensitive enough that the charging of a nearby QD with just a single electron exerts sufficient influence to close an additional transport channel in the QPC. The presence of an electron in the QD is thus observed as a change in the current through the QPC and in this way, the passage of single electrons can be detected. Figure 9.1 shows some experimental details from

the group of R. Haug in Hannover.

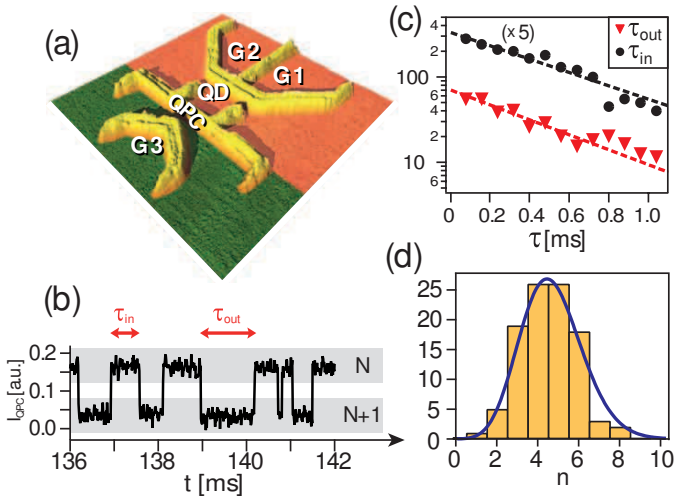

Figure 9.1: Electron counting experiment. (a) QD with QPC detector. (b) time trace of QPC current showing single-electron charging processes. (c) distribution of times of electron in and out of dot. (d) Distribution $P(n;t)$ of the number of electrons transmitted . Fricke *et al.*, Phys. Rev. B **76**, 155307 (2007).

In this chapter we learn how to calculate the FCS in the quantum master-equation approach (Bagrets and Nazarov 2003, Gurvitz 1996/7). In doing so we shall develop a theory of shotnoise in interacting systems, including at finite-frequency.

9.1 n-resolved master equation

The theory of FCS in the master-equation approach bears many similarities to the theory of photon-counting statistics from quantum optics. Our first task is to derive the n-resolved master equation (R.J. Cook 1981).

Consider the Liouvillian of single resonant level in the infinite-bias limit:

$$L = \begin{pmatrix} -\Gamma_L & \Gamma_R \\ \Gamma_L & -\Gamma_R \end{pmatrix}. \tag{9.1}$$

Let us concentrate on counting electrons as they enter the collector (the right lead). For this purpose, we divide the Liouvillian into two parts: the

jump operator

$$J_R = \begin{pmatrix} 0 & \Gamma_R \\ 0 & 0 \end{pmatrix}, \tag{9.2}$$

which transfers an electron from the dot into the collector; and

$$L_0 = \begin{pmatrix} -\Gamma_L & 0 \\ \Gamma_L & -\Gamma_R \end{pmatrix}, \tag{9.3}$$

which leaves the number of electrons in the collector unchanged. The propagator for the system in Laplace-Liouville-space can be written

$$\Omega(z) = \frac{1}{z - L} = \frac{1}{z - L_0 - J_R}, \tag{9.4}$$

which we expand as

$$\begin{aligned} \Omega(z) &= \Omega_0(z) + \Omega_0(z) J_R \Omega_0(z) + \Omega_0(z) J_R \Omega_0(z) J_R \Omega_0(z) + \dots \\ &= \sum_{n=0}^{\infty} \Omega_0(z) \left[J_R \Omega_0(z) \right]^n , \end{aligned} \tag{9.5}$$

with $\Omega_0(z) = 1/(z - L_0)$. The density matrix in Laplace-space is then

$$\rho(z) = \sum_{n=0}^{\infty} \Omega_0(z) \left[J_R \Omega_0(z) \right]^n \rho(t_0), \tag{9.6}$$

and we define the partial density matrix

$$\rho^{(n)}(z) = \Omega_0(z) \left[J_R \Omega_0(z) \right]^n \rho(t_0), \tag{9.7}$$

such that $\rho(z) = \sum_n \rho^{(n)}$. Since partial density matrix $\rho^{(n)}(z)$ consists of a total of n jump operators acting (at various times) on the initial state, it represents that component of the density matrix with n electrons having been transferred to the collector. If we start counting as $t = t_0$, the initial conditions read: $\rho^{(0)}(t_0) = \rho(t_0)$ and $\rho^{(n)}(t_0) = 0;\ n \neq 0$.

We now construct equations of motion for these n-resolved components. For $n = 0$, we have from Eq. (9.7)

$$\begin{aligned} \rho^{(0)}(z) &= \frac{1}{z - L_0} \rho(t_0) \\ \Rightarrow z\rho^{(0)}(z) - \rho^{(0)}(t_0) &= L_0 \rho^{(0)}(z). \end{aligned} \tag{9.8}$$

Performing the inverse Laplace transform, we find

$$\dot{\rho}^{(0)}(t) = L_0 \rho^{(0)}(t). \tag{9.9}$$

For $n \neq 0$, Eq. (9.7) yields the recursion relation

$$\rho^{(n)}(z) = \Omega_0(z) J_R \rho^{(n-1)}(z), \tag{9.10}$$

from which we obtain

$$\dot{\rho}^{(n)}(t) = L_0 \rho^{(n)}(t) + J_R \rho^{(n-1)}(t). \tag{9.11}$$

With the the convention $\rho^{(-n)} = 0$, we can combine these results and write

$$\boxed{\dot{\rho}^{(n)}(t) = L_0 \rho^{(n)}(t) + J_R \rho^{(n-1)}(t)} \tag{9.12}$$

for all n. This is the n-resolved master equation (for a single one-electron jump process).

This can be generalised to include processes which transfer an arbitrary number of electrons to the collector as

$$\dot{\rho}^{(n)}(t) = \sum_{n'=0}^{n} W(n-n') \rho^{(n')}(t). \tag{9.13}$$

It is also possible to generalise to multiple counting fields and to nonMarkovian kernels (Braggio, Flindt).

9.1.1 The counting field, χ

The equation set (9.12) can be solved with a Fourier transform that introduces the *counting field* χ as the variable conjugate to n. We define

$$\rho(\chi; t) = \sum_n \rho^{(n)} e^{in\chi}. \tag{9.14}$$

Multiplying Eq. (9.12) with $e^{in\chi}$ and summing over n, we obtain

$$\dot{\rho}(\chi; t) = \left(L_0 + e^{i\chi} J_R \right) \rho(\chi; t) \tag{9.15}$$

or

$$\boxed{\dot{\rho}(\chi; t) = L(\chi) \rho(\chi; t)}, \tag{9.16}$$

where we have defined the χ-dependent Liouvillian

$$\boxed{L(\chi) = L_0 + e^{i\chi} J_R}. \tag{9.17}$$

This is the χ-resolved master equation, which is identical to the normal master equation but with the χ-dependent Liouvillian $L(\chi)$. $L(\chi)$ is itself the same as the normal Liouvillian, but with the jump operator J_R multiplied with $e^{i\chi}$. This form can be generalised such that processes which transfer m electrons to lead α acquire a factor $e^{im\chi_\alpha}$ and processes in which m electrons are transferred from lead α acquire a factor $e^{-im\chi_\alpha}$.

Equation (9.16) is easily solved in Laplace space:

$$\rho(\chi; z) = \Omega(\chi; z)\rho(t_0) \tag{9.18}$$

with the χ-dependent propagator

$$\Omega(\chi; z) = \frac{1}{z - L(\chi)}. \tag{9.19}$$

9.2 Vector representation

For practical calculations it is useful to utilise the representation of Chapter 7 in which L is a matrix and ρ a vector. The eigendecomposition of L reads

$$L = \sum_{k=0}^{N-1} \lambda_k |\phi_k\rangle\!\rangle\langle\!\langle \phi_k|, \tag{9.20}$$

with eigenvalues λ_k, and right and left eigenvectors $|\phi_k\rangle\!\rangle$ and $\langle\!\langle\phi_k|$ respectively. We choose the labelling such that $\lambda_0 = 0$ with corresponding right eigenvector $|\phi_0\rangle\!\rangle = |\rho_{\text{stat}}\rangle\!\rangle$, the stationary state, which we assume unique and normalised. From orthonormality $\langle\!\langle\phi_j|\phi_k\rangle\!\rangle = \delta_{jk}$, the left eigenvector $\langle\!\langle\phi_0|$ has entries 1 at all positions corresponding to populations and 0 elsewhere. Thus the action of multiplying from the left with $\langle\!\langle\phi_0|$ is equivalent to taking the trace in the normal Fock space.

We introduce a similar notation for the eigendecomposition of the χ-dependent Liouvillian:

$$L(\chi) = \sum_{k=0}^{N-1} \lambda_k(\chi) |\phi_k(\chi)\rangle\!\rangle\langle\!\langle \phi_k(\chi)|. \tag{9.21}$$

We have $\lambda_k(\chi = 0) = \lambda_k$, and similarly for the eigenvectors.

9.3 Electron counting statistics

We begin with definitions of the moment and cumulants generating functions (MGF: $G(\chi;t)$ and CGF: $F(\chi;t)$):

$$G(\chi) = e^{F(\chi;t)} = \sum_{n=0}^{\infty} P(n;t)e^{in\chi} \tag{9.22}$$

From these functions we can obtain all the moments/cumulants of distribution $P(n;t)$ via simple differentiation. In particular, the kth cumulant can be obtained as

$$\langle (\delta n)^k \rangle = \frac{\partial^k}{\partial (i\chi)^k} F(\chi;t)\bigg|_{\chi=0}. \tag{9.23}$$

The distribution and generating functions are easily obtainable from the n-resolved approach. The probability of n electrons having passed after time t is simply

$$P(n;t) = \mathrm{Tr}\left\{\rho^{(n)}(t)\right\}, \tag{9.24}$$

and the generating function is therefore

$$e^{F(\chi;t)} = \sum_{n=0}^{\infty} \mathrm{Tr}\left\{\rho^{(n)}(t)e^{in\chi}\right\} = \mathrm{Tr}\left\{\rho(\chi;t)\right\}. \tag{9.25}$$

Inverse Laplace-transforming Eq. (9.19), we can write the CGF

$$e^{F(\chi;t)} = \mathrm{Tr}\left\{e^{L(\chi)t}\rho(t_0)\right\}. \tag{9.26}$$

For studying the long-time limit, we start the system in its stationary state$\rho(t_0) = \rho_{\mathrm{stat}}$. Employing the vector notation, we have

$$e^{F(\chi;t)} = \langle\langle \phi_0 | e^{L(\chi)t} | \phi_0 \rangle\rangle. \tag{9.27}$$

We then use the eigendecomposition of $L(\chi)$ to write

$$e^{F(\chi;t)} = \sum_k \langle\langle \phi_0 | \phi_k(\chi) \rangle\rangle \langle\langle \phi_k(\chi) | \phi_0 \rangle\rangle e^{\lambda_k(\chi)t}. \tag{9.28}$$

In the long time limit, the only term that survives is that with $\lambda_0(\chi)$ in the exponent, since all other terms yield exponentially-damped contributions to any and every cumulant. We have, therefore

$$e^{F(\chi;t)} \sim c(\chi)e^{\lambda_0(\chi)t}, \tag{9.29}$$

with $c(\chi) = \langle\langle\phi_0|\phi_0(\chi)\rangle\rangle\langle\langle\phi_0(\chi)|\phi_0\rangle\rangle$. Taking logarithms, we obtain

$$F(\chi;t) = \lambda_0(\chi)t + \ln c \tag{9.30}$$

and, therefore, to exponential accuracy,

$$\boxed{F(\chi;t) = \lambda_0(\chi)t}. \tag{9.31}$$

From this we can easily obtain any cumulant via multiple differentiation. In addition, we can obtain the distribution $P(n;t)$ via the inverse Fourier transform.

$$P(n;t) = \int_{-\pi}^{\pi} \frac{d\chi}{2\pi} e^{F(\chi;t)-in\chi} \tag{9.32}$$

This is often evaluated using a saddle-point method.

9.4 Examples

9.4.1 Poissonian Process

As with the noise, we use a generic Poissonian process as benchmark. The CGF is

$$F(\chi) = t\gamma(e^{i\chi} - 1), \tag{9.33}$$

such that all the cumulants are equal $\langle(\delta n)^k\rangle = \gamma t$.

9.4.2 Single resonant level

The χ-dependent Liouvillian for the SRL is

$$L(\chi) = \begin{pmatrix} -\Gamma_L & \Gamma_R e^{i\chi} \\ \Gamma_L & -\Gamma_R \end{pmatrix}. \tag{9.34}$$

Diagonalisng, we find the CGF:

$$F(\chi) = \frac{\Gamma t}{2}\left\{\sqrt{1 - \frac{4\Gamma_L\Gamma_R}{\Gamma^2}(1 - e^{i\chi})} - 1\right\} \tag{9.35}$$

with $\Gamma = \Gamma_L + \Gamma_R$. The first three cumulants are

$$\begin{aligned} \langle n\rangle &= t\frac{\Gamma_L\Gamma_R}{\Gamma} \\ \langle(\delta n)^2\rangle &= t\frac{\Gamma_L\Gamma_R}{\Gamma^3}\left(\Gamma_L^2 + \Gamma_R^2\right) \\ \langle(\delta n)^3\rangle &= t\frac{\Gamma_L\Gamma_R}{\Gamma^5}\left(\Gamma_R^4 - 2\Gamma_L^3\Gamma_R + 6\Gamma_L^2\Gamma_R^2 - 2\Gamma_L\Gamma_R^3 + \Gamma_R^4\right) \end{aligned} \tag{9.36}$$

A typical $P(n;t)$ distribution is shown in Fig. 9.1 alongside experimental results for a single QD. Note that in the limit in which $4\Gamma_L\Gamma_R/\Gamma^2 \ll 1$, the becomes

$$F(\chi) \approx \frac{\Gamma_L\Gamma_R t}{\Gamma}(e^{i\chi} - 1), \tag{9.37}$$

recovering the Poisson limit.

9.4.3 Double Quantum dot

This theory of FCS applies equally as well to systems with internal coherences. For a DQD in the strong Coulomb blockade regime (0 or 1 electrons). χ-dependent Liouvillian in basis $(\rho_{00}, \rho_{LL}, \rho_{RR}, \rho_{LR}, \rho_{RL})$ reads:

$$L(\chi) = \begin{pmatrix} -\Gamma_L & 0 & \Gamma_R e^{i\chi} & 0 & 0 \\ \Gamma_L & 0 & 0 & iT_c & -iT_c \\ 0 & 0 & -\Gamma_R & -iT_c & iT_c \\ 0 & iT_c & -iT_c & -i\epsilon - \Gamma_R/2 & 0 \\ 0 & -iT_c & iT_c & 0 & i\epsilon - \Gamma_R/2 \end{pmatrix}. \tag{9.38}$$

I skip the details here but refer you to Fig. 9.2 for some interesting results concerning the Fano factor of this model.

9.5 Finite-frequency FCS

In this section we look at how to calculate FCS at finite-frequencies. We follow the approach of Emary *et al.* PRB 2007. In doing so, we also derive an alternative method of evaluating specific cumulants (Hershfield 1993, Flindt 2005), which is particularly suited to situations with large Liouvillians.

9.6 Multi-time generating function

We are interested in N-point correlation functions, such as $\langle n(t_3)n(t_2)n(t_1)\rangle$, which correlates the number of electrons that have been passed to the collector at N different times. With each electron number, $n(t_k)$, we associate a separate counting field χ_k. We then view the evolution of the system as a series of propagations, first $t_0 \to t_1$, then $t_1 \to t_2$, and finally $t_{N-1} \to t_N$. As Fig. 9.3 shows, in each propagation interval more than one counting field can be active. In fact, in interval $\tau_k \equiv t_{k+1} - t_k$, counting fields $\sigma_k \equiv \sum_{i=N+1-k}^{N} \chi_i$ are active.

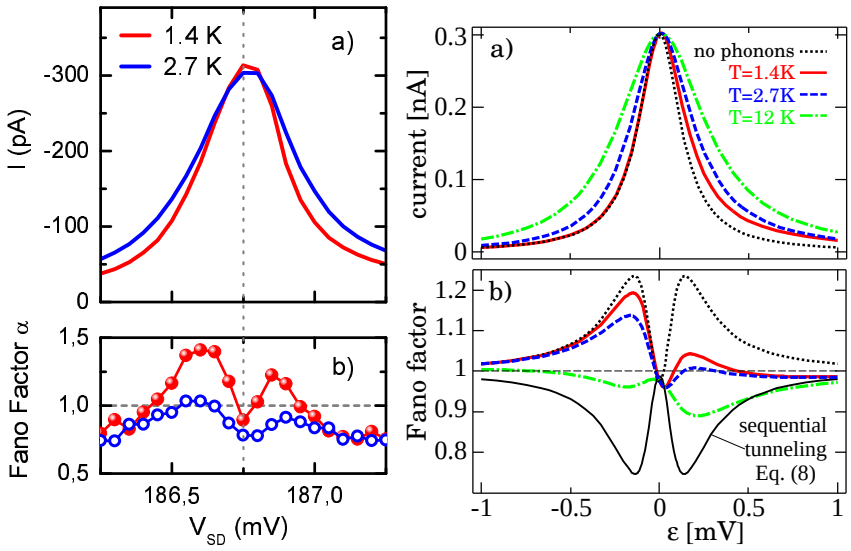

Figure 9.2: Mean current and Fano factor through an asymmetric DQD from both experiment (LEFT) and theory (RIGHT). Of particular interest is the superPoissonian Fano factor, an effect which is diminished with increasing temperature. This superPoissonian Fano factor is also absent from calculations with sequential tunnelling between the dots, indicating that $F > 1$ is a coherent effect. From G. Kiesslich et al., Phys. Rev. Lett. **99**, 206602 (2007).

We want to calculate the CGF for such a set of intervals, as this allows us to calculate any cumulant of the form $\langle (\delta n(t_N))^{p_N} (\delta n(t_{N-1}))^{p_{N-1}} \dots (\delta n(t_1))^{p_1} \rangle$, where p_k are integers. Here we just give recipe for the CGF, which is (hopefully) plausible — details can be found in Emary 2007 and Marcos 2009 (in preparation!). The multi-time CGF for a given set of intervals can be obtained by taking Eq. (9.27), dividing the propagator up into separate propagators for each interval, and inserting the appropriate set of counting fields σ_k in place of χ. This gives

$$e^{\mathcal{F}^{>}(\boldsymbol{\chi};\boldsymbol{t})} = \langle\!\langle \prod_{k=1}^{N} \Omega(\sigma_k; \tau_{N-k}) \rangle\!\rangle, \tag{9.39}$$

where $\boldsymbol{\chi} \equiv (\chi_1, \dots, \chi_N)$, $\boldsymbol{t} \equiv (t_1, \dots, t_n)$. We have labelled the CGF here $\mathcal{F}^{>}$ because the above form assumes a specific time ordering: $t_N > t_{N-1} > \dots > t_1 > t_0$. To obtain the full CGF we need to include all time-orderings,

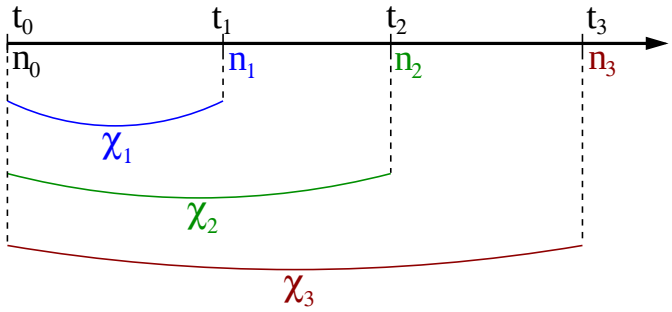

Figure 9.3: Time intervals, electron numbers, and counting fields for a $N = 3$ correlation function. In interval $t_0 \to t_1$ all three counting fields are active, in interval $t_1 \to t_2$, fields χ_2 and χ_3 are active, and in the final interval $t_2 \to t_3$, only χ_3 is active.

and this we do with the use of the time-ordering operator $\mathcal{T}$. We obtain

$$e^{\mathcal{F}(\boldsymbol{\chi};\boldsymbol{t})} = \mathcal{T}\, \langle\!\langle \prod_{k=1}^{N} \Omega(\sigma_k;\tau_{N-k})\boldsymbol{\rho}(t_0)\rangle\!\rangle, \tag{9.40}$$

Note that this form relies on the Markovian nature of the time-evolution.

The N-time current-cumulant ($e = 1$) is calculated using:

$$\begin{aligned} &S^{(N)}(t_1,\ldots,t_N) \equiv \langle \delta I(t_1)\ldots\delta I(t_N)\rangle = \\ &= \partial_{t_1}\ldots\partial_{t_N}\langle \delta n(t_1)\ldots\delta n(t_N)\rangle = \\ &= (-i)^N \partial_{t_1}\ldots\partial_{t_N}\partial_{\chi_1}\ldots\partial_{\chi_N}\mathcal{F}(\boldsymbol{\chi};\boldsymbol{t})\Big|_{\boldsymbol{\chi}=\mathbf{0}}. \end{aligned} \tag{9.41}$$

Note that, in the QME approach, the number of electrons in a lead is essentially a classical variable — this arises because we assume that no phase coherence exists between tunnelling events (in the sequential regime, at least). Correspondingly, the number and current correlation functions need not be symmetrised in the usual QM fashion. For noise, we have therefore

$$S(t_2,t_1) \equiv \frac{1}{2}\langle \delta I(t_2)\delta I(t_1) + \delta I(t_1)\delta I(t_2)\rangle = \langle \delta I(t_2)\delta I(t_1)\rangle. \tag{9.42}$$

9.6.1 Finite-frequency shotnoise

The two-time cumulant generating function (CGF) is

$$e^{\mathcal{F}(\chi_2,\chi_1;t_2,t_1)} = \mathcal{T}\, \langle\!\langle \Omega(\chi_2, t_2 - t_1)\Omega(\chi_1+\chi_2, t_1 - t_0)\rangle\!\rangle, \tag{9.43}$$

and we want to evaluate

$$S(\omega_1, \omega_2) \equiv 2 \int_{-\infty}^{\infty} dt_1 \int_{-\infty}^{\infty} dt_2 e^{i\omega_1 t_1 + i\omega_2 t_2} S(t_1, t_2). \tag{9.44}$$

(Note that the 2 in the front is to agree with the definition in the Büttiker review) The correlator $S(t_1, t_2)$ of Eq. (9.42) has the properties: 1) time-translational invariance $S(t_1 + \tau, t_2 + \tau) = S(t_1, t_2)$, and 2) symmetry under exchange of indices: $S(t_2, t_1) = S(t_1, t_2)$ (symmetrised, or here classical).

We can take into account the $\mathcal{T}$ operator by rearranging the frequency integrals. First, we write Eq. (9.44) as

$$S(\omega_1, \omega_2) = 2 \int_{-\infty}^{\infty} dt_1 dt_2 e^{i\omega_1 t_1 + i\omega_2 t_2} S(t_1, t_2) \left[\theta(t_2 - t_1) + \theta(t_1 - t_2)\right]. \tag{9.45}$$

Exchanging variables in the second term we have

$$S(\omega_1, \omega_2) = 2 \int_{-\infty}^{\infty} dt_1 dt_2 \left(e^{i\omega_1 t_1 + i\omega_2 t_2} + e^{i\omega_2 t_1 + i\omega_1 t_2}\right) S(t_1, t_2) \theta(t_2 - t_1), \tag{9.46}$$

due to the symmetry of $S(t_1, t_2)$. Now let's change variables to t_1 and $\tau = t_2 - t_1$

$$S(\omega_1, \omega_2) = 2 \int_{-\infty}^{\infty} dt_1 d\tau e^{i\widetilde{\omega} t_1} \left(e^{i\omega_2 \tau} + e^{i\omega_1 \tau}\right) S(t_1, t_1 + \tau) \theta(\tau), \tag{9.47}$$

where $\widetilde{\omega} = \omega_1 + \omega_2$.

Now split t_1 integral and use translational-invariance, $S(-t_1, -t_1 + \tau) = S(t_1, t_1 + \tau)$, to obtain

$$S(\omega_1, \omega_2) = 2 \int_{0}^{\infty} dt_1 d\tau \left(e^{i\widetilde{\omega} t_1} + e^{-i\widetilde{\omega} t_1}\right) \left(e^{i\omega_2 \tau} + e^{i\omega_1 \tau}\right) S(t_1, t_1 + \tau). \tag{9.48}$$

Therefore, we are able to write

$$S(\omega_1, \omega_2) = 2 \left(\widetilde{S}(\widetilde{\omega}, \omega_2) + \widetilde{S}(\widetilde{\omega}, \omega_1) + \widetilde{S}(-\widetilde{\omega}, \omega_2) + \widetilde{S}(-\widetilde{\omega}, \omega_1)\right) \tag{9.49}$$

with

$$\widetilde{S}(\widetilde{\omega}, \omega_2) = \int_{0}^{\infty} dt_1 d\tau e^{i\widetilde{\omega} t_1 + i\omega_2 \tau} S(t_1, t_1 + \tau). \tag{9.50}$$

The symmetry properties of S are thus clear. Finally, let us write $\widetilde{S}$ as a Laplace transform

$$\widetilde{S}(\widetilde{z}, z_2) = \int_{0}^{\infty} dt_1 d\tau e^{-\widetilde{z} t_1 - z_2 \tau} S(t_1, t_1 + \tau), \tag{9.51}$$

with $\widetilde{z} = -i\widetilde{\omega}$ and $z_i = -i\omega_i$.

Now, writing cumulants in terms of moments, we have

$$\begin{aligned} S(t_1, t_1+\tau) &= \langle \delta I(t_1)\delta I(t_1+\tau)\rangle \\ &= \langle I(t_1)I(t_1+\tau)\rangle - \langle I(t_1)\rangle\langle I(t_1+\tau)\rangle \\ &= \langle I(t_1)I(t_1+\tau)\rangle - \langle I(t_1)\rangle\langle I(\tau)\rangle, \end{aligned} \tag{9.52}$$

where the last line follows once again from the translational invariance of the mean current. The currents can be expressed as time-derivatives of electron numbers:

$$\begin{aligned} S(t_1, t_1+\tau) &= \frac{\partial^2}{\partial t_1 \partial t_2}\langle n(t_1)n(t_1+\tau)\rangle - \frac{\partial^2}{\partial t_1 \partial \tau}\langle n(t_1)\rangle\langle n(\tau)\rangle \\ &= \left(\frac{\partial^2}{\partial t_1 \partial \tau} - \frac{\partial^2}{\partial \tau^2}\right)\langle n(t_1)n(t_1+\tau)\rangle - \frac{\partial^2}{\partial t_1 \partial \tau}\langle n(t_1)\rangle\langle n(\tau)\rangle. \end{aligned} \tag{9.53}$$

Placing this result into Eq. (9.50), we obtain

$$\begin{aligned} \widetilde{S}(\widetilde{z}, z_2) &= z_2\left(\widetilde{z} - z_2\right)\int_0^\infty dt_1 d\tau e^{-\widetilde{z}t_1 - z_2\tau}\langle n(t_1)n(t_1+\tau)\rangle \\ &\quad - z_2\widetilde{z}\int_0^\infty dt_1 d\tau e^{-\widetilde{z}t_1 - z_2\tau}\langle n(t_1)\rangle\langle n(\tau)\rangle. \end{aligned} \tag{9.54}$$

The number correlators are obtained from our moment-generating-functions as

$$\begin{aligned} \widetilde{S}(\widetilde{z}, z_2) &= z_2\left(\widetilde{z} - z_2\right)\int_0^\infty dt_1 d\tau e^{-\widetilde{z}t_1 - z_2\tau}\frac{1}{i^2}\frac{\partial^2}{\partial\chi_1\partial\chi_2}\langle\!\langle \Omega\left(\chi_2, \tau\right)\Omega\left(\chi_1+\chi_2, t_1\right)\rangle\!\rangle \\ &\quad - z_2\widetilde{z}\int_0^\infty dt_1 e^{-\widetilde{z}t_1}\frac{1}{i}\frac{\partial}{\partial\chi_1}\langle\!\langle \Omega\left(\chi_1, t_1\right)\rangle\!\rangle\int_0^\infty d\tau e^{-z_2\tau}\frac{1}{i}\frac{\partial}{\partial\chi_2}\langle\!\langle \Omega\left(\chi_2, \tau\right)\rangle\!\rangle \\ &= z_2\left(\widetilde{z} - z_2\right)\frac{1}{i^2}\frac{\partial^2}{\partial\chi_1\partial\chi_2}\langle\!\langle \Omega\left(\chi_2, z_2\right)\Omega\left(\chi_1+\chi_2, \widetilde{z}\right)\rangle\!\rangle \\ &\quad - z_2\widetilde{z}\frac{1}{i}\frac{\partial}{\partial\chi_1}\langle\!\langle \Omega\left(\chi_1, \widetilde{z}\right)\rangle\!\rangle\frac{1}{i}\frac{\partial}{\partial\chi_2}\langle\!\langle \Omega\left(\chi_2, z_2\right)\rangle\!\rangle \end{aligned} \tag{9.55}$$

where we have introduced the propagator in Laplace space

$$\Omega(\chi; z) = \int_0^\infty e^{-zt}\Omega(\chi; t) = \left(z - L(\chi)\right)^{-1}. \tag{9.56}$$

Can now expand the propagators as

$$\Omega(\chi, z) = \left[z - L - L_\chi\right]^{-1} = \Omega(z) + \Omega(z)L_\chi\Omega(z) + \Omega(z)L_\chi\Omega(z)L_\chi\Omega(z) + . \tag{9.57}$$

with $\Omega(z) = [z - L]^{-1}$. Now, since $L_\chi = J(e^{i\chi} - 1)$, we can further expand as functions of χ and only keep the terms that match with the derivatives in Eq. (9.55). For the current-squared term we require

$$\begin{aligned} \frac{1}{i}\frac{\partial}{\partial\chi}\langle\!\langle \Omega(\chi, z)\rangle\!\rangle &= \frac{1}{i}\frac{\partial}{\partial\chi}\langle\!\langle \Omega(z) + \Omega(z)\left(i\chi - \chi^2/2 + \ldots\right) J\Omega(z) + \ldots\rangle\!\rangle \\ &= \langle\!\langle \Omega(z) J \Omega(z)\rangle\!\rangle. \end{aligned} \tag{9.58}$$

Similarly, for the two-point generating function, we have

$$\begin{aligned} &\frac{1}{i^2}\frac{\partial^2}{\partial\chi_1\partial\chi_2}\langle\!\langle \Omega(\chi_2, z_2)\,\Omega(\chi_1 + \chi_2, \widetilde{z})\rangle\!\rangle \\ &\qquad = \langle\!\langle \Omega(z_2)\left(1 + 2\Omega(\widetilde{z})J + J\Omega(z_2)\right)\Omega(\widetilde{z})J\Omega(\widetilde{z})\rangle\!\rangle \end{aligned} \tag{9.59}$$

With the "amputation rules" $\langle\!\langle \ldots \Omega(z)\rangle\!\rangle = \langle\!\langle \Omega(z)\ldots\rangle\!\rangle = (z)^{-1}\langle\!\langle \ldots\rangle\!\rangle$, we have

$$\begin{aligned} &\frac{1}{i^2}\frac{\partial^2}{\partial\chi_1\partial\chi_2}\langle\!\langle \Omega(\chi_2, z_2)\,\Omega(\chi_1 + \chi_2, \widetilde{z})\rangle\!\rangle \\ &\qquad = \frac{1}{z_2\widetilde{z}^2}\left\{\langle\!\langle J\rangle\!\rangle + 2\langle\!\langle J\Omega(\widetilde{z})J\rangle\!\rangle + \widetilde{z}\langle\!\langle J\Omega(z_2)\Omega(\widetilde{z})J\rangle\!\rangle\right\}, \end{aligned} \tag{9.60}$$

and will also use the trick

$$\Omega(z_2)\Omega(\widetilde{z}) = \frac{1}{\widetilde{z} - z_2}\left(\Omega(z_2) - \Omega(\widetilde{z})\right). \tag{9.61}$$

Placing these results into Eq. (9.55), gives us

$$\widetilde{S}(\widetilde{z}, z_2) = \frac{\widetilde{z} - z_2}{(\widetilde{z})^2}\langle\!\langle J\rangle\!\rangle + \frac{\widetilde{z} - 2z_2}{(\widetilde{z})^2}\langle\!\langle J\Omega(\widetilde{z})J\rangle\!\rangle + \frac{1}{\widetilde{z}}\langle\!\langle J\Omega(z_2)J\rangle\!\rangle - \frac{1}{\widetilde{z}z_2}\langle\!\langle J\rangle\!\rangle^2 \tag{9.62}$$

We then employ the eigendecomposition of L to write

$$\begin{aligned} \Omega(z) &= \frac{1}{z - L} = \sum_{k=1}^{N-1}\frac{|\phi_k\rangle\!\rangle\langle\!\langle\phi_k|}{z - \lambda_k} + \frac{|\phi_0\rangle\!\rangle\langle\!\langle\phi_0|}{z} \\ &= R(z) + \frac{P}{z}. \end{aligned} \tag{9.63}$$

The object $P = |\phi_0\rangle\!\rangle\langle\!\langle\phi_0|$ is the projector onto the steady-state, and $R(z)$ is the pseudo-inverse of $z - L$, i.e. the inverse of the part of $z - L$ that is non-singular in the $z \to 0$ limit. This gives, in particular

$$\frac{1}{\widetilde{z}}\langle\!\langle J\Omega(z_2)J\rangle\!\rangle = \frac{1}{\widetilde{z}}\langle\!\langle JR(z_2)J\rangle\!\rangle + \frac{1}{\widetilde{z}z_2}\langle\!\langle JPJ\rangle\!\rangle \tag{9.64}$$

The second term of this then cancels with the current-squared contribution, to give

$$\widetilde{S}(\widetilde{z}, z_2) = \frac{\widetilde{z} - z_2}{(\widetilde{z})^2}\langle\langle J\rangle\rangle + \frac{\widetilde{z} - 2z_2}{(\widetilde{z})^2}\langle\langle JR(\widetilde{z})J\rangle\rangle + \frac{1}{\widetilde{z}}\langle\langle JR(z_2)J\rangle\rangle. \tag{9.65}$$

We can now use our symmetrization results of Eq. (9.49). First, we find

$$\widetilde{S}(\widetilde{z}, z_2) + \widetilde{S}(\widetilde{z}, z_1) = \frac{1}{\widetilde{z}}\left\{\langle\langle J\rangle\rangle + \langle\langle JR(z_1)J\rangle\rangle + \langle\langle JR(z_2)J\rangle\rangle\right\}, \tag{9.66}$$

where the term containing $R(\widetilde{z})$ has cancelled. We then symmetrize over $\widetilde{z}$ and, because the two contributions originally come from different halves of the $\tilde{z}$ axis, they have opposite convergence factors, giving

$$\begin{aligned} S(z_1, z_2) &= 2\left(\frac{1}{\widetilde{z} + \eta} + \frac{1}{-(\widetilde{z} - \eta)}\right)\left\{\langle\langle J\rangle\rangle + \langle\langle JR(z_1)J\rangle\rangle + \langle\langle JR(z_2)J\rangle\rangle\right\} \\ &= 2\frac{2\eta}{\widetilde{z}^2 + \eta^2}\left\{\langle\langle J\rangle\rangle + \langle\langle JR(z_1)J\rangle\rangle + \langle\langle JR(z_2)J\rangle\rangle\right\} \end{aligned} \tag{9.67}$$

In the limit that $\eta \to 0$, we obtain

$$S(z_1, z_2) = 2\left(2\pi\delta\left(z_1 + z_2\right)\right)\left\{\langle\langle J\rangle\rangle + \langle\langle JR(z_1)J\rangle\rangle + \langle\langle JR(z_2)J\rangle\rangle\right\} \tag{9.68}$$

The $2\pi\delta(z_1 + z_2)$ forefactor originates from the time-translational invariance of the correlator. Translating back into Fourier space, we have then

$$\boxed{S(\omega) = 2\left\{\ \langle\langle J\rangle\rangle + \langle\langle JR(\omega)J\rangle\rangle + \langle\langle JR(-\omega)J\rangle\rangle\right\}} \tag{9.69}$$

with

$$R(\omega) \equiv Q\frac{-1}{i\omega + L}Q \tag{9.70}$$

where $Q = 1 - |\phi_0\rangle\rangle\langle\langle\phi_0|$ is the projector out of the null-space of L. In this same notation, the current is

$$\boxed{\langle I\rangle = \langle\langle J\rangle\rangle}. \tag{9.71}$$

The zero frequency noise is then

$$\boxed{S(0) = 2\left\{\ \langle\langle J\rangle\rangle + 2\langle\langle JR(0)J\rangle\rangle\right\}} \tag{9.72}$$

9.6.2 Total current and the Ramo-Shockley theorem

The above frequency-dependent result does not directly give the finite-frequency noise measured in experiment since this result, just as Eq. (8.12), describes the particle current only and neglects displacement currents arising from charge accumulation. Note that the zero-frequency result does not suffer in the same way as the charge accumulation contribution disappears in this limit. Fortunately, the effect of the displacement current can be easily incorporated with help of the Ramo-Shockley theorem (1938/39), which states that the total instantaneous current through a two barrier system of capacitances C_L and C_R is given by

$$I(t) = \frac{C_R}{C_L + C_R} I_L(t) + \frac{C_L}{C_L + C_R} I_R(t) = \alpha I_L(t) + \beta I_R(t), \tag{9.73}$$

with $\alpha+\beta = 1$. Translating this into QM operators, we see that the shotnoise in frequency-domain will have the form

$$S(\omega) = \alpha^2 S_{LL}(\omega) + \beta^2 S_{RR}(\omega) + \alpha\beta \left(S_{LR}(\omega) + S_{LR}(\omega)\right) \tag{9.74}$$

where the noise correlator S_{XY} correlates currents through leads X and Y. These correlation functions can be evaluated as in the preceding subsection with the following modifications. We write the Liouvillian in terms of both left and right current superoperators, and associate with each its own counting field: $L(\chi) = L_0 + e^{i\chi_R} J_R + e^{i\chi_L} J_L$. The auto-correlation functions $S_{XX}(\omega)$; $X = L, R$ are then obtained from twice differentiation of the CGF with respect to the single counting field χ_X and yield forms identical to Eq. (9.69). The cross-correlators $S_{XY}(\omega)$; $X, Y = L, R$ are obtained from differentiation of the CGF once with respect to χ_L and once with respect to χ_R in the appropriate interval (z-variable). The cross-correlators are thus found to be

$$S_{XY}(\omega) = 2 \Big\{ \langle\langle J_X R(\omega) J_Y \rangle\rangle + \langle\langle J_X R(-\omega) J_Y \rangle\rangle \Big\}. \tag{9.75}$$

In this way, the total noise can be determined in the master equation approach.

The Ramo-Shockley result can be expressed as

$$S(\omega) = \alpha S_{LL}(\omega) + \beta S_{RR}(\omega) - \alpha\beta\omega^2 S_Q(\omega) \tag{9.76}$$

where $S_Q(\omega)$ is the charge-charge correlation function of the dot. This latter form shows how the charge-accumulation contribution disappears for $\omega \to 0$ and that the noise with this contribution is always less than that without, since $S_Q(\omega) > 0$.

9.6.3 Double Quantum dot

An interesting model in which to study finite frequency noise is the DQD since the existence of an internal quantum degree of freedom is visible in the finite-frequency noise as a resonant structure. Figure Fig. 9.4 shows some finite-frequency results for the DQD (Aguado Brandes). The previous

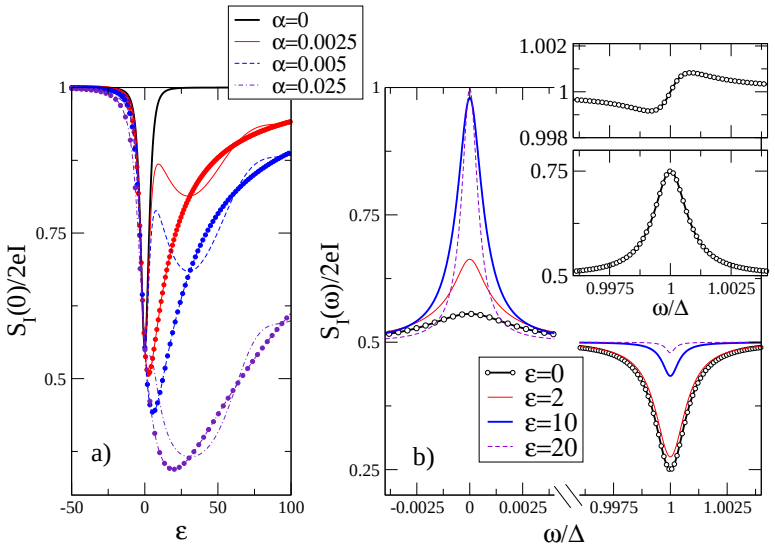

Figure 9.4: a) Fano factor vs. bias ε for different dissipative couplings α. Parameters $T_c = 3$, $\Gamma = 0.15$, $\omega_c = 500$, $\omega_d = 10$, $T = 2$ (in μeV) correspond to typical experimental values in double quantum dots. Lines: acoustic phonons, circles: generic ohmic environment $\omega_d = 0$ (see text). b) Frequency dependent current noise ($\alpha = 0$, $T = 0$, $\Gamma = 0.01$). Inset: (Top) Contribution to noise from particle currents $S_{I_R}(\omega)/2eI$. (Bottom) Charge noise contribution $\omega^2 S_Q(\omega)/8eI$. $a = b = 1/2$. From Aguado & Brandes, Phys. Rev. Lett. **92**, 206601 (2004)

calculation is also capable for giving higher-order frequency-dependent correlators. In Fig. 9.5 some results for the frequency-dependent skewness are given (Emary 2007).

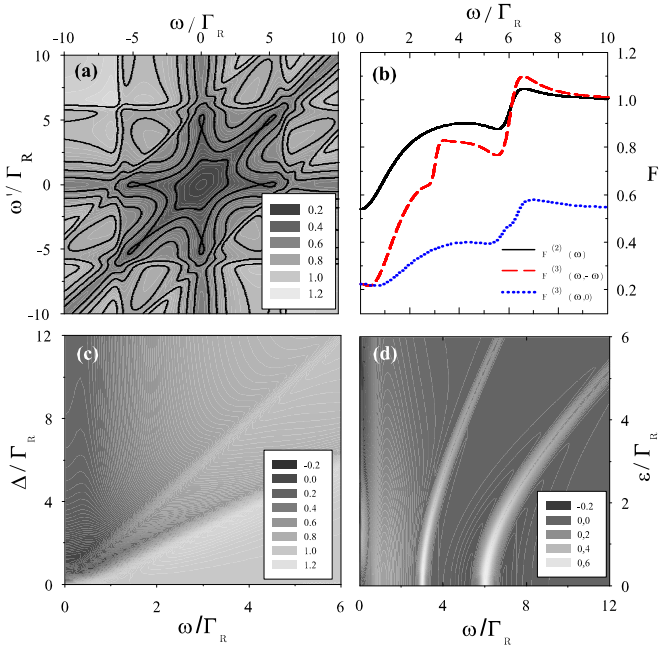

Figure 9.5: Frequency-dependent Fano skewness for the double quantum dot in Coulomb blockade. **(a)** Contour plot in the strong coupling regime, $T_c = 3\Gamma_R$, with $\Gamma_L = \Gamma_R$ and $\epsilon = 0$. **(b)** Sections $F^{(3)}(\omega, 0)$ and $F^{(3)}(\omega, -\omega)$, and shotnoise $F^{(2)}(\omega)$ show a series of abrupt increases with increasing ω. Both noise and skewness exhibit both sub- and super- Poissonian behaviour **(c)** Varying the internal coupling T_c, the skewness shows rapid increases along the lines $\omega = \Delta$ and $\omega = \Delta/2$. For $\omega > \Delta$ the system is Poissonian (slightly super-Poissonian for $\omega \gtrsim \Delta$), while for $\omega < \Delta$ the transport is always sub-Poissonian. The skewness is strongly suppressed at low frequencies. **(d)** The derivative $dF^{(3)}(\omega, -\omega)/d\omega$ as a function of frequency and detuning ϵ for $T_c = 3\Gamma_L = 3\Gamma_R$. Resonances occur at $\omega = \Delta$, $\Delta/2$ and $\sim \Gamma_R$.